INTERNATIONAL ATOMIC ENERGY AGENCY
UNITED NATIONS EDUCATIONAL, SCIENTIFIC AND CULTURAL ORGANIZATION

INTERNATIONAL CENTRE FOR THEORETICAL PHYSICS
34100 TRIESTE (ITALY) - P.O.B. 586 - MIRAMARE - STRADA COSTIERA 11 - TELEPHONES: 224281/2/3/4/5/6
CABLE: CENTRATOM - TELEX 460392-1

SMR/115 - 50

WINTER COLLEGE ON LASERS, ATOMIC AND MOLECULAR PHYSICS

(21 January - 22 March 1985)

SPIN-POLARIZED HYDROGEN

D. KLEPPNER
Massachusetts Institute of Technology
Research Laboratory of Electronics
Cambridge, Mass. 02139
U.S.A.

LES HOUCHES

SESSION XXXVIII

28 Juin–29 Juillet 1982

TENDANCES ACTUELLES

EN PHYSIQUE ATOMIQUE

NEW TRENDS

IN ATOMIC PHYSICS

GILBERT GRYNBERG et RAYMOND STORA

VOLUME II

NORTH-HOLLAND PUBLISHING COMPANY
AMSTERDAM · NEW YORK · TOKYO

COURSE 11

LECTURES ON SPIN-POLARIZED HYDROGEN

Thomas J. GREYTAK and Daniel KLEPPNER

Department of Physics
Massachusetts Institute of Technology
Cambridge, Massachusetts 02139, U.S.A.

G. Grynberg and R. Stora, eds.
Les Houches, Session XXXVIII, 1982 – Tendances actuelles en physique atomique / New trends in atomic physics

Contents

1. Introduction

Recent years have witnessed a flowering of theoretical and experimental interest in spin-polarized hydrogen, its growth propelled in no small part by the final realization of techniques for creating the substance in the laboratory, and for studying it. These lectures attempt to portray the main body of the research: the intellectual problems which sparked first interest, the theoretical studies of spin-polarized hydrogen, the experimental techniques for creating it, the results of the initial experiments, the new scientific opportunities which have been generated by these developments. We do not, however, attempt to offer a comprehensive review, and we apologize in advance to our colleagues whose work may not be adequately represented. The field is so diverse that such a review would conflict with the spirit of these lectures, and in any case the work is moving so rapidly that it would soon become obsolete.

A number of summary articles have been published and will be cited in the text. We wish to make reference here, however, to three articles by prime movers in the field: Nosanow [1], Silvera [2], and Hardy and Berlinsky [3].

1.1. Background

Statistical mechanics originated with Boltzmann's probabilistic analysis of the motion of ideal gas atoms. The velocity distribution for a gas of atoms of mass M at temperature T is described by the well-known Maxwell–Boltzmann law:

$$f(v) = \frac{1}{(\sqrt{\pi}\alpha)^3} \exp(-v^2/\alpha^2), \tag{1.1}$$

where $\alpha = \sqrt{2kT/M}$ (k is Boltzmann's constant.) In a stream of atoms effusing into a vacuum, an atomic beam, the distribution of speeds is

$$g(v) = (1/\alpha^4)v^3 \exp(-v^2/\alpha^2)\,. \tag{1.2}$$

The Maxwell–Boltzmann law was tested by Otto Stern in 1920 with a primitive atomic beam experiment in which the time of flight of the atoms was manifested as a smear in the beam's image on a rotating drum. Much more refined studies of velocities in atomic and molecular beams were carried out by Estermann and by Kusch in the 1950s. Recent experiments by laser spectroscopy have confirmed the accuracy of the Maxwell–Boltzmann distribution to high precision. The limitations of Boltzmann's theory are now well understood: the Maxwell–Boltzmann law is only accurate for weakly interacting atoms at high temperature. In the absence of interactions, departures from the Maxwell–Boltzmann law are insignificant until quantum mechanical effects assert themselves; this does not occur until the temperature is so low that an atom's deBroglie wavelength becomes comparable with the mean distance between particles.

The characteristic wavelength for a gas in thermal equilibrium is the "thermal" deBroglie wavelength

$$\Lambda(T) = (2\pi\hbar^2/MkT)^{1/2}\,. \tag{1.3}$$

If the particle density is n, the mean distance between particles is $n^{-1/3}$ and the quantum effects are to be expected when $n^{-1/3} \sim \Lambda(T)$. Consider, for instance, an intense atomic beam of sodium. Taking $T = 900\,\mathrm{K}$ and $n = 10^{16}\,\mathrm{cm}^{-3}$, then $n^{-1/3} = 5\times10^{-6}\,\mathrm{cm} \gg \Lambda \cong 10^{-9}\,\mathrm{cm}$. This system is safely in the classical regime. To witness quantum effects one evidently needs atoms of low mass at low temperature and a relatively high density. Helium is the obvious candidate. Unfortunately, as the gas density is increased at constant temperature the saturated vapor pressure is reached and the helium liquifies before the quantum regime is achieved in the gas. Instead of a simple weakly interacting gas one is presented with the complex problem of a strongly interacting liquid. Other substances are worse; they form solids long before quantum effects can occur. As a result, the quantum mechanical ideal gas has *never* been observed, nor even the quantum mechanical weakly interacting gas. A fundamental branch of statistical mechanics remains experimentally unexamined.

These lectures describe an attack on the problem of finding an atomic system which remains gaseous in the quantum regime. The atom is hydrogen. It is believed that spin-polarized atomic hydrogen never condenses under its own pressure and remains a gas at temperatures down to absolute zero. As a testing ground for the quantum theory of fluids, hydrogen would be unique. As an experimental medium, however, atomic hydrogen has a serious flaw: the atoms invariably combine to form molecules. Dramatic progress toward overcoming this problem has been made recently. The enterprise has caused renewed interest in quantum fluids, and the experimental advances have already led to numerous interesting applications.

These lectures summarize the theoretical foundations of the study of spin-polarized hydrogen and describe the experimental achievements. A concluding section discusses some potential applications for spin-polarized hydrogen.

1.2. *Elementary picture of Bose–Einstein condensation*

Because hydrogen is composed of two fermions, an electron and a proton, the atom as a whole obeys Bose statistics. The most dramatic feature of quantum behavior in a Bose gas is the Bose–Einstein transition, which we now briefly review.

Our starting point is the result for the mean occupation number of non-interacting particles in a state with momentum $\boldsymbol{p}$ and energy $\varepsilon_{\boldsymbol{p}}$.

$$\bar{N}_{\boldsymbol{p}} = \begin{cases} \dfrac{1}{\exp\beta(\varepsilon_{\boldsymbol{p}}-\mu)-1} & \text{Bose particles}\,, \\ \dfrac{1}{\exp\beta(\varepsilon_{\boldsymbol{p}}-\mu)+1} & \text{Fermi particles}\,, \\ \exp-\beta(\varepsilon_{\boldsymbol{p}}-\mu) & \text{Boltzmann law – classical limit}\,. \end{cases} \tag{1.4}$$

These results are obtained from the grand canonical ensemble. In this ensemble the *mean* total energy, E, and the *mean* number of particles N, are specified by constraint equations. As usual, $\beta \equiv 1/kT$. Hence

$$\sum \varepsilon_{\boldsymbol{p}}\bar{N}_{\boldsymbol{p}} = E\,, \tag{1.5a}$$

$$\sum \bar{N}_{\boldsymbol{p}} = N\,. \tag{1.5b}$$

The normalization equation, (1.5b), determines the chemical potential

μ as a function of N and T. The chemical potential is adjusted so that $\Sigma \bar{N}_p = N$ as follows: the system is taken to be in a box of volume $V = L^3$. Imposing periodic conditions on the momenta yields:

$$p_x = \frac{2\pi\hbar}{L} j_x, \qquad p_y = \frac{2\pi\hbar}{L} j_y, \qquad p_z = \frac{2\pi\hbar}{L} j_z, \tag{1.6}$$

where j_x, j_y, j_z are integers. Each state is specified by the set of three integers, (j_x, j_y, j_z), and the sum over states can be converted to an integral over momenta:

$$\sum_i \to (L/2\pi\hbar)^3 \int\int\int \mathrm{d}p_x\, \mathrm{d}p_y\, \mathrm{d}p_z = \int\int\int D(\boldsymbol{p})\, \mathrm{d}p_x\, \mathrm{d}p_y\, \mathrm{d}p_z, \tag{1.7}$$

where $D(\boldsymbol{p}) = V/(2\pi\hbar)^3$ is the density of states in momentum space. For a non-interacting gas, $\varepsilon_p = p^2/2M$ and $p^2\,\mathrm{d}p \to \sqrt{2M^3}\sqrt{\varepsilon}\,\mathrm{d}\varepsilon$. Hence

$$\sum_i \to \frac{V}{(2\pi)^2}\left(\frac{2M}{\hbar^2}\right)^{3/2} \int \sqrt{\varepsilon}\,\mathrm{d}\varepsilon = \int D(\varepsilon)\,\mathrm{d}\varepsilon, \tag{1.8}$$

where $D(\varepsilon)$ is the density of states as a function of energy:

$$D(\varepsilon) = \frac{V}{(2\pi)^2}\left(\frac{2M}{\hbar^2}\right)^{3/2} \sqrt{\varepsilon}. \tag{1.9}$$

$\bar{N}(\varepsilon)$ must satisfy

$$N = \int \bar{N}(\varepsilon) D(\varepsilon)\,\mathrm{d}\varepsilon, \tag{1.10}$$

where

$$\bar{N}(\varepsilon) = \frac{1}{\exp\beta(\varepsilon - \mu) - 1}. \tag{1.11}$$

Figure 1.1(a) illustrates several features of $\bar{N}(\varepsilon)$. Notice that the mean number of atoms occupying any single particle state is of the order of 1. The integrand in eq. (1.10) is the product of $\bar{N}(\varepsilon)$ and $D(\varepsilon)$, shown in fig. 1.1(b). The width of $\bar{N}(\varepsilon)$ decreases with temperature so

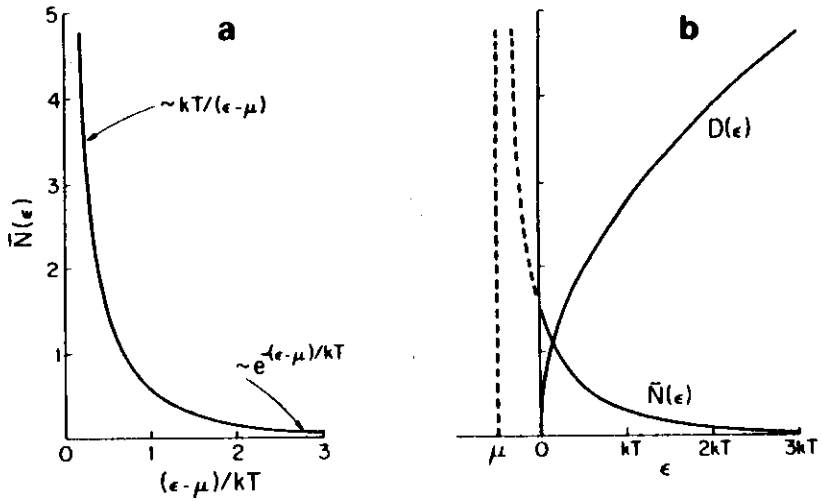

Fig. 1.1. (a) Mean occupation number $\bar{N}(\varepsilon)$ of a state with energy ε for the ideal Bose gas with chemical potential μ and temperature T. (b) $\bar{N}(\varepsilon)$ and density of states $D(\varepsilon)$ for ideal Bose gas. The chemical potential adjusts itself so that $\int \bar{N}(\varepsilon)D(\varepsilon)\,\mathrm{d}\varepsilon = N$. As the temperature decreases, μ increases. For $\mu > 0$ the integral would diverge; the Bose-Einstein transition takes place when $\mu = 0$.

that for the area under $\bar{N}(\varepsilon)D(\varepsilon)$ to remain constant as T decreases, μ must increase. However, μ cannot be positive: the divergence in $\bar{N}(\varepsilon)$ for $\varepsilon = \mu$ would cause the integral to diverge. Hence, the behavior changes abruptly at the temperature T_0 for which $\mu = 0$. This temperature is found from

$$N = \frac{V}{(2\pi)^2}\left(\frac{2M}{\hbar^2}\right)^{3/2} \int \frac{\sqrt{\varepsilon}\,\mathrm{d}\varepsilon}{\mathrm{e}^{\beta\varepsilon} - 1} = V\left(\frac{MkT}{2\pi\hbar^2}\right)^{3/2} \frac{2}{\sqrt{\pi}} \int_0^\infty \frac{\sqrt{x}\,\mathrm{d}x}{\mathrm{e}^x - 1}$$
$$= V\frac{1}{\Lambda(T_0)^3} \times 2.612. \tag{1.12}$$

(The integral is discussed later.) This result defines the transition temperature

$$T_0 = \frac{2\pi\hbar^2}{kM}\left(\frac{n}{2.612}\right)^{2/3}. \tag{1.13}$$

Provided that $T > T_0$, the above procedure can be used to find the

value of μ; if $T < T_0$, however, the procedure fails – the system is unable to accommodate all the particles in the available energy states. Before dealing with this difficulty, note that it would not arise if we were considering a *two-dimensional* gas. The density of states in two dimensions is $D(\varepsilon) = 32\pi M/\hbar^2$, which is independent of ε. In particular, $D(\varepsilon)$ remains finite at $\varepsilon = 0$. As a result eq. (1.10) can be solved for a physical μ (that is, μ is less than or equal to 0) for all temperatures:

$$\mu = kT \ln\{1 - \exp(-N[\Lambda(T)]^2/A)\}, \tag{1.14}$$

where A is the area of the sample.

What happens in the three-dimensional case when $T < T_0$? The excess particles start to populate the zero-energy state. This particular state was dropped in the process of transforming the sum over states into an integral over energy, eq. (1.8). It plays a unique role, however, for the energy of the system is unaffected by its occupation number. Below T_0 a finite fraction of the particles, that is a number of the order of N, occupies the zero-energy state. The mean occupation number as a function of energy then consists of a continuous part given by eq. (1.11) plus a discrete part, $\bar{N}_0\delta(\varepsilon)$. This is shown in fig. 1.2(a).

For $T < T_0$ one can show that the chemical potential is "pinned" at $\mu = 0$. The number of positive energy particles N' is

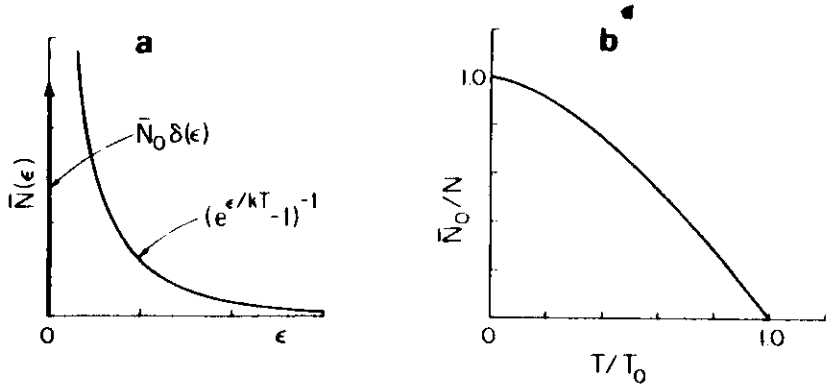

Fig. 1.2. (a) Mean occupation number in an ideal Bose condensed gas. The delta function at $\varepsilon = 0$ describes the finite occupation of the zero-energy state. (b) The fraction of Bose particles in the $\varepsilon = 0$ state as a function of the temperature. T_0 is the transition temperature.

$$N' = V\left(\frac{kTM}{2\pi\hbar^2}\right)^{3/2}\frac{2}{\sqrt{\pi}}\int_0^\infty \frac{\sqrt{x}\,dx}{e^x - 1} = N\left(\frac{T}{T_0}\right)^{3/2} \tag{1.15}$$

Thus the number of particles in the zero-energy state is

$$\bar{N}_0 = N - N' = N[1 - (T/T_0)^{3/2}]. \tag{1.16}$$

This is shown in fig. 1.2(b).

The abrupt occurrence of a finite occupation in a single particle state at T_0 indicates a spontaneous change in the symmetry of the system, albeit an ordering in momentum space rather than in real space, and therefore a thermodynamic phase change. One says that at $T = T_0$ the system undergoes a *Bose–Einstein transition* to a condensed state. The condensate fraction, $\bar{N}_0/N$, is the squared magnitude of the "order parameter" in the low temperature phase. In the modern theory of phase transitions, a transition is first order if there is a discontinuous change in the order parameter at the transition temperature and second order if the order parameter goes smoothly to zero at T_0. According to this classification, fig. 1.2(b) indicates that the Bose–Einstein transition is second order.

1.3. Evidence for the Bose–Einstein transition

In searching for a system in which to observe the Bose–Einstein transition, most gases can be rejected immediately because the transition temperature T_0 is so low that the system is no longer a gas, it is a solid. The possible exception is helium. In 1938 Fritz London pointed out that if liquid ^{4}He were treated as an ideal Bose gas with a density equal to that of the liquid, 2.20×10^{22} atoms cm^{-3}, the transition temperature would be $T_0 = 3.15$ K. This is remarkably close to the temperature at which superfluidity occurs, $T_\lambda = 2.17$ K. The fact that ^{3}He, a fermion, did not display superfluidity gave added weight to his suggestion that superfluidity is due to a Bose transition.

London's suggestion has tantalized theoretical and experimental condensed matter physicists for decades. It motivated much of the theoretical development of the weakly interacting Bose gas. Unfortunately, liquid helium is manifestly *not* a weakly interacting gas, and no microscopic theory of the liquid has yet been developed. Nevertheless, effects related to the Bose–Einstein transition are pre-

dicted, though they are small. According to the best estimates, the Bose condensate fraction at zero temperature is only about 0.1.

The experimental task of measuring the momentum distribution in the liquid is formidable. One possible approach is to use neutron spectroscopy, but until recently the results were inconclusive. Sears et al. [4] have reported measurements that yield $\bar{N}_0(0)/N = 0.139(23)$, and $\bar{N}_0(T)/\bar{N}_0(0) = (1 - (T/T_\lambda)^\alpha)$, where $\alpha = 3.6(14)$. Their results are shown in fig. 1.3, along with theoretical estimates. Thus, 44 years after London's original suggestion, there is reason to believe that Bose condensation has been observed. As an ideal gas, however, liquid helium leaves much to be desired. Are there better candidates for laboratory study? What is required is smaller mass and lower liquifaction temperature. Aside from ^{3}He, which obeys Fermi statistics, the only possibility is H (see postscript).

Atomic hydrogen is not an obvious candidate for study since under

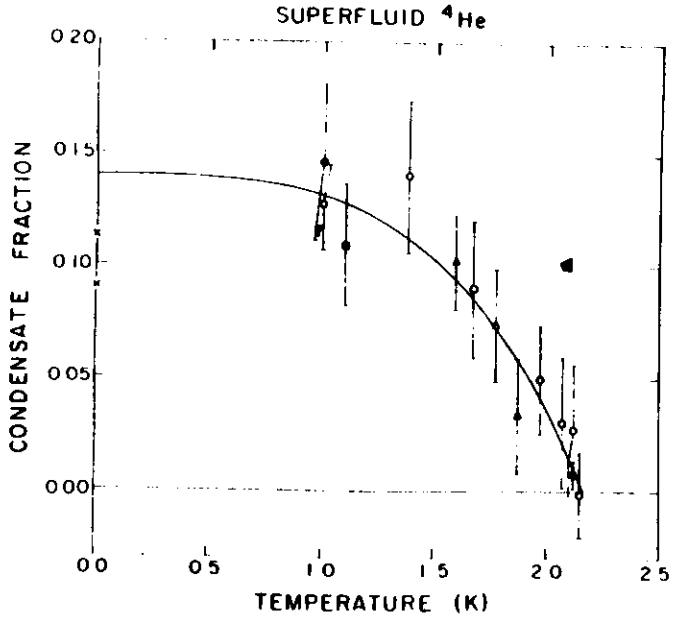

Fig. 1.3. The condensate fraction in superfluid ^{4}He (ref. [4]). Filled symbols are values obtained from $N(p)$ using inelastic neutron diffraction; open symbols are from observations of the temperature variation of the pair correlation function by using elastic neutron and X-ray diffraction. The ×'s are theoretical values. Courtesy of E.C. Svensson.

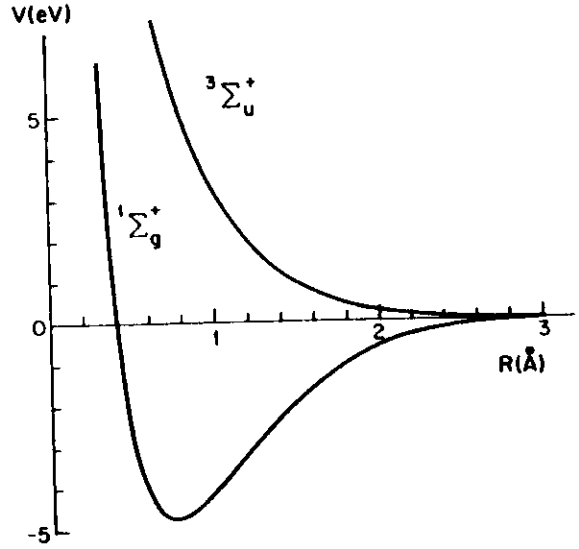

Fig. 1.4. Interatomic potentials for two hydrogen atoms, calculated by Kolos and Wolniewicz [5].

ordinary circumstances it forms a molecular gas, H_2, which liquifies at 20 K. The molecule is tightly bound, as the potential curve in fig. 1.4 shows. The dissociation energy of the $^1\Sigma_g$ state is 4.48 eV. The $^3\Sigma_u$ potential, however, is essentially repulsive and supports no bound states. Hydrogen with the electron spins all pointing in the same direction, spin-polarized hydrogen (H↓), interacts according to this potential and should form a close-to-ideal Bose gas. The quest to create H↓ is the subject of these lectures.

1.4. A short history of spin-polarized hydrogen

We present here an abbreviated history of gaseous spin-polarized hydrogen. Numerous important contributions are omitted, though many of these will be discussed later.

1959: Hecht [6] points out that if H could be spin-polarized, for instance by using a high magnetic field so that the reaction H + H → H_2 is suppressed, the system should remain a gas even at zero temperature. The gas should undergo a Bose condensation and become a superfluid. The paper is ahead of its time: experimental techniques,

particularly superconducting magnets and dilution refrigerators, are not yet available, and the paper does not attract attention for many years.

1973: Dugan and Etters [7] calculate the ground-state energy of spin-polarized hydrogen and deuterium, H↓ and D↓. They conclude that neither is bound at $T = 0$.

1975: Etters et al. [8] report more detailed calculations of H, D and T. T↓ is found to be a liquid at $T = 0$.

1975: Miller et al. [9] demonstrate the power of the law of corresponding states to predict liquid–gas transitions at $T = 0$ as a function of the system parameters.

1976: Stwalley and Nosanow [10] point out and extend the calculations of Etters et al. The Letter urges experimentalists to get to work. They do.

1979: Crampton et al. [11] and Hardy et al. [12] report observation of hyperfine resonance in H at 4.2 K, using a H_2-lined cell, and demonstrate the ability to thermalize and transport atomic hydrogen at 4.2 K.

1980: Silvera and Walraven [13] create spin-polarized hydrogen. H↓ is observed in a helium-lined cell at a temperature of 270 mK with a density of at least $1.8 \times 10^{14}\,\mathrm{cm}^{-3}$. H↓ is officially launched as an experimental field!

1980: Meeting on spin-polarized quantum fluids is held in Aussois, France [14]. Theoretical results and experimental problems are discussed. The MIT group reports production of H↓ at a density of $2 \times 10^{16}\,\mathrm{cm}^{-3}$.

1981: Morrow et al. [15] report values for adsorption energy and recombination rates of unpolarized H in a He-lined cell at zero magnetic field.

1981: Cline et al. [16] obtain proton-polarized H↓ and demonstrate that nuclear polarization plays a key role in the dynamics of molecular recombination. Attainment of high nuclear polarization opens the way to technical applications including polarized sources and targets for nuclear and particle physics.

Several groups have now made H↓. The maximum density so far achieved at 0.3 K is about $3 \times 10^{17}\,\mathrm{cm}^{-3}$. Higher densities appear to be possible*, but it is difficult to predict whether the Bose–Einstein transition can be achieved. There is hope; the sweepstakes is still on!

* See Postscript.

1.5. Some parallel history

The earliest theoretical study of H↓ was a 1958 report by Jones et al. [17] on the use of H↓ as a rocket fuel:

$$H + H \rightarrow H_2 + 4.8\,\mathrm{eV}\,.$$

Hydrogen has by far the highest energy per unit mass. Example:

$H_2 + \frac{1}{2}O_2 \rightarrow H_2O + 2.5\,\mathrm{eV}$	$(1.3 \times 10^{11}\,\mathrm{erg\,g^{-1}})$
$\frac{1}{2}H_2 + \frac{1}{2}F_2 \rightarrow HF + 2.8\,\mathrm{eV}$	$(1.3 \times 10^{11}\,\mathrm{erg\,g^{-1}})$
$H + H \rightarrow H_2 + 4.8\,\mathrm{eV}$	$(2.2 \times 10^{12}\,\mathrm{erg\,g^{-1}})$.

Because most of the mass of a rocket at takeoff is in its fuel, the potential advantages of H↓ are enormous. Jones et al. concluded (incorrectly) that H↓ could not be stabilized. Nevertheless, at present it seems unlikely that high enough densities of H↓ can be created for use as a rocket fuel.

During the late 1950s interest grew in the use of inert surfaces to inhibit nuclear and electronic spin relaxation in gases due to wall collisions. About 1960 it was discovered by Berg and Kleppner [18] that Teflon is a suitable material for storing atomic hydrogen – the possibility of such a surface is the central idea of the hydrogen maser. A typical density of polarized H atoms in a maser is $10^{11}\,\mathrm{cm}^{-3}$, about 8 orders of magnitude too low to see the Bose–Einstein transition.

In 1968 Kastler [19] proposed inhibiting the formation of diatomic alkali metal molecules by optically pumping the atoms so that the electrons are polarized. Atoms would then collide in the molecular triplet state. The effect was observed by Alzetta et al. [20].

1.6. The motivation for studying H↓

No one doubts the essential correctness of quantum statistical mechanics, and so it is worth asking why one should study yet another elementary system. There are a number of reasons:

–The theory for H↓ *exists*, and it can be refined to essentially any required precision. This is possible because the Bose–Einstein transition occurs at such a low density that the separation between atoms is

large compared to the range of the interatomic force. Perturbation methods are excellent; the results should converge without the need of going to high order.

–A Bose gas is expected to be a superfluid. Superfluidity in a gas has never been observed. Thus one has the opportunity to study new phenomena.

–The transport properties of a spin-polarized gas are of considerable interest in their own right because of the dramatic effect of quantum properties on macroscopic behavior. The theory is discussed by Lhuillier and Laloë [21, 22].

–The experimental challenge of creating H↓ is attractive because one may reasonably expect new scientific opportunities, and possibly technological advances. As we shall see, this has been born out.

–Underlying all the activity is the thought that the most dramatic transport phenomena, supercondictivity and superfluidity, were *discovered*, not predicted. There is always the hope that Nature has further surprises.

1.7. How to create H↓

To make the discussion more concrete, we briefly summarize the experimental steps in creating H↓. More details will be given later.

The method centers on what might be called a "magnetic bottle" [23]. The hyperfine energy for the ground state of hydrogen in a magnetic field is illustrated in fig. 1.5. States **a** and **b** are essentially electron spin "down" states, whereas states **c** and **d** are spin "up". Atoms in states **a** and **b** are attracted into a high magnetic field; atoms in **c** and **d** are repelled. In thermal equilibrium at a temperature of 0.3 K, the ratio of the populations is $n(\uparrow)/n(\downarrow) \simeq \exp(-14\,\mathrm{K}/0.3\,\mathrm{K}) \simeq 10^{-20}$.

The principle of operation is shown in fig. 1.6. Atoms in states **a** and **b** are pulled into the solenoid. They thermalize by collisions with the helium-lined walls and become trapped in the magnetic potential well. Atoms in states **c** and **d**, on the other hand, are strongly repelled by the magnet. The magnetic field selects the spin state with essentially 100% efficiency. In addition, it confines the atoms and inhibits spin depolarization due to collisions.

This method has yielded densities up to $3 \times 10^{17}\,\mathrm{cm}^{-3}$, and may be capable of achieving somewhat larger values. Substantially higher density will require additional steps. Work continues.

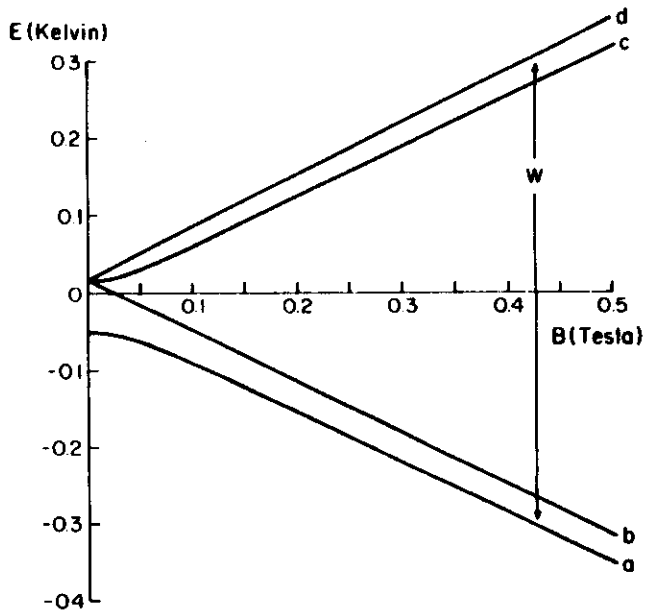

Fig. 1.5. Energy level diagram for the ground electronic state of hydrogen in a magnetic field. In a field of 10 T, $W = 13.5$ K.

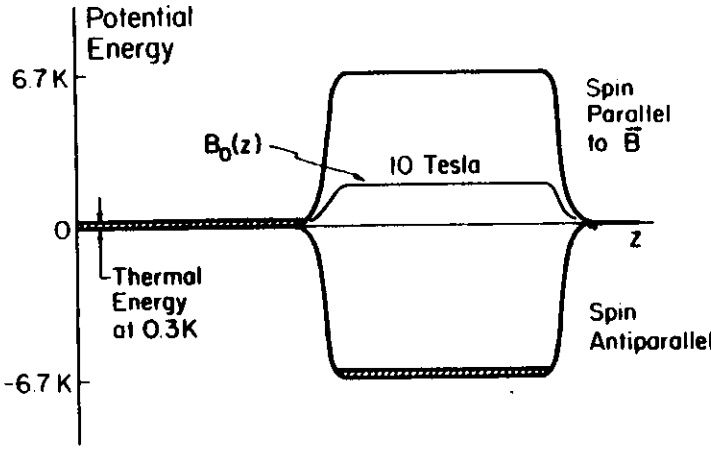

Fig. 1.6. Schematic picture of "magnetic bottle" confinement of H↓. The magnetic field spin selects, stabilizes, and confines the atomic hydrogen.

1.8. What has been learned so far?

The quest to witness the Bose–Einstein transition in hydrogen has stimulated a great deal of new science and technology – certainly enough to justify the effort irrespective of whether the final goal is achieved. Scientific accomplishments include studies of
- binding energies of H (and D) on H_2, He^4, He^3
- recombination processes
- hyperfine perturbations in H–He systems
- nuclear relaxation
- transport properties.

Experimental advances include developing methods for
- efficient production of H at 4 K and <0.3 K
- magnetic confinement of H↓
- efficient methods for producing *proton*-polarized H↓.

Proposed applications for H↓ and the H↓ techniques include
- atomic physics with cold (4 K) and very cold ($T<0.5$ K) hydrogen
- a low temperature H maser
- a cold tritium source for neutrino rest mass experiments
- polarized proton (and deuteron) sources and targets for nuclear and particle physics
- a polarized deuterium and tritium source for fusion reactors.

2. The ideal Bose gas

Spin-polarized hydrogen is a weakly interacting Bose gas. The starting point for understanding its properties is the theory of the ideal Bose gas, which we review in this section. Useful references are: K. Huang, *Statistical Mechanics* (Wiley, 1963); L.D. Landau and E.M. Lifshitz, *Statistical Physics*, Part 1 (Pergamon, 1980); F. London, *Superfluids*, Vol. II (Wiley, 1954).

2.1. The grand partition function

In statistical mechanics based on the grand canonical ensemble, thermodynamic information about a system is obtained from the grand partition function, $\Xi(z, V, T)$. This function depends on the temperature T, the volume V, and the variable z which is a measure of the

chemical potential μ ($z \equiv e^{\beta\mu}$). The pressure P and the mean number of particles N are found from

$$PV = kT \ln \Xi(z, V, T), \tag{2.1}$$

$$N = z\frac{\partial}{\partial z}(\ln \Xi(z, V, T))_{V,T}. \tag{2.2}$$

In order to find the equation of state for the system, $P(N, V, T)$, these two equations can be combined so as to eliminate z.

The grand partition function for a non-interacting Bose gas (Huang, p. 199) is

$$\Xi(z, V, T) = \prod_p \frac{1}{1 - z\exp -\beta\varepsilon_p}, \tag{2.3}$$

where Π_p indicates a product over all single particle states indexed by their momentum p. (The particles are assumed to have spin 0). In general $N = \Sigma_p \bar{N}_p$. An alternative expression is obtained from eqs. (2.3) and (2.2):

$$N = \sum_p \frac{1}{z^{-1}\exp(\beta\varepsilon_p) - 1}. \tag{2.4}$$

Evidently the mean occupation number of a single particle state is

$$\bar{N}_p = \frac{1}{\exp[\beta(\varepsilon_p - \mu(T))] - 1}. \tag{2.5}$$

This result was used in section 1.2. The probability that a particular single particle state is occupied by exactly N_p atoms can be found from the grand canonical ensemble – it is described by a simple geometric distribution:

$$\text{prob}(N_p) = \frac{1}{1 + \bar{N}_p}\left(\frac{\bar{N}_p}{1 + \bar{N}_p}\right)^{N_p}. \tag{2.6}$$

Figure 2.1 shows this probability density for $\bar{N}_p = 4$.

Before deriving the thermodynamic functions it is worth noting a valuable constitutive relation. For a *non-interacting* gas one can show

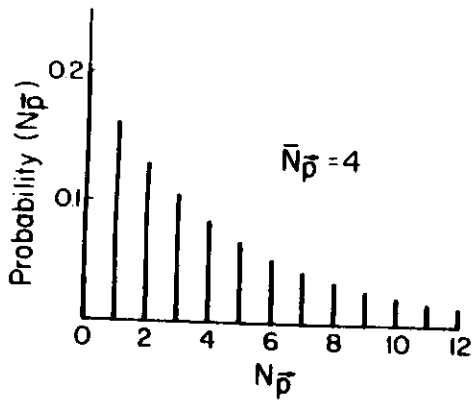

Fig. 2.1. Probability that N_p Bose particles occupy a state whose average occupation number is 4.

that

$$E = -\frac{\partial}{\partial\beta}(\ln \Xi(z, V, T))_{z,V}. \tag{2.7}$$

This expression, together with eq. (2.1), gives

$$E = \tfrac{3}{2}PV \tag{2.8}$$

for any non-interacting gas. The same result can, of course, be derived from simple kinetic theory arguments.

2.2. *Thermodynamic functions*

The thermodynamic functions can be obtained from eqs. (2.1)–(2.3). The density is found from eq. (2.4) by carrying out the sum over states. The sum over p can be converted to an integral as in section 1.2, with one important modification; the zero momentum state is explicitly retained.

$$\sum_p \bar{N}_p = 4\pi \frac{V}{(2\pi\hbar)^3} \int \bar{N}_p p^2\, dp + \bar{N}_0. \tag{2.9}$$

The reason for retaining the term $\bar{N}_0$ is that although particles in the zero-momentum state make no contribution to the integral, their number can be large. $\bar{N}_0 = z(1-z)^{-1}$, which diverges as $z \to 1$. Combining eqs. (2.5) and (2.9) yields

$$N = 4\pi \frac{V}{(2\pi\hbar)^3} \int_0^\infty \frac{1}{z^{-1}\exp(+\beta\varepsilon_p) - 1} p^2\, dp + \bar{N}_0, \tag{2.10}$$

$$\frac{N}{V} = \frac{1}{\Lambda^3}\frac{2}{\sqrt{\pi}} \int_0^\infty \frac{\sqrt{x}\, dx}{z^{-1}e^x - 1} + \frac{1}{V}\frac{z}{1-z}, \tag{2.11}$$

where $\Lambda(T) = (2\pi\hbar^2/MkT)^{1/2}$. Similarly

$$\frac{P}{kT} = -\frac{1}{\Lambda^3}\frac{2}{\sqrt{\pi}} \int_0^\infty \sqrt{x} \ln(1 - z\, e^{-x})\, dx - \frac{1}{V}\ln(1-z). \tag{2.12}$$

The integrals are discussed in Landau and Lifshitz, and in London. Defining

$$g_n(z) = \sum_{l=1}^{\infty} \frac{z^l}{l^n}, \tag{2.13}$$

it can be shown that

$$-\frac{2}{\sqrt{\pi}} \int_0^\infty \sqrt{x} \ln(1 - z\, e^{-x})\, dx = g_{5/2}(z), \tag{2.14}$$

$$\frac{2}{\sqrt{\pi}} \int_0^\infty \frac{\sqrt{x}}{z^{-1}e^x - 1}\, dx = g_{3/2}(z). \tag{2.15}$$

The value of $g_n(z)$ at $z = 1$ is $\zeta(n)$, the Riemann zeta function with argument n [$\zeta(3/2) = 2.612\ldots$; $\zeta(5/2) = 1.342\ldots$]. Thus

$$\frac{N}{V} = \frac{1}{\Lambda(T)^3} g_{3/2}(z) + \frac{1}{V}\frac{z}{1-z}, \tag{2.16}$$

$$\frac{P}{kT} = \frac{1}{\Lambda(T)^3} g_{5/2}(z) - \frac{1}{V}\ln(1-z). \tag{2.17}$$

These define the equation of state for the ideal Bose gas. For instance, given N, V and T, one can solve for P. Equation (2.16) can be rewritten,

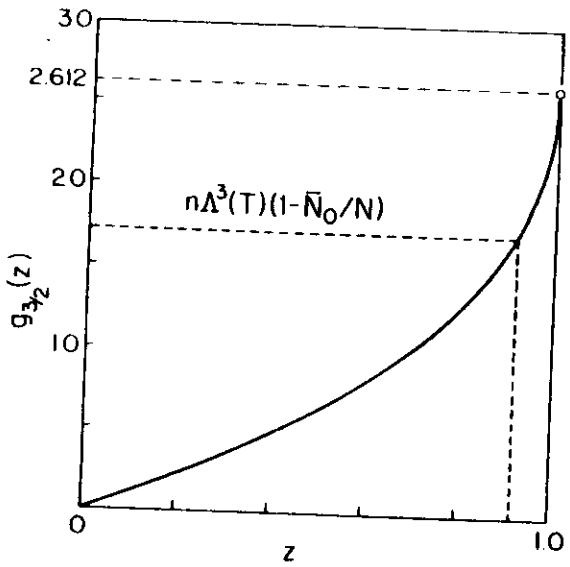

Fig. 2.2. $g_{3/2}(z)$ vs z. The solution of eq. (2.18) is illustrated.

$$n\Lambda^3(T)(1-\bar{N}_0/N) = g_{3/2}(z)\,. \tag{2.18}$$

The behavior of $g_{3/2}(z)$ is shown in fig. 2.2. From the drawing one sees that eq. (2.18) can be solved by setting $\bar{N}_0/N \sim 1/N$ (as would be given by eq. (2.5)) as long as

$$n\Lambda^3(T) < g_{3/2}(1)\,. \tag{2.19}$$

When this condition holds, $z < 1$ and $\mu < 0$. At $z = 1$, however, $g_{3/2}(z)$ attains its maximum value, 2.612. For values of $n\Lambda^3(T) > 2.612$, z remains "pinned" at 1 and $\bar{N}_0/N$ becomes finite:

$$\begin{aligned}\bar{N}_0/N &= 1 - 2.612/n\Lambda^3(T) \\ &= 1 - [T/T_0(n)]^{3/2}\,.\end{aligned} \tag{2.20}$$

This result was found in section 1.2 by a more physical argument.

Bose–Einstein condensation occurs when $z \to 1$ or equivalently, when $n \to n_0$:

$$n_0 = \frac{\zeta(3/2)}{\Lambda^3} = 2.612\left(\frac{MkT}{2\pi\hbar^2}\right)^{3/2}\,. \tag{2.21}$$

Table 2.1
Density and mean atomic separation for hydrogen at the Bose–Einstein transition

T_0 (K)	n_0 (cm^{-3})	l (Å)
1	4.95×10^{20}	13
0.3	8.13×10^{19}	23
0.1	1.57×10^{19}	40
0.03	2.59×10^{18}	73
0.01	4.98×10^{17}	126

Values of n_0 for atomic hydrogen are shown in table 2.1.

Below the transition temperature the second term on the right in eq. (2.16) is negligible and the thermodynamic equation of state is given by

$$P/kT = \frac{1}{\Lambda(T)^3}\,\zeta(5/2)\,. \tag{2.22}$$

The pressure is independent of the density at constant temperature. Above the transition temperature the $1/V$ terms in eqs. (2.16) and (2.17) are negligible. The equation of state can be found numerically by eliminating z between the two expressions

$$P/kT = \frac{1}{\Lambda(T)^3}\,g_{5/2}(z)\,, \tag{2.23}$$

$$n = \frac{1}{\Lambda(T)}\,g_{3/2}(z)\,. \tag{2.24}$$

At high temperatures (low z) one can use the leading terms in the power series expansion of $g_n(z)$ to find the leading quantum correction to the ideal gas law for spinless bosons:

$$P \sim \frac{NkT}{V}\,[1 - 2^{-5/2}n\Lambda^3(T)]\,. \tag{2.25}$$

The plot of the equation of state, fig. 2.3, shows that in the condensed state the pressure is independent of the density at constant temperature. This can be explained on kinetic grounds: pressure depends on the thermal distribution of velocities and on the density n of particles. At high temperature the velocity distribution is independent of n so that at constant temperature the pressure is propor-

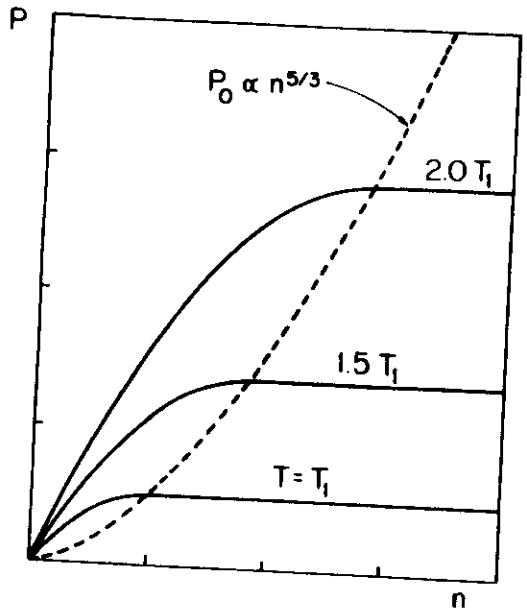

Fig. 2.3. Equation of state of the ideal Bose gas for three temperatures. In the condensed state the pressure is independent of density.

tional to n. Below T_0, $\mu = 0$ and the velocity distribution is again independent of n. However, the density of particles having that distribution is a constant, $n_{\text{mobile}} = 2.612[\Lambda(T)]^{-3}$. As the total density is increased at constant T, only the density in the zero-momentum state increases. These atoms make no contribution to the pressure.

Figure 2.3 shows that the isothermal compressibility $\kappa_T \equiv -(1/V)(\partial V/\partial P)_{N,T}$ is infinite below the transition. As a result, the fluctuations in that region are anomalous, for according to the theory of thermodynamic fluctuations (Landau and Lifshitz, Chapter XII) the mean square density fluctuation is proportional to κ_T:

$$\overline{(\Delta N)^2}/N^2 = \frac{kT}{V}\kappa_T. \tag{2.26}$$

The divergence of the fluctuations is actually a consequence of the macroscopic occupation of a single-particle state, as the following argument demonstrates: The variance of the occupation number of any

single-particle state can be found from eq. (2.6),

$$\overline{(\Delta N_p)^2} = \bar{N}_p(\bar{N}_p + 1). \tag{2.27}$$

For all states, except possibly the ground state, this is a number of order 1. In the grand canonical ensemble for non-interacting particles, the single-particle states are statistically independent. Thus, the variance in the total number of particles is the sum of the variances for the single-particle states:

$$\overline{(\Delta N)^2} = \bar{N}_0(\bar{N}_0 + 1) + \sum_{p \neq 0} \bar{N}_p(\bar{N}_p + 1). \tag{2.28}$$

The second term on the right is of order N. Below the transition, however, the first term is of order N^2 so that $\overline{(\Delta N)^2}/N^2$ is of order 1 and the fluctuations are anomalous.

An experimental consequence of the anomalous fluctuations is that the non-interacting Bose gas exhibits critical opalescence below its transition. A theoretical consequence is that one must worry about the validity of thermodynamically derived quantities below T_0, for thermodynamics is based on the assumption that fluctuations in the variables are negligible compared to the means. As we shall see in the next section, this problem is avoided if there is the slightest interaction between the particles.

3. The weakly interacting Bose gas

References: K. Huang, *Studies in Statistical Mechanics II* (J. DeBoer and G.E. Uhlenbeck editors, North-Holland, 1964); E.M. Lifshitz and L.P. Pitaevskii, *Statistical Physics*, Part 2 (Pergamon, 1980).

Although the theory of the imperfect Bose gas was originally motivated by the problem of superfluid helium, liquid helium bears such little resemblance to a gas that this application of the theory has not been particularly successful. The theory of the imperfect Bose gas is a perturbation theory, however, and for $H \downarrow$ it should be excellent. This is fortunate considering the many unphysical properties of the ideal Bose gas. (Some of these were mentioned in the previous chapter.) The existence of even a tiny interaction between the particles can drastically change the properties of a Base gas.

3.1. The simplifying approximations

The interaction between two particles is normally described by a potential $V(r_1 - r_2)$, but it can alternatively be described by the wave-vector dependent partial-wave phase shifts, $\delta_l(k)$. These phase shifts determine the form of the scattering cross section. At sufficiently low energies only S-wave scattering need be considered. (An exception occurs when S-wave scattering is forbidden by the particle statistics, as in the case of polarized spin 1/2 fermions [24]). The S-wave scattering length, a, is defined by

$$\lim_{k\to 0} k \cot \delta_0(k) = -1/a . \tag{3.1}$$

The total scattering cross section at low energy is

$$\lim_{k\to 0} \sigma_{\text{total}} = 4\pi a^2 . \tag{3.2}$$

Equation (3.2) also describes the quantum result for hard spheres of diameter a. Therefore, in the weakly interacting gas as long as $a > 0$, a may be thought of as an effective hard core diameter. We shall assume that the scattering is predominantly S-wave. This is valid if the temperature is sufficiently low that

$$a/\Lambda(T) \ll 1 . \tag{3.3}$$

In addition, we shall also assume that the density is small enough for three-body collisions to be neglected. This is true if

$$an^{1/3} \ll 1 . \tag{3.4}$$

When both the temperature restriction, eq. (3.3), and the density restriction eq. (3.4) are satisfied, the many-body behavior of the system depends solely on a single parameter, the S-wave scattering length a. The particular features of the potential are unimportant; a gas of Lennard–Jones particles and a gas of hard spheres will behave identically provided that their scattering lengths are equal.

The S-wave scattering length for spin-polarized hydrogen has been calculated by Friend and Etters [25] using the potential of Kolos and Wolniewicz [5]. They found

$$a = 0.72 \text{ Å} . \tag{3.5}$$

Because the form of the interatomic potential is unimportant at low temperature and low density, we are free to choose any form which is computationally convenient. A point contact, or delta function, potential is most often used,

$$V(r_1 - r_2) = V_0 \delta(r_1 - r_2) , \tag{3.6}$$

where V_0 is related to a by

$$V_0 = \frac{4\pi\hbar^2}{M} a . \tag{3.7}$$

3.2. Self-consistent field approximation

The simplest calculations of the equation of state for the weakly interacting Bose gas are based on the self-consistent field approximation. An immediate result is that at zero temperature the mean energy per particle, $E(0)/N$, increases linearly with the number density. For the model potential of eq. (3.6),

$$E(0)/N = \tfrac{1}{2} V_0 n . \tag{3.8}$$

Because the mean energy increases linearly with the density, many unphysical features of the non-interacting gas are eliminated. For example, the pressure at $T = 0$ no longer vanishes; it is proportional to the density squared,

$$P(T=0) = -\left.\frac{\partial E}{\partial V}\right|_N = \tfrac{1}{2} V_0 n^2 . \tag{3.9}$$

Consequently, the isothermal compressibility remains finite, the density fluctuations do not diverge and the system can be described by thermodynamic equilibrium states.

The increase in interaction energy with density eliminates another non-physical phenomenon: spatial collapse of the system into a single-particle ground state. At $T = 0$ the density of a non-interacting gas confined by walls at $x = 0$ and $x = L$ is proportional to $\sin^2 \pi x/L$; the atoms tend to bunch in the center of the container. In a 1 cm^3 volume

the zero-point energy of each particle is less than 10^{-14} K. The density in such a system would be supersensitive to applied potentials. A small harmonic potential would force the density into a narrow Gaussian distribution; a gravitational field could flatten the gas against the bottom of the container.

Ginzburg and Pitaevskii [26] and Gross [27] have considered the spatial behavior of the superfluid condensate wavefunction in a weakly interacting Bose gas using the self-consistent field approximation. They find that in a box with rigid walls the condensate density $\bar{N}_0/V$ is *constant* everywhere except near a wall where it goes to zero as $\tanh^2(x/\eta)$. The healing length η is

$$\eta = \hbar/(2MV_0 n)^{1/2}. \tag{3.10}$$

Substitution of eq. (3.7) into eq. (3.10) gives $\eta = (8\pi an)^{-1/2}$ Physically, the healing length is the distance in which the zero-point energy becomes comparable to the interaction energy. For H ↓ at a density of 10^{18}, the healing length is 235 Å.

The self-consistent field equations for the condensate density $\bar{N}_0(r)/V$ can be solved for an inhomogeneous external potential $U(r)$. Assuming that $U(r)$ does not vary significantly over distances as small as η, the condensate density is given by

$$\bar{N}_0(r)/V \quad \frac{1}{V_0}(E \quad U(r)), \quad E \cdot U(r), \qquad \cdot$$

$$\cdot 0 \qquad\qquad E \prec U(r), \tag{3.11}$$

where E is a normalization constant with the dimensions of energy. Consider a gas of H ↓ trapped by the magnetic field near the center of a superconducting solenoid. Along the axis the field decreases parabolically from its maximum value and the potential energy increases parabolically. Equation (3.11) predicts a parabolic decrease of $\bar{N}_0(r)/V$ along the axis. The width of this distribution is much larger than that associated with a non-interacting gas, but it is narrower than the thermal distribution of "non-condensate" atoms. Walraven and Silvera [28] have suggested that the change in the total density profile at T_0 might be used to detect the transition.

3.3. The Bogoliubov theory

In a classic paper Bogoliubov [29] in 1947 presented a theory of a weakly interacting Bose gas at temperatures far below the transition temperature. He found that if a measurement were made of the momenta of the individual atoms when the system is in its ground state ($T = 0$), a finite number

$$\bar{N}_0 = N[1 - \tfrac{8}{3}(a^3 n/\pi)^{1/2}] \tag{3.12}$$

would be found to have zero momentum. One says that $\bar{N}_0$ atoms are in the "condensate". The remainder of the atoms, $N - \bar{N}_0$, have finite momenta. The probability density for the momenta of the non-condensate atoms has a maximum near the characteristic momentum $p_0 = \sqrt{2}\hbar/\eta$ (see fig. 3.1), though it is important to realize that because of the interactions the momenta of individual atoms are not constants of motion. Another result is that the finite condensate fraction no longer causes a divergence of the fluctuations, since the motion of the individual atoms is now correlated.

Low-lying excited states of a weakly interacting Bose gas can be described in terms of a collection of elementary excitations, each indexed by its momentum p and having an energy $\varepsilon(p)$. The excitations behave as an ideal Bose gas of "quasi-particles". The mean number in a given momentum state is represented by a function of the

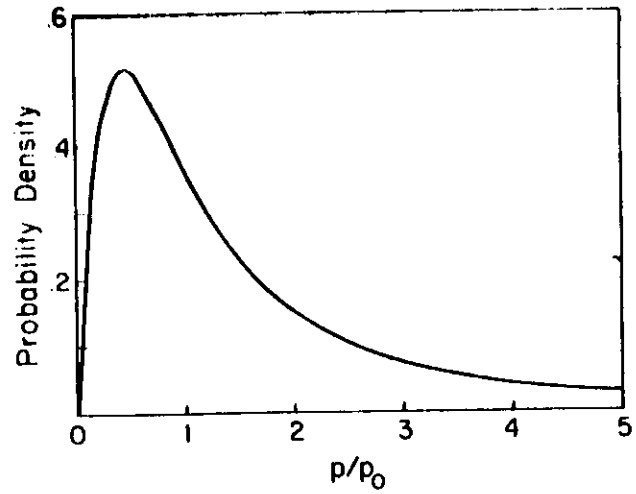

Fig. 3.1. Probability density for the magnitude of the momenta of non-condensate atoms in a Bose-condensed system of weakly interacting particles according to the Bogoliubov theory. $p_0 = (4MV_0 n)^{1/2}$ is a characteristic momentum.

form of eq. (2.5) with $\mu = 0$. Because of the interactions, the quasi-particles cannot be identified with individual atoms. The dispersion curve $\varepsilon(p)$ is shown in fig. (3.2). When $p \ll p_0$, $\varepsilon(p)$ is of the phonon form, $\varepsilon = up$, where the sound velocity u is given by

$$u = \frac{p_0}{2M} = \frac{\hbar}{M}(4\pi an)^{1/2}. \tag{3.13}$$

When $p \gg p_0$, $\varepsilon(p)$ becomes free-particle-like, $\varepsilon \sim p^2/2M$.

Describing a many-body system in terms of elementary excitations is a powerful and widely used technique. The weakly interacting Bose gas is one of the rare systems for which the properties of these excitations can be calculated directly.

The number of elementary excitations in a weakly interacting Bose gas is zero at $T = 0$ and increases as T increases. A corresponding change takes place in the momentum distribution of the individual

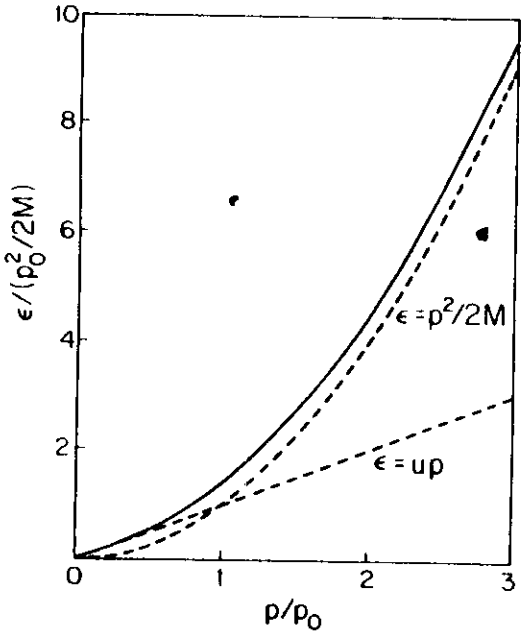

Fig. 3.2. Dispersion curve for elementary excitations in a weakly interacting Bose gas when $V(r) = V_0\delta(r)$. At low energies it represents phonons of velocity $u = (nV_0M)^{1/2}$; at high energies it is larger than the free particle result by an amount nV_0.

atoms as the temperature is raised. The number of atoms with zero momentum decreases from the $T = 0$ value given in eq. (3.12),

$$\frac{\bar{N}_0(T) - \bar{N}_0(0)}{\bar{N}_0(0)} = -\frac{Mk^2T^2}{12nuh^3}, \tag{3.14}$$

and the momentum distribution of the remaining atoms changes from that pictured in fig. 3.1. The Bogoliubov theory applies only when the fraction of atoms *not* in the condensate, $(N - \bar{N}_0)/N$, is much less than one. For temperatures near T_0 the condensate fraction approaches zero and a more extensive theory is required.

3.4. Superfluidity

Landau [30] has shown that a fluid will exhibit superfluidity if the dispersion curve for every set of elementary excitations in the system is such that $\varepsilon(p)/p > v_c$ for all momenta p. v_c is a critical flow velocity below which the fluid cannot lose energy to the walls of the confining channel. From fig. 3.2 one sees that $v_c = u$; therefore the weakly interacting Bose gas is a superfluid near absolute zero. The non-interacting Bose gas is not a superfluid because its elementary excitations are single particles, and $\varepsilon(p) = p^2/2M$ for which $v_c = 0$. These arguments only apply near $T = 0$. Whether the superfluid–normal fluid transition occurs at the Bose–Einstein transition T_0, or some lower temperature, appears to be an open question [10].

3.5. Hard sphere Bose gas

In 1957 Lee et al. [31] published the results of an extensive theoretical study of a Bose gas of hard spheres of diameter a. (Recall that a is also the S-wave scattering length for scattering of these hard spheres.) The reference by Huang listed at the beginning of this section presents a thorough review of that work. We summarize here some results which are relevant to spin-polarized hydrogen:

– The pair distribution function which describes the relative probability of finding two particles a distance r apart exhibits a "correlation length" r_0 given by

$$r_0 = (8\pi an)^{-1/2}. \tag{3.15}$$

This is identical to the expression for the healing length which came from the self-consistent field approximation. It also sets the scale for the characteristic momenta of elementary excitations in the Bogoliubov theory.

– The dispersion curve for elementary excitations $\epsilon(p)$ depends on the temperature T. It reduces to the Bogoliubov form when $T \ll T_0$.

– The temperature T_0 and the mean volume per particle $1/n_0$ at the Bose–Einstein transition exceed their values in the non-interacting gas, but only by corrections which are of order $(a^3 n)^{1/2}$.

– The calculations for the hard sphere Bose gas apply for a wide range of values of the dimensionless parameter $na\Lambda^2(T)$. When this parameter is much less than unity, however, the thermodynamic functions assume simple analytic forms. This condition can be written

$$kT \gg \frac{2\pi\hbar^2 a}{M} n = \tfrac{1}{2} V_0 n = E(0)/N . \tag{3.16}$$

In words, the thermal energy is large compared to the mean interaction energy. By using eq. (1.13) for T_0, it can be shown that this is equivalent to

$$T/T_0 \gg (2.612)^{2/3} a n^{1/3} \sim 2(a/l) , \tag{3.17}$$

where l is the mean spacing between the particles. For example, in a H↓ gas of density $10^{18}\,\mathrm{cm}^{-3}$ the expressions given below for the thermodynamic quantities are valid for reduced temperatures T/T_0 as small as 0.1. (The general limits imposed on the temperature, eq. (3.3), and the density, eq. (3.4), must also be satisfied.)

– The temperature dependence of the condensate fraction is difficult to calculate in general. It can, however, be expressed analytically in two limits. Near $T = 0$, where $(N - \tilde{N}_0)/N \ll 1$, the condensate fraction is given by eq. (3.12) and (3.14). Near the transition, where the inequality (3.17) holds, the ideal gas result applies:

$$\tilde{N}_0(T)/N = 1 - (T/T_0)^{3/2} . \tag{3.18}$$

In mean field theories of second-order phase transitions the order parameter goes to zero as $[(T_c - T)/T_c]^{1/2}$. Since $\tilde{N}_0(T)$ is the squared magnitude of the order parameter in this system, the behavior given by eq. (3.18) and sketched in fig. 1.2(b) is consistent with mean field behavior.

The thermodynamic functions are given in table 3.1 in terms of the density n and the temperature T. The equations have been simplified by using the temperature-dependent density at the transition

$$n_0(T) = \zeta(3/2)\frac{1}{\Lambda^3(T)} = 2.612\left(\frac{MkT}{2\pi\hbar^2}\right)^{3/2} . \tag{3.19}$$

When $T > T_0$, the value of z is determined from the relation

$$g_{3/2}(z) = \zeta(3/2) n/n_0(T) . \tag{3.20}$$

These thermodynamic functions possess a simple scaling behavior when they are suitably normalized, usually to their values at $T = T_0$ and $V_0 = 0$. At constant density the scaled functions depend only on the reduced temperature $t \equiv T/T_0$, and at constant temperature they depend only on the reduced density n/n_0. The natural unit for the interaction strength is

$$a' \equiv \frac{n_0 V_0}{kT_0} = 2\zeta(3/2)\frac{a}{\Lambda(T_0)} . \tag{3.21}$$

The scaled functions are simplified by introducing the following

Table 3.1
Thermodynamic functions for the weakly interacting Bose Gas

Pressure	
$P(n,T) = \frac{\zeta(5/2)}{\zeta(3/2)} kT n_0(T) + \frac{V_0}{2}[n_0^2(T) + n^2]$	$T < T_0$
$= \frac{g_{5/2}(z)}{\zeta(3/2)} kT n_0(T) + V_0 n^2$	$T > T_0$
Entropy	
$S(n,T)/Nk = \frac{5}{2}\frac{\zeta(5/2)}{\zeta(3/2)}\frac{n_0(T)}{n} - \frac{3}{2}\frac{n_0(T)V_0}{kT}\left[1 - \frac{n_0(T)}{n}\right]$	$T < T_0$
$= \frac{5}{2}\frac{g_{5/2}(z)}{\zeta(3/2)}\frac{n_0(T)}{n} - \ln z$	$T > T_0$

Table 3.1 *Continued*

Internal energy

$$U(n,T)/Nk = \frac{3}{2}\frac{\zeta(5/2)}{\zeta(3/2)}T\frac{n_0(T)}{n} + \frac{nV_0}{2k}\left[1 - \frac{n_0(T)}{n} + 2\left(\frac{n_0(T)}{n}\right)^2\right] \qquad T < T_0$$

$$= \frac{3}{2}\frac{g_{5/2}(z)}{\zeta(3/2)}T\frac{n_0(T)}{n} + \frac{nV_0}{k} \qquad T > T_0$$

Specific heat at constant volume

$$C_V(n,T)/Nk = \frac{15}{4}\frac{\zeta(5/2)}{\zeta(3/2)}\frac{n_0(T)}{n} - \frac{3}{4}\frac{n_0(T)V_0}{kT}\left[1 - 4\frac{n_0(T)}{n}\right] \qquad T < T_0$$

$$= \frac{15}{4}\frac{g_{5/2}(z)}{\zeta(3/2)}\frac{n_0(T)}{n} - \frac{9}{4}\frac{g_{3/2}(z)}{g_{1/2}(z)} \qquad T > T_0$$

Specific heat difference

$$(C_P(n,T) - C_V(n,T))/Nk = \frac{kT}{nV_0}\left[\frac{5}{2}\frac{\zeta(5/2)}{\zeta(3/2)}\frac{n_0(T)}{n} + \frac{3}{2}\frac{n_0^2(T)V_0}{nkT}\right]^2 \qquad T < T_0$$

$$= \left[\frac{g_{3/2}(z)}{g_{1/2}(z)} + \frac{2nV_0}{kT}\right]^{-1} \times \left[\frac{5}{2}\frac{g_{5/2}(z)}{\zeta(3/2)}\frac{n_0(T)}{n} - \frac{3}{2}\frac{g_{3/2}(z)}{g_{1/2}(z)}\right]^2 \qquad T > T_0$$

Isothermal compressibility: $\kappa_T \equiv -\frac{1}{V}\frac{\partial V}{\partial P}\Big|_{N,T}$

$$\kappa_T^{-1}(n,T) = V_0 n^2 \qquad T < T_0$$

$$= 2V_0 n^2 + \frac{g_{3/2}(z)}{g_{1/2}(z)}nkT \qquad T > T_0$$

Adiabatic compressibility: $\kappa_S \equiv -\frac{1}{V}\frac{\partial V}{\partial P}\Big|_{N,S}$

$$\kappa_S^{-1}(n,T) = V_0 n^2 + \tfrac{5}{3}nkT\left[\frac{\zeta(5/2)}{\zeta(3/2)}\frac{n_0(T)}{n} + \frac{3}{5}\frac{n_0^2(T)V_0}{nkT}\right]^2 \qquad T < T_0$$

$$\times\left[\frac{\zeta(5/2)}{\zeta(3/2)}\frac{n_0(T)}{n} - \frac{1}{5}\frac{n_0(T)V_0}{kT}\left(1 - 4\frac{n_0(T)}{n}\right)\right]^{-1}$$

$$= 2V_0 n^2 + \frac{5}{3}\frac{g_{5/2}(z)}{\zeta(3/2)}n_0(T)kT \qquad T > T_0$$

Expansion coefficient: $\alpha \equiv \frac{1}{V}\frac{\partial V}{\partial T}\Big|_{N,P}$

$$\alpha(n,T) = \frac{5}{2}\frac{\zeta(5/2)}{\zeta(3/2)}\frac{kn_0(T)}{n^2V_0} + \frac{3}{2}\frac{1}{T}\left(\frac{n_0(T)}{n}\right)^2 \qquad T < T_0$$

$$= \frac{5}{2}\frac{1}{T}\left[\frac{g_{5/2}(z)}{\zeta(3/2)}\frac{n_0(T)}{n} - \frac{3}{5}\frac{g_{3/2}(z)}{g_{1/2}(z)}\right]\left[\frac{g_{3/2}(z)}{g_{1/2}(z)} + \frac{2nV_0}{kT}\right]^{-1} \qquad T > T_0$$

parameters:

$$c \equiv \zeta(3/2)/\zeta(5/2) = 1.95\ldots,$$
$$b(z) \equiv g_{5/2}(z)/\zeta(5/2), \qquad b(1) = 1, \tag{3.22}$$
$$f(z) \equiv g_{3/2}(z)/g_{1/2}(z), \qquad f(1) = 0.$$

In terms of the pressure P_0 of the non-interacting gas at the transition

$$P_0 = \zeta(5/2)(M/2\pi\hbar^2)^{3/2}(kT)^{5/2} \tag{3.23}$$

the scaled equation of state for an isotherm (pressure as a function of density at constant temperature) is

$$\frac{P}{P_0} = 1 + \tfrac{1}{2}ca'[1 + (n/n_0)^2] \qquad n/n_0 > 1,$$
$$= b(z) + ca'(n/n_0)^2, \qquad n/n_0 < 1. \tag{3.24}$$

Figure 3.3 shows the behavior of this scaled equation of state. It demonstrates a unique feature of the weakly interacting Bose gas: the

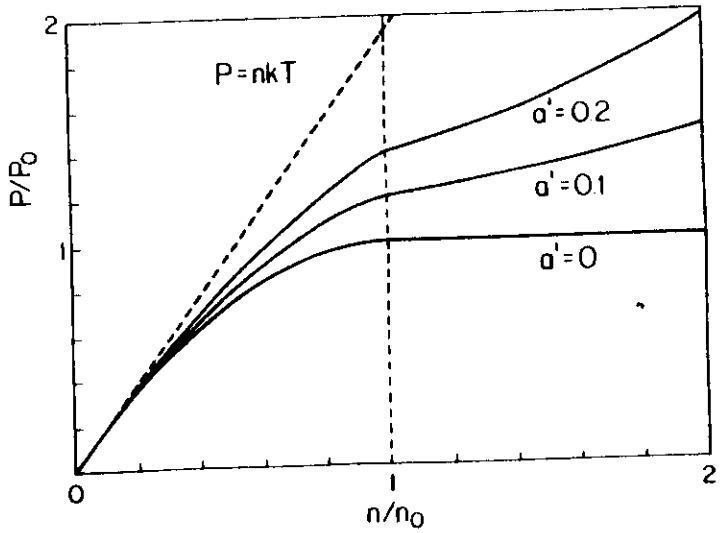

Fig. 3.3. Equation of state for a weakly interacting Bose gas. a' is the reduced scattering length, eq. (3.19). $a' = 0$ describes the ideal Bose gas. For H↓ at 0.3 K, $a' \approx 0.1$.

Table 3.2
Scaled thermodynamic functions at constant density

Pressure: $P_0(n) = \frac{2\pi\zeta(5/2)\hbar^2}{M}\left[\frac{n}{\zeta(3/2)}\right]^{5/3}$

$$P/P_0 = t^{5/2} + \tfrac{1}{2}ca'(1 + t^3) \qquad t < 1$$
$$= b(z)t^{5/2} + ca' \qquad t > 1$$

Entropy: $S_0(n) = \frac{5}{2}Nk/c$

$$S/S_0 = t^{3/2} - \tfrac{1}{2}ca't^{3/2}(1 - t^{3/2}) \qquad t < 1$$
$$= b(z)t^{3/2} - \tfrac{3}{2}c \ln z \qquad t > 1$$

Internal energy: $U_0(n) = \frac{3\pi N\hbar^2}{M}\left[\frac{n}{\zeta(3/2)}\right]^{2/3}$

$$U/U_0 = t^{5/2} + \tfrac{1}{3}ca'(1 - t^{3/2} + 2t^3) \qquad t < 1$$
$$= b(z)t^{5/2} + \tfrac{1}{3}ca' \qquad t > 1$$

Specific heat

$$C_V/\tfrac{3}{2}Nk = \tfrac{5}{4}c^{-1}t^{3/2} - \tfrac{1}{4}a't^{1/2}(1 - 4t^{3/2}) \qquad t < 1$$
$$= \tfrac{5}{4}c^{-1}b(z)t^{3/2} - \tfrac{1}{4}f(z) \qquad t > 1$$

Specific heat difference

$$\left(\frac{C_P - C_V}{Nk}\right)^{-1} = a't^{-1}(\tfrac{5}{4}c^{-1}t^{3/2} + \tfrac{3}{4}a't^2)^{-2} \qquad t < 1$$
$$= [2a't^{-1} + f(z)][\tfrac{5}{4}c^{-1}b(z)t^{3/2} - \tfrac{1}{4}f(z)]^{-2} \qquad t > 1$$

Isothermal compressibility

$$\kappa_T^{-1}/nkT_0 = a' \qquad t < 1$$
$$= 2a' + f(z)t \qquad t > 1$$

Adiabatic compressibility

$$\kappa_S^{-1}/\tfrac{5}{3}nkT_0 = \tfrac{3}{5}a' + t[c^{-1}t^{3/2} + \tfrac{3}{5}a't^2][c^{-1}t^{3/2} - \tfrac{1}{5}a't^{1/2}(1 - 4t^{3/2})]^{-1} \qquad t < 1$$
$$= \tfrac{6}{5}a' + c^{-1}b(z)t^{5/2} \qquad t > 1$$

Expansion coefficient

$$\alpha^{-1}/T_0 = a'[\tfrac{5}{2}c^{-1}t^{3/2} + \tfrac{3}{2}a't^2]^{-1}$$
$$= [2a' + f(z)t]\left[\frac{5}{2c}b(z)t^{3/2} - \tfrac{1}{2}f(z)\right]^{-1}$$

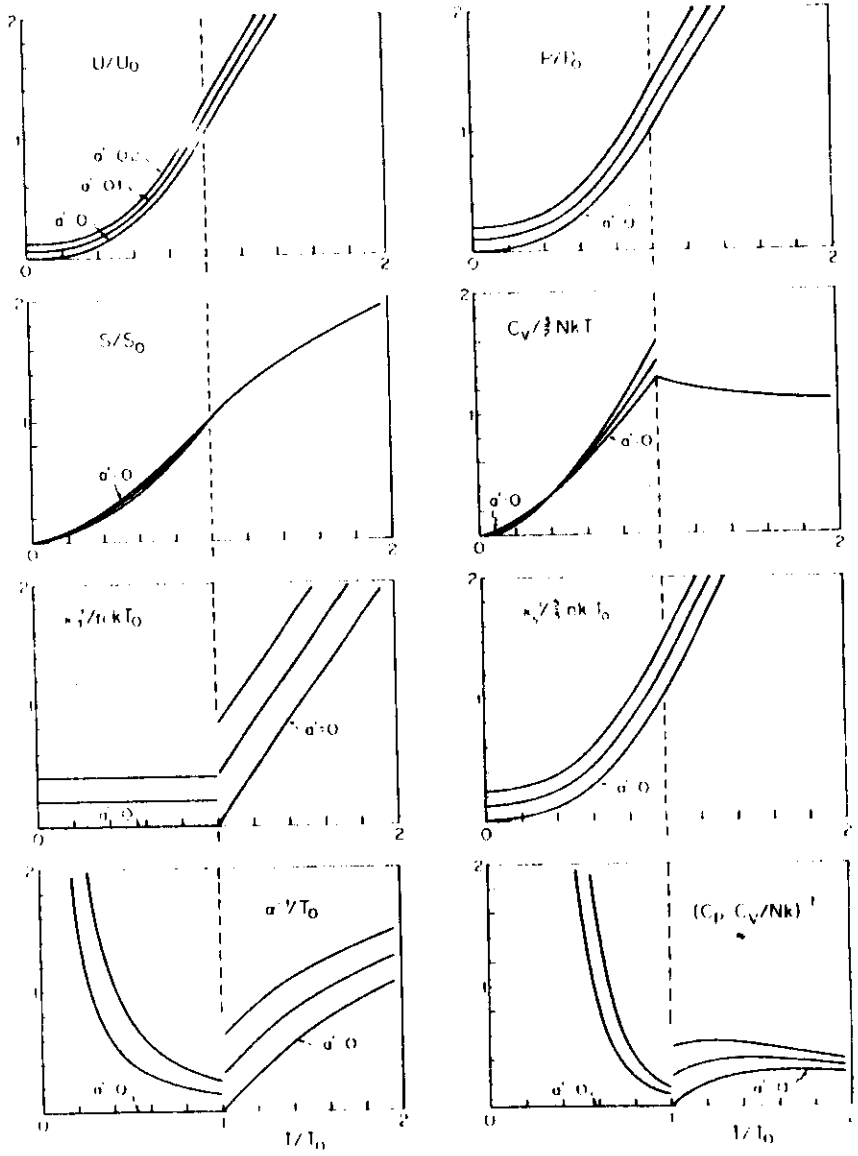

Fig. 3.4. Thermodynamic functions for a weakly interacting Bose gas at constant density.

slope of an isotherm changes by a factor of 2 at the transition, corresponding to a discontinuous increase by a factor of 2 in the isothermal compressibility as the system enters the ordered phase. This effect could serve as an experimental signature of the Bose–Einstein transition in H↓.

The dependence of the scaled thermodynamic functions on temperature at constant density are presented in table 3.2 and illustrated in fig. 3.4. Because of the interactions, the pressure and internal energy are non-vanishing at $T = 0$. The entropy and specific heat at constant volume are independent of the interaction strength V_0 when $T > T_0$. The specific heats, the expansion coefficient, and the isothermal compressibility are all discontinuous at the transition, providing possibilities for detecting the transition as well as for measuring the strength of the interaction. For example, the discontinuity in the constant volume specific heat is directly proportional to a:

$$C_V(t = 1-) - C_V(t = 1+) = \tfrac{9}{2}\zeta(3/2)Nka/\Lambda(T_0)\,. \tag{3.25}$$

The adiabatic compressibility, however, shows no anomolous behavior at T_0, precluding the use of the velocity of sound as a signature of the transition. Finally, note that for the ideal Bose gas $(C_P - C_V)^{-1}$ is zero for $T < T_0$. This reflects the unphysical result that for the non-interacting gas C_P is infinite below T_0.

It must be borne in mind that the results presented in tables 3.1 and 3.2 and displayed in fig. 3.4 are subject to the inequality (3.17): they are not valid near $T = 0$. Consider, for example, the specific heat. For the interacting gas in the limit of small momentum or energy the elementary excitations are phonons; therefore as $T \to 0$ the specific heat should be proportional to T^3. In the analytic forms of tables 3.1 and 3.2, however, as $T \to 0$ the specific heat is proportional to $T^{3/2}$, as is the case in an *ideal* Bose gas. This is consistent with eq. (3.16) (which implies that the mean thermal energy of an atom must be large compared to its interaction energy) and with the fact that the dispersion curve for the elementary excitations, fig. 3.2, approaches the free atom result at high energies.

3.6. *Critical behavior near T_0*

The Bose–Einstein transition is one member of a large class of phase transitions which are the subject of modern theories of critical

phenomena. From the point of view of these theories all second-order phase transitions can be grouped into what are called *universality classes* [32]. Members of the same class exhibit similar behavior at the transition, notwithstanding that their non-critical characteristics may vary widely. A universality class is defined by the spatial dimensionality, d, of the system and the number of components, n, in the order parameter. For the free gas of H↓, $d = 3$. (For a phase transition in the film of H↓ adsorbed on a He coated surface, $d = 2$.) The order parameter for the Bose–Einstein transition is a complex scalar [33] so that $n = 2$, corresponding either to its real and imaginary parts or to its amplitude and phase. Other systems in the same universality class include superconductivity, superfluidity in ^{4}He, and magnetism in a three-dimensional planar ferromagnet.

In principle, to predict the behavior at the Bose–Einstein transition in H↓ one need only examine the transition in a superconductor or the lambda transition in ^{4}He. For one of the most important experimental parameters, however, the specific heat at constant pressure, there appears to be a paradox. As fig. 3.5 shows, C_P behaves in qualitatively different manners in the superconductor and in the superfluid. To explain this apparent violation of universality, one must consider the role of fluctuations near the transition.

A characteristic of second-order phase transitions is that the magnitude of the order parameter decreases with increasing temperature,

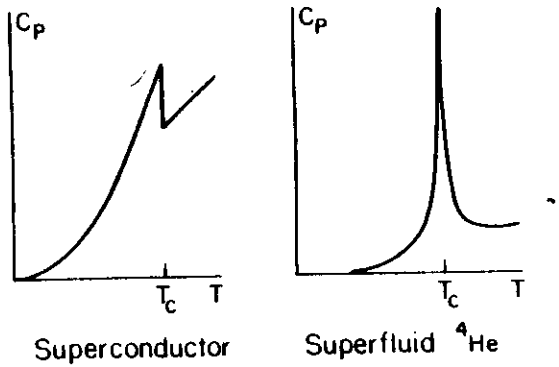

Fig. 3.5. Mean field behavior of C_P at a second-order phase transition (left). Critical behavior of C_P at a second-order phase transition (right). Which behavior is observed experimentally depends on the fractional width of the critical region. H↓ is expected to display mean field behavior.

going smoothly to zero at the transition temperature, T_c. In contrast, fluctuations in the order parameter grow as T_c is approached, and diverge at the transition. At temperatures well below T_c the fluctuations are small and the behavior of the system can be described in terms of the mean value of the order parameter. Theories which neglect the fluctuations are called *mean field* theories. These include the BCS and the Ginzburg–Landau theories of superconductivity, and the various theories of the weakly interacting Bose gas.

If one approaches T_c so closely that fluctuations in the order parameter dominate the behavior of the system, the mean field theories no longer apply and one is said to be in the critical region. No theories describe behavior in this region directly, though one can resort to indirect means such as scaling laws and renormalization group calculations [32]. It is only in the critical region that systems approach their universal behavior.

Ginzburg [34] has obtained an approximate expression for the value of the reduced temperature difference $\varepsilon \equiv (T_c - T)/T_c$ at which one passes from mean field to true critical behavior.

$$\varepsilon \sim \frac{k^2}{32\pi^2 r_0^4 (\Delta C_P/V)^2}, \tag{3.26}$$

where ΔC_P is the jump in constant pressure specific heat at T_c based on a mean field model, and r_0 is a $T = 0$ non-critical correlation length.

For superconductors, ε is too small to permit exploration of the critical region by existing (μK) techniques. Thus, the plot of C_P for a superconductor in fig. 3.5 (left) displays mean field behavior. For ^{4}He, however, $\varepsilon \sim 10^{-1}$ and the plot of C_P for a superfluid in fig. 3.5 (right) displays true critical behavior.

The theory of the weakly interacting Bose gas is the mean field theory for H↓. By evaluating ε we can determine whether H↓ is likely to display mean field or critical behavior. The value of r_0 can be found from eq. (3.15) and ΔC_P can be obtained from table 3.1:

$$\Delta C_P \equiv C_P(t = 1-) - C_P(t = 1+) = \frac{25}{8}\frac{Nk}{c^2 a'}[1 + \tfrac{4}{3}ca']^2. \tag{3.27}$$

For our purposes the bracketed term can be taken to be unity. Using eqs. (3.15) and (3.27), the Ginzburg criterion (3.26) becomes

$$\varepsilon \sim \frac{1}{\pi}\left(\frac{8}{5}\right)^4 \frac{\zeta^7(3/2)}{\zeta^4(5/2)}\left(\frac{a}{\Lambda(T_0)}\right)^5 = 533\left(\frac{a}{\Lambda(T_0)}\right)^5. \tag{3.28}$$

As might be expected, the behavior is governed by the ratio of scattering length to De Broglie wavelength. However, the fact that ε depends on the fifth power of this ratio means that a system is likely to display decisively one form of behavior or the other.

Consider H↓ with $T_0 = 0.1$ K, which corresponds to a density of 1.57×10^{19} cm^{-3} and $\Lambda(T_0) = 55$ Å. Under these circumstances $\varepsilon \sim 2 \times 10^{-7}$. The cross-over from mean field to critical behavior occurs less than 10^{-7} K from T_0. Thus a mean field description, in particular the theory of the hard sphere Bose gas, should be adequate for experiments on H↓ in the foreseeable future (see Postscript).

3.7. *Extensions of the theory for H↓*

Interest in H↓ has motivated several extensions of the theory of a weakly interacting Bose gas. We summarize three of these.

Lantto and Nieminen [35] have carried out numerical calculations of the ground-state properties of a Bose gas using the accurate Kolos–Wolniewicz potential [5]. They considered densities as high as 4×10^{21} cm^{-3}, where $a^3 n = 0.11$. The calculations yielded the ground-state energy, the condensate fraction, the radial distribution function, the static structure factor, and the wave-vector dependent exchange energy. At low densities the results are in accord with those of the hard sphere Bose gas, but at higher densities substantial deviations are observed. These deviations would be interesting to study, but for reasons to be described later it seems unlikely that high enough densities of H↓ can be achieved for them to be important.

Siggia and Ruckenstein [36] examined the consequences of having two hyperfine states in the Bose gas. They found that atoms in the two states could constitute two separate gases, each with its own transition temperature. When both gases are in the condensed phase in a high magnetic field, a rotating transverse magnetization should spontaneously appear. The situation is complicated by the possibility of magnetic domains and phase separation. Unfortunately, a practical requirement for achieving densities high enough for the Bose transition is that the gas be prepared in a single hyperfine state, which makes it unlikely that this collection of magnetic phenomena can be observed.

Following the original suggestion by Walraven and Silvera [28], various groups [37–39] have considered the spatial dependence of the density in an inhomogeneous magnetic field. The motivation is that a change in $n(r)$ at the transition can signal the onset of condensation, and the precise shape of $n(r)$ for $T < T_0$ can provide quantitative information about the equation of state. A feature common to these calculations is that the gradient of $n(r)$ increases by a factor of approximately 2 where the condensate first appears in the cell. This can be explained physically as follows.

For a magnetic field B varying along the x-axis hydrostatic equilibrium requires that

$$\frac{dP}{dx} = n(x)\mu_e \frac{dB}{dx}, \tag{3.29}$$

where μ_e is the magnetic moment of the electron. In a system at uniform temperature

$$\left.\frac{\partial P}{\partial x}\right|_T = \left.\frac{\partial P}{\partial n}\right|_T \left.\frac{dn}{dx}\right|_T = \frac{1}{n\kappa_T}\left.\frac{dn}{dx}\right|_T. \tag{3.30}$$

Combining these two equations yields an expression for the density gradient in terms of the isothermal compressibility

$$\left.\frac{dn(x)}{dx}\right|_T = n^2\kappa_T\mu_e \frac{dB}{dx}. \tag{3.31}$$

This result is valid both above and below the transition. The factor of 2 increase in the gradient is a consequence of the doubling of the isothermal compressibility κ_T as one enters the condensed phase. Equation (3.31) can be integrated to obtain the density profile. Below the transition temperature where $\kappa_T = 1/V_0 n^2$ the result is

$$n(x) = \frac{\mu_e}{V_0} B(x) + \text{constant}. \tag{3.32}$$

(Recall that V_0 is defined in eq. (3.7). It has the dimension of energy times volume.) These simple arguments assume that $n(x)$ is approximately constant over distances of the order of the healing length. Under these circumstances eq. (3.31) reproduces many of the useful results of the more involved calculations.

4. Adsorbed H↓ : a two-dimensional Bose gas

The need to find suitable surfaces to help to confine gaseous H↓ constitutes a serious experimental problem, but it also provides scientific opportunities. In most experiments H↓ recombines predominantly on the surface; from this point of view the surface is an undoubted nuisance. On the other hand, the adsorbed layer of H↓ forms a weakly interacting Bose gas which is of considerable interest in its own right. The gas is predicted to undergo a two-dimensional phase transition, a Kosterlitz–Thouless transition [40]. This surface transition may occur before the Bose–Einstein transition takes place in the gas.

In addition to confining the atoms, the surface serves another experimental role: it is the site at which heat is extracted from the gas, allowing (one hopes) thermal equilibrium to be attained. At high densities the question of heat transport can assume major importance, but the mechanisms are not well understood at present and we will not discuss the problem here.

4.1. *The antiferromagnetic instability*

Adsorption of H↓ can cause high densities on the walls of the container. This is potentially worrisome for the following reason.

Berlinsky et al. [41] have pointed out that for sufficiently high density H↓ becomes unstable with respect to perturbations in the uniform parallel spin alignment, even in a high magnetic field. The effect is usually discussed in terms of an antiferromagnetic exchange interaction between neighboring atoms. For three-dimensional solid H↓ the instability is associated with the spontaneous creation of spin waves; the depolarized spins would cause rapid recombination. Such an instability is not limited to the solid: the gas [35] and the two-dimensional array of H↓ on a surface [42] are also unstable. Precise calculations are difficult because they depend sensitively on the radial distribution function. For example, recent calculations by Kagan and Shlyapnikov [43] find that the critical density is somewhat higher than that calculated by Berlinsky et al. [41]. However, the origin of the

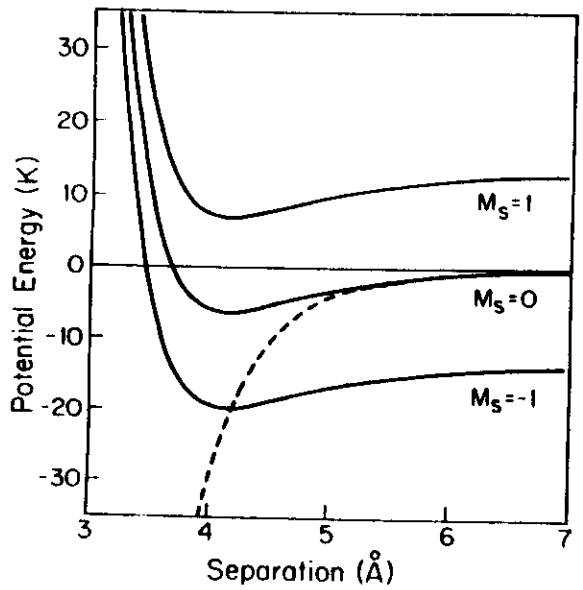

Fig. 4.1. Interatomic potentials for H in the triplet state in a field of 10 T. The dashed line indicates the singlet potential.

effect can be understood and an estimate of the critical densities can be obtained from simple energy considerations.

Figure 4.1 shows the potential for a pair of hydrogen atoms in a 10 T magnetic field. The $m_S = -1$ triplet state is stable only as long as the separation is greater than about 4 Å; for smaller separations the energy of covalent bonding in the singlet state exceeds the Zeeman energy due to spin polarization. We infer that a solid, a gas, or a two-dimensional layer of H↓ will be unstable when the mean spacing between the atoms is of the order of 4 Å. This corresponds to bulk densities of order $10^{22}\,\mathrm{cm}^{-3}$. Such densities lie beyond the goals of current research, however, so at least for the present this instability is unimportant in the bulk. The critical surface density is somewhat above $10^{14}\,\mathrm{cm}^{-2}$. This can be exceeded at low temperatures unless the adsorption of H↓ on the walls is extremely weak.

4.2. *Surface adsorption*

Hydrogen atoms are attracted to the walls of the container by Van der Waals forces. To minimize this interaction the surfaces should be a material of low density and low polarizability. One material which must be considered is molecular hydrogen, for at low temperature almost any other surface adsorbs hydrogen so strongly that it will recombine to form H_2, building up a blanketing layer.

In thermal equilibrium the surface density σ of a classical non-interacting two-dimensional gas is related to the volume density n by

$$\sigma = n\Lambda(T)\exp(+E_b/kT), \tag{4.1}$$

where E_b is the (positive) binding energy of an atom on the surface. This expression holds for real gases at low temperatures provided that the mean spacing between atoms on the surface and in the gas is much larger than the De Broglie wavelength $\Lambda(T)$.

The binding energy of H↓ on solid H_2 has been measured by Crampton et al. [44] to be about 34 K. Consider the adsorption of H↓ on H_2 when $n = 10^{14}\,\mathrm{cm}^{-3}$. At $T = 4$ K the surface density is reasonable: $\sigma = 4\times10^{10}\,\mathrm{cm}^{-2}$. At 1 K, however, the surface density would be unphysically large: $10^{22}\,\mathrm{cm}^{-2}$. Molecular hydrogen walls are useful (and perhaps unavoidable) for transport of atomic hydrogen at temperatures down to 4 K, but for transport and storage at lower temperatures some other wall coating is needed.

The only atoms with a lower Van der Waals attraction than H_2 are ^{3}He and ^{4}He. The Van der Waals attraction between H and *atomic* helium is identical for the two He isotopes. As a surface coating, each isotope has its own advantage. ^{4}He forms a superfluid below 2.17 K. The superfluid flows up the walls of any vessel containing it and forms a self-healing film of thickness $d \sim 300\,\text{Å}/h^{1/3}$, where h is the height in centimeters of the film above a liquid puddle. This constitutes an ideal arrangement for applying the surface coating. Liquid ^{3}He is not a superfluid, but because of its lower mass and larger zero-point motion, its density is about 25% less than that of liquid ^{4}He. As a result the binding energy of H↓ on liquid ^{3}He is significantly less than on liquid ^{4}He, which is an important advantage.

4.3. *Binding energies for hydrogen on helium*

The potential energy $V(z)$ for motion perpendicular to a helium surface is essentially independent of which isotope of hydrogen is being considered. The systematics of binding energies for hydrogen on

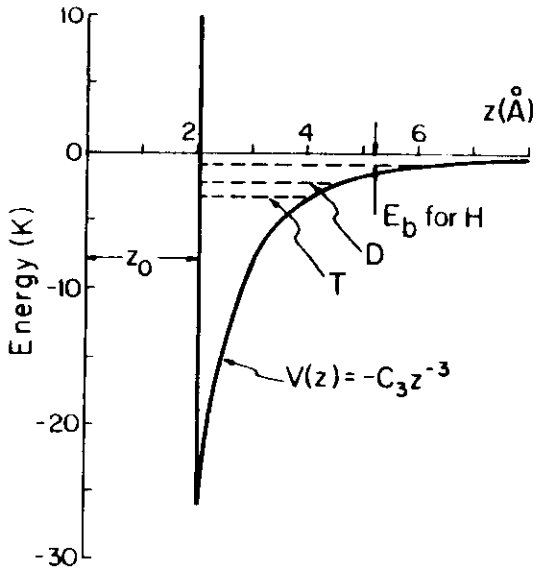

Fig. 4.2. Model potential for atom–surface interactions, according to Stwalley [45]. The surface is treated as a hard surface with a z^{-3} Van der Waals attraction. The values of z_0 and c_3 are those appropriate to a ^{4}He coated surface.

helium have been studied by Stwalley [45] using scaling arguments based on a simplified model for the surface potential. His model for $V(z)$ is shown in fig. 4.2. The z^{-3} behavior is appropriate to the Van der Waals attraction of a wall. The cut-off at z_0 replaces the complicated hard core repulsion at short distances. Table 4.1 presents the results for the binding energies based on this model. In some cases there is a second bound surface state, but the binding energies are so low that the occupation probability is negligible. Although the results in table 4.1 are intended primarily to demonstrate how the energy depends on the adsorbent and adsorbate masses, they are, in fact, remarkably close to the measured values.

Mantz and Edwards [46] have calculated the binding of the hydrogen isotopes on liquid ^{4}He taking into account various details of the free ^{4}He surface. The approximations involved are expected to give genuine lower limits to the binding energies. They find 0.62 K for H, 1.39 K for D, and 1.83 K for T. Another calculation based on different approximations by Guyer and Miller [47] gives 0.10 K for H, 1.1 K for D and 2.4 K for T.

Table 4.1
Binding energies from the Stwalley model

System	v	E_b (K)
H on ^{4}He	0	0.85
D on ^{4}He	0	2.2
	1	0.0013
T on ^{4}He	0	3.2
	1	0.028
H on ^{3}He	0	0.36
D on ^{3}He	0	1.2
	1	5.6×10^{-6}
T on ^{3}He	0	1.9
	1	0.0030

v is the bound state quantum number (from ref. [45]).

Experimental measurements of E_b are discussed in sections 6 and 7 and results to date are listed in table 4.2. Note that the ratios E_b (D on ^{4}He)/E_b (H on ^{4}He) and E_b (H on ^{3}He)/E_b (H on ^{4}He) are close to those suggested by Stwalley's analysis. It is puzzling, however, that the

Table 4.2
Measured adsorption energies

Adsorbent	Adsorbate	E_b(K)	Reference
H	^{4}He	1.15(5)	Morrow et al. [15]
		1.01(6)	Cline et al. [16]
		0.89(7)	Matthey et al. [48]
H	^{3}He	0.42(5)	Jochemsen et al. [49]
H	^{3}He–^{4}He	0.34(3)	Van Yperen et al. [50]
D	^{4}He	2.5(4)	Silvera and Walraven [51]

Table 4.3
Surface density of adsorbed atomic hydrogen

T (K)	^{4}He	^{3}He
0.3	8.9×10^{10}	1.2×10^{10}
0.2	5.8×10^{11}	2.9×10^{10}
0.1	1.2×10^{14}	3.0×10^{11}

Density (atoms cm^{-2}) calculated from the classical absorption isotherm, eq. (4.1). Bulk density $n = 10^{16}$ cm^{-3}; binding energy 1.0 K for ^{4}He, 0.4 K for ^{3}He.

measured adsorption energy for H on ^{3}He is larger than for H on a solution of ^{3}He and ^{4}He; physically one would expect the reverse.

Table 4.3 displays values of the surface density of H↓ from eq. (4.1), using binding energies of 1.0 K for ^{4}He and 0.4 K for ^{3}He. In the case of ^{4}He at 0.1 K the surface density is so high that interactions between the H↓ atoms must be considered and eq. (4.1) no longer applies. We next consider these interactions and their implications.

4.4. *Interactions between H↓ atoms on the surface*

The problem of a Bose gas confined in a vessel with interacting walls provides another example of how one can be misled by neglecting interactions between the atoms. For an ideal gas the chemical potential μ_A for the H↓ on the surface is given by eq. (1.14) with an additional term, $-|E_b|$, due to adsorption

$$\mu_A = -|E_b| + kT \ln[1 - \exp(-\sigma\Lambda^2(T))]\,. \tag{4.2}$$

The chemical potential for the H↓ in bulk, μ_V, can be obtained from eq. (2.18) and the definition $\mu = kT \ln(z)$. In equilibrium $\mu_A = \mu_V$; this relation determines the adsorption isotherm $\sigma(n, T)$. Note that μ_A is always less than $-|E_b|$, whereas Bose–Einstein condensation in the bulk requires $\mu_V = 0$. As a result, adsorption on the surface prevents the Bose–Einstein transition from occurring in the bulk. The atoms find it energetically preferable to adsorb on the walls rather than to build up the bulk densities needed for condensation.

This situation is unphysical because it assumes that the surface density can increase without limit. (It is also unphysical in that it assumes the atoms can interact with the surface but not with each other.) In reality the density of adsorbed atoms saturates at the point where the cost in interaction energy for adding one more atom to the surface exceeds the adsorption energy. Once the surface saturates, μ_V is free to rise to zero.

The first study of interactions between H↓ atoms on a surface was undertaken by Miller and Nosanow [52] who verified that the adsorbate would form a two-dimensional gas rather than a two-dimensional liquid. They showed that the energy per atom at $T = 0$, $E(0)/N$, is a monotonically increasing function of σ. (A liquid would have a minimum in $E(0)/N$ at a finite σ rather than at $\sigma = 0$.) Their calculations were based on the quantum theory of corresponding states

using a Lennard–Jones potential whose parameters were chosen to fit the Kolos–Wolniewicz potential (see sections 5.2, 5.3). The results for $E(0)/N$ are shown in fig. (4.3) along with the results of Lantto and Nieminen [42] who employed a different technique based directly on the K–W potential. In both cases $E(0)/N$ is linear in σ for small σ. The shape of $E(0)/N$ gives the surface interaction strength γ:

$$\lim_{\sigma \to 0} E(0)/N = \gamma\sigma\,. \tag{4.3}$$

Miller and Nosanow found $\gamma = 0.97 \times 10^{-14}$ Kcm^2 while Lantto and Nieminen obtained $\gamma = 0.65 \times 10^{14}$ Kcm^2. The chemical potential of the two-dimensional gas at $T = 0$ can be obtained from eq. (4.3).

$$\mu|_{T=0} = \left.\frac{\partial E(0)}{\partial N}\right|_A = \frac{\partial}{\partial N}\left(\frac{\gamma N^2}{A}\right) = 2\gamma\sigma\,. \tag{4.4}$$

To determine the adsorption isotherms for H↓ we need expressions for μ_V and μ_A, including the interactions. To obtain μ_V we use the thermodynamic identity

$$\mu = (E + PV - TS)/N\,, \tag{4.5}$$

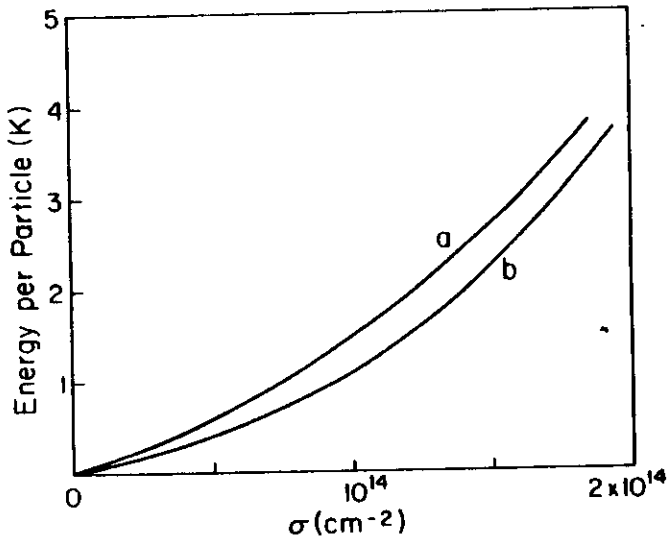

Fig. 4.3. Mean energy per particle vs surface density for H↓ in strictly two-dimensional motion. Curve (a), Miller and Nosanow [52]; curve (b), Lantto and Nieminen [42].

and the thermodynamic functions for a weakly interacting Bose gas from table 3.1. The result is

$$\mu_V = \mu_V^{(0)} + 2V_0 n\,, \qquad T > T_0\,,$$
$$= \mu_V^{(0)} + V_0(n + n_0(T))\,, \qquad T < T_0\,. \tag{4.6}$$

Here $\mu_V^{(0)}$ is the chemical potential of the non-interacting gas ($\mu_V^{(0)} = 0$ when $T < T_0$), V_0 is the effective scattering strength given by eq. (3.7), and $n_0(T)$ is the density at the transition given by eq. (2.21). Note that the result $\mu_V(T = 0) = V_0 n$ could be obtained directly from eq. (3.8) for $E(0)/N$:

$$\mu_V(T = 0) = \frac{\partial E(0)}{\partial N}\bigg|_V = \frac{\partial}{\partial N}\left(\frac{V_0 N^2}{2V}\right) = V_0 n\,. \tag{4.7}$$

Edwards and Mantz [53] have considered the interaction of two H↓ atoms adsorbed on the surface of ^{4}He. Their calculations differ from a strictly two-dimensional model in that the finite spread of the H↓ wavefunctions perpendicular to the surface is taken into account. (Two atoms can pass "over" as well as "around" each other.) They define an effective surface interaction strength $V_0^{(S)}$ and find it to be proportional to the V_0 used for interactions in the three-dimensional gas:

$$V_0^{(S)} = (0.095 \times 10^8\ \mathrm{cm}^{-1})\,V_0\,. \tag{4.8}$$

The chemical potential for H↓ on the surface is the sum of three separate contributions: an adsorption term, $-|E_b|$; a term representing the kinetic energy, eq. (1.14); and an interaction term, $2V_0^{(S)}\sigma$, analogous to that used in eq. (4.6) for $T > T_0$. (Because Bose–Einstein condensation does not occur in two dimensions the result for $T < T_0$ does not apply.)

$$\mu_A = -|E_b| + 2V_0^{(S)}\sigma + kT\ln[1 - \exp(\sigma\Lambda^2(T))]\,. \tag{4.9}$$

It is worthwhile comparing the interaction contribution to μ_A used here, $2V_0^{(S)}\sigma$, to the rigorous two-dimensional result $2\gamma\sigma$ of eq. (4.4). Using the generally accepted value of $a = 0.72$ Å from Friend and Etters [25], $V_0^{(S)} = 0.41 \times 10^{-14}$ K cm^2. This is less than the values of γ discussed earlier [44, 52], 0.94 and 0.65×10^{-14} K cm^2, which probably

reflects the "softening" of the interaction due to the finite extent of the wavefunctions perpendicular to the surface.

The adsorption isotherms obtained by eliminating $\mu_A = \mu_B$ from eq. (4.6) and eq. (4.9) are shown in fig. 4.4. At low density and high temperature the adsorption isotherms reduce to eq. (4.1). At high density and low temperature, they approach a limiting behavior,

$$\lim_{T\to 0}\sigma = \frac{|E_b|}{2V_0^{(S)}} + \frac{V_0}{2V_0^{(S)}}(n + n_0(T))\,. \tag{4.10}$$

Under the experimental conditions which are expected to apply to H↓, the second term in eq. (4.10) is much smaller than the first. In this case the surface density σ saturates at a value $|E_b|/2V_0^{(S)}$.

Adsorption isotherms for H↓ were first discussed by Edwards and Mantz [53] and by Silvera and Goldman [54]. Those calculations contained a factor of 2 error in the interaction contributions to the chemical potentials which was corrected by Goldman and Silvera [55].

The form of the interaction contribution for μ_A used in eq. (4.9) assumes a weakly interacting surface gas of H↓ atoms for which the mean energy per particle is linear in the surface density σ. This assumption can be compared with the strictly two-dimensional results at $T = 0$ shown in fig. 4.3. In that case E/N is noticeably higher than a linear extrapolation of the low σ result by the time σ reaches 10^{14} cm^{-2}. If the actual hydrogen film shows the same behavior, then eq. (4.9) underestimates the interaction contribution to μ_A near saturation. This would lead to a saturated density somewhat lower than that given in eq. (4.10) and displayed in fig. 4.4.

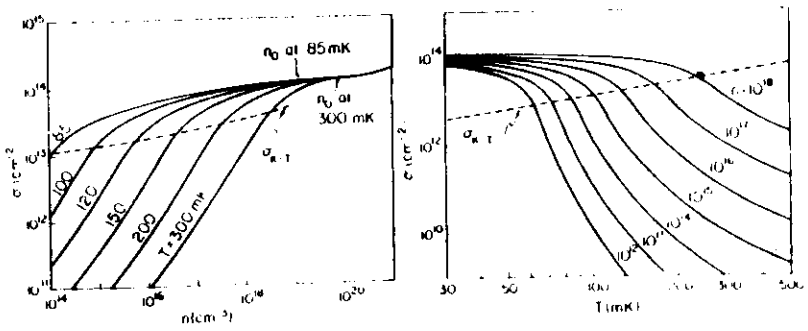

Fig. 4.4. Adsorption isotherms for H↓ (left). Adsorption "isochores" for H↓ (right).

4.5. The Kosterlitz–Thouless transition

Edwards and Mantz [53] have suggested that a Kosterlitz–Thouless transition [40] to a superfluid state may occur in the H↓ adsorbed on the walls, analogous to a transition which has been observed in thin adsorbed films of ^{4}He [56, 57]. It is qualitatively different from the superfluid transition in three dimensions because fluctuations are more important in two dimensions than in three. Conventional long-range order, a non-zero limit at large distances in the correlation function for the order parameter, is impossible in two dimensions. This implies the absence of a finite condensate fraction. Nonetheless, systems of the Kosterlitz–Thouless type undergo a phase transition to an ordered state at a finite temperature T_c.

Below T_c the two-dimensional system is a superfluid. It can be described by two-fluid hydrodynamics involving a superfluid density $\rho_s^{(2)}(T)$ and a normal fluid density $\rho_n^{(2)}(T) = M\sigma - \rho_s^{(2)}(T)$. Bose–Einstein condensation does not occur, however, since the fraction of atoms with zero momentum is never finite.

In a three-dimensional system the superfluid density goes smoothly to zero at T_c; in two dimensions $\rho_s^{(2)}(T)$ drops discontinuously to zero at T_c. Nelson and Kosterlitz [58] have shown that the ratio of the discontinuity in the superfluid mass density to the transition temperature is a universal constant:

$$\rho_s^{(2)}(T_c^-)/T_c = \frac{2k}{\pi}\left(\frac{M}{\hbar}\right)^2 . \tag{4.11}$$

This prediction has been confirmed in the experiments on ^{4}He films [56, 57].

Because of the unique nature of the Kosterlitz–Thouless transition it would be valuable to observe the transition in a system as simple and mathematically tractable as H↓ on ^{4}He. Edwards [59] has argued that the jump in the superfluid density at the transition should be very close to the total surface density:

$$\rho_s^{(2)}(T_c^-) \sim M\sigma . \tag{4.12}$$

Using this approximation in eq. (4.11) gives the following estimate for T_c:

$$T_c \sim \pi\hbar^2\sigma/2Mk . \tag{4.13}$$

The two-dimensional transition temperature eq. (4.13) is shown on the adsorption isotherms in fig. 4.4. The transition lies within a temperature and density range which may be achieved in H↓ experiments; indeed, it may be easier to attain the Kosterlitz–Thouless transition on the surface than the Bose–Einstein transition in the bulk.

Unfortunately, a Kosterlitz–Thouless transition in H↓ will not be easy to detect. There is no measurable anomaly in the specific heat as there is in superfluid ^{4}He and the weakly interacting Bose gas. The torsional oscillator technique used by Bishop and Reppy [57] relies on the slipping of $\rho_s^{(2)}$ relative to an oscillating substrate below T_c. In all experiments with H↓ so far, the substrate has been superfluid. In such a case no change in the moment of inertia would occur when the layer underwent a superfluid transition. The oscillator technique seems to require a pure ^{3}He surface to avoid superfluidity in the substrate. It is not yet known whether H↓ can be stabilized under these conditions, though only small amounts would be required.

Guyer and Miller [60] have proposed using third sound in ^{4}He to study the Kosterlitz–Thouless transition in H↓. Third sound is a density oscillation in superfluid films. They point out that a *normal* layer of H↓ adsorbed on superfluid ^{4}He would shift the resonance frequency of a third sound oscillator by an amount which depends on the H↓ coverage. Moreover, when the H↓ layer becomes a superfluid, two separate resonance frequencies should appear where there was only one before. Possibly the high resolution third sound resonance methods which have been used to study ^{4}He films [61, 62] can be adapted to the study of adsorbed H↓.

4.6. Effect of dynamical modes of the surface

So far the helium on the walls has been treated as a flat immobile surface whose only effect on the hydrogen is to provide bound surface states. This picture is inconsistent, however, since adsorption of atoms from the gas onto the surface requires inelastic collisions; the surface must have degrees of freedom to accommodate the energy lost by the atoms. These degrees of freedom are the elementary excitations associated with surface waves on an incompressible fluid, usually referred to as *ripplons*. The surface is distorted in the vicinity of the H↓; this distortion can move with the atom. The resulting complex is called a *surface polaron* in analogy with the problem of an electron moving in an ionic lattice. The first calculations [63, 64] indicated that the interaction is so strong that the H↓ is effectively localized on the

surface. Subsequent calculations [65, 66], however, have concluded that the interaction is weak, its primary effect being to replace the actual mass M of H↓ by an effective mass M^*. The calculations indicate that M^* is only a few percent larger than M. A value of $M^* = 1.11\,M$ was estimated by Edwards [59] using a semi-classical approach.

The fact that the adsorption rate is governed by the surface excitations may have important experimental consequences. It is known that the probability for a H↓ atom to be adsorbed during a collision with a He wall is small. Jochemsen et al. [49] measured the "sticking probability" for H to be 0.035(4) on ^{4}He and 0.016(5) on ^{3}He in the temperature range 0.18–0.27 K. Zimmerman and Berlinsky [67] and Kagan and Shlyapnikov [68] have calculated the temperature dependence of the sticking probability and find that it approaches zero as $T \to 0$. An interesting and perhaps important physical consequence of such a temperature dependence has been pointed out by Kagan and Shlyapnikov [68]: the decrease in the sticking probability may be helpful in attaining the Bose–Einstein transition in the millikelvin region. The reasoning is as follows.

We shall see in section 7.6 that the lifetime of samples with densities near the critical value $n_0(T)$ may be limited by three-body collisions. The lifetime could be too short to permit observing the transition in the 300 mK region. This problem can be avoided by working at lower temperatures, below 100 mK, where $n_0(T)$ is smaller and the three-body recombination rate in the gas is much reduced. Unfortunately, as the temperature is lowered the surface density $\sigma(T)$ increases rapidly and the atomic lifetime decreases due to recombination on the surface (see section 6.2). It is possible that there is no temperature at which the lifetime is long enough to permit a quantitative study of the transition: this can only be determined by further experiments. The above argument, however, assumes that $\sigma(T)$ is in thermal equilibrium with $n(T)$. Kagan and Shlyapnikov [68] point out that the small sticking probability at low temperature may prevent establishment of this equilibrium. This would cause σ to be smaller, and the lifetime to be longer, than the equilibrium calculations indicate. They predict that σ will begin to fall below its equilibrium value (in this case the saturated value of about $10^{14}\,\mathrm{cm}^{-2}$) at a temperature of the order of 5 mK. They also point out that the sticking probability decreases even more rapidly with decreasing temperature once the Bose–Einstein transition occurs, since the atoms in the condensate are effectively at zero temperature and cannot be adsorbed.

5. Equations of state for H↓

It is a tautology that H↓ cannot be viewed as a weakly interacting Bose gas unless it is a gas, but is not *a priori* obvious that H↓ will never liquify under its own vapor pressure. In this section we review the theoretical studies of the equations of state of H↓ and its isotopes. The statistics of particles can have a decisive effect on their equations of state; our starting point is a discussion of the Bose properties of H↓.

5.1. *Why is H↓ a Bose system?*

Underlying our discussion of H↓ as a Bose gas is the assumption that H↓ obeys Bose statistics. The argument is essentially that two fermions make a boson. More specifically, one can interchange two atoms by first exchanging the electrons, reversing the sign of the wavefunction, and then exchanging the protons, restoring the original sign. Here is the abstract of the paper which first discussed the role of symmetry on diatomic molecular systems, a 1931 article by Paul Ehrenfest and J. Robert Oppenheimer [69].

From Pauli's exclusion principle we devise the rule for the symmetry of the wave functions in the coordinates of the center of gravity of two similar stable clusters of electrons and protons, and justify the assumption that the clusters obey the Einstein–Bose or Fermi–Dirac statistics according to whether the number of particles in each cluster is even or odd. The rule is shown to become invalid only when the interaction between the clusters is large enough to disturb their internal motions.

By way of illustration, note that in molecular physics the deuteron is treated as a boson though in fact it consists of a proton and a neutron, two fermions. At nuclear energies, MeV's, the deuteron must be regarded as a system of fermions, whereas at chemical energies, eV's, it behaves like a single Bose particle. The large ratio in the energies, $\sim 10^6$, assures that the approximation is safe. Similarly, a hydrogen atom must be treated as a system of 2 fermions for energies which approach electronic excitation, about 10 eV. The H↓–H↓ molecular interaction is about 10^{-3} eV. The energy ratio is about 10^4, which justifies the assumption.

There are, however, conceptual problems when one considers interactions which depend on the internal variables, for instance exchange interactions which depend on the electron spin coordinates. A sys-

tematic study of the role of symmetry on the equation of state of hydrogen has been carried out by Lefevre–Seguin et al. [70]. These authors calculated the second virial coefficient for hydrogen, and showed that the interactions can be classified according to their dependence on the internal coordinates. As anticipated, at low temperature the system behaves like a simple Bose gas. In principle, however, a complete description of the system requires consideration of collisions in which electrons or protons are separately exchanged.

5.2. *The role of zero-point energy*

The H↓–H↓ potential is not dramatically different from the ^{4}He–^{4}He potential (see fig. 5.1), and ^{4}He is a liquid in the Bose transition region. Why then does H↓ remain a gas down to absolute zero?

The decisive difference between H↓ and He is not the slightly deeper potential for He but the factor of 4 in the mass. At low temperature the state of a system is determined by the conflict between the attractive potential energy and the zero point kinetic energy. In ^{4}He neither wins: ^{4}He does not form the most ordered state, a solid, nor does it remain a gas. Rather, the system collapses to a state of

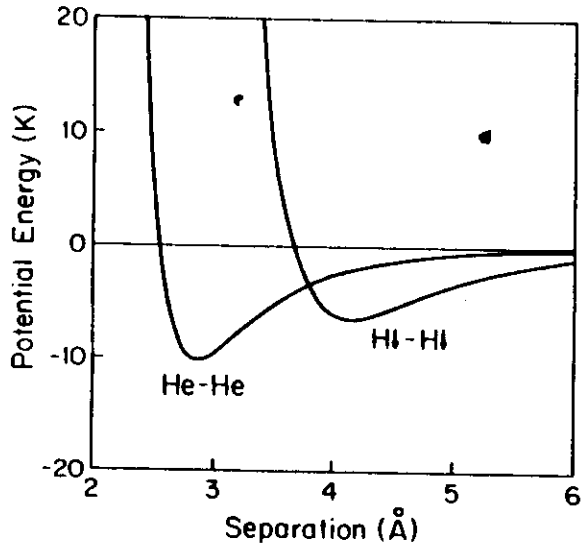

Fig. 5.1. Interatomic potentials, helium and hydrogen.

intermediate order, a liquid. (Nevertheless, the density of the liquid is dramatically lowered by the zero-point motion. If absent, the density would be 6×10^{22} cm^{-3}. The actual density is 2×10^{22} cm^{-3}.) In H↓ the zero point energy is so large that the system *never* liquifies under its own pressure.

Hecht's original conjecture that H↓ is a gas at $T=0$ was based on the ***quantum theorem of corresponding states***. This theorem provides a powerful guide to predicting the properties of diverse systems by simple scaling arguments. We briefly summarize it here.

5.3. *The quantum theorem of corresponding states*

The interatomic potentials for many simple diatomic species are so similar that they can often be characterized by just a few parameters. A common example is the Lennard–Jones potential

$$V(r)=4\varepsilon[(\sigma/r)^{12}-(\sigma/r)^{6}]\,. \tag{5.1}$$

It seems reasonable that the thermodynamic properties of all such systems should have basic similarities. To make use of this idea one introduces dimensionless variables:

$$r^*=r/\sigma,\quad v^*=V(\sigma r^*)/\varepsilon,\quad T^*=kT/\varepsilon,\quad V^*=V/N\sigma^3\,. \tag{5.2}$$

σ is a scale length, and $1/V^*$ is the density in volume units of σ^3. The following dimensionless quantity plays a key role:

$$\eta=\hbar^2/M\varepsilon\sigma^2\,. \tag{5.3}$$

The parameter η describes the competition between zero point kinetic energy and the potential energy: it is this competition which determines the state of the system at low temperature. To see why this is so, consider a harmonic oscillator potential drawn tangent to the minimum of an interatomic potential $V(r)$. The curvature is $V''|_{r_m}$. By dimensional arguments

$$V''|_{r_m}=C\varepsilon/\sigma^2\,, \tag{5.4}$$

where C is a numerical constant which depends on the shape of the potential. The zero-point energy is

$$\varepsilon_0 = \tfrac{1}{2}\hbar\omega = \tfrac{1}{2}\hbar(V''/M)^{1/2} \tag{5.5}$$

The ratio of zero-point energy to the potential well depth ε is

$$\frac{\varepsilon_0}{\varepsilon} = \frac{C^{1/2}}{2}\left(\frac{\hbar^2}{Me\sigma^2}\right)^{1/2} = \text{const}\sqrt{\eta}\,. \tag{5.6}$$

Because η is proportional to the square of this ratio it is evident that large η corresponds to the case where zero-point energy of a system is important compared to the binding energy, i.e. the quantum limit, whereas small η describes a classical system where zero point energy is unimportant.

The quantum theorem of corresponding states asserts that for all systems which can be described by a potential having the same form, the free energy (or any other thermodynamic potential) can be written in a reduced form,

$$F(T, V, N) = \varepsilon F^*(T^*, V^*, N, \eta)\,. \tag{5.7}$$

F^* depends only on the form of the potential and on the statistics of the system (Bose–Einstein or Fermi–Dirac). Once F^* is known, the thermodynamic properties of the entire class of systems is determined. Nosanow et al. [71] made use of this result to survey the nature of zero-temperature liquid-to-crystal phase transitions in quantum systems. The theorem provides a natural starting point for a study of the gas to liquid transition.

5.4. *Equations of state for H and its isotopes*

5.4.1. *Etters, Dugan and Palmer*

Following Hecht's short note [6], the first detailed calculations on the properties of H↓ were carried out by Dugan and Etters [7], and Etters et al. [8]. The work follows W.L. McMillan's study of the properties of ^{4}He as an interacting Bose gas [72]. The Kolos–Wolniewicz potential (fig. 4.1) is fit to the Morse form

$$V(r) = \varepsilon\{\exp[2c(1 - r/r_0)] - 2\exp[c(1 - r/r_0)]\}\,. \tag{5.8}$$

The wave function for an N-particle system is taken to be of the Jastrow type

$$\psi(r_1, r_2, \ldots, r_n) = \prod_{i<j}^{N} \exp[-b_1 \exp(-b_2 r_{ij})]\,. \tag{5.9}$$

This function leaves the atoms uncorrelated at large distances, but rapidly vanishes as they start to overlap. It is symmetric under interchange of any two particles as required for bosons. b_1 and b_2 are treated as variational parameters. $\langle E\rangle = \langle T\rangle + \langle V\rangle$ is calculated for particles in a box by Monte Carlo methods using random configurations, typically for 32 particles. As the system is compressed, the energy per atom at $T = 0$ is found continually to increase for hydrogen and deuterium, but initially to decrease for tritium. Thus H and D are predicted to be a gas at $T = 0$, whereas tritium is a liquid.

5.4.2. *Miller, Nosanow and Parish* [9]

In this work the reduced pressure and energy for boson and fermion systems interacting via a Lennard–Jones potential is studied as a function of η. The results are illustrated in fig. 5.2. For Bose systems, the energy increases with density provided η exceeds a critical value, $\eta_c = 0.45$. Thus, whether or not a weakly interacting Bose system liquifies at $T = 0$ depends on whether or not η exceeds 0.45. For Fermi systems, the energy initially increases with density due to the "Pauli pressure" of the gas. However, if the attractions are great enough (i.e., if η is small enough) there is a minimum in the energy at a finite density, so the system will be a liquid.

Generalizations based on the quantum theorem of corresponding states depend, of course, on the assumed form of the potential. The Lennard–Jones potential is expected to be more reliable than the Morse potential because it has the correct long-range behavior; it is the long-range force which determines the onset of a gas to liquid transition. In cases where a system is on the border of a phase transition, however, conclusions based on any simple model potential are suspect.

5.4.3. *Stwalley and Nosanow* [10]

The results of the previous studies were applied by these authors to hydrogen and its isotopes. Because the quantum parameter varies with the inverse of the mass, its value differs significantly among the isotopes. The values are

$$\text{H}\downarrow:\ \eta = 0.55, \qquad \text{D}\downarrow:\ \eta = 0.27, \qquad \text{T}\downarrow:\ \eta = 0.18\,.$$

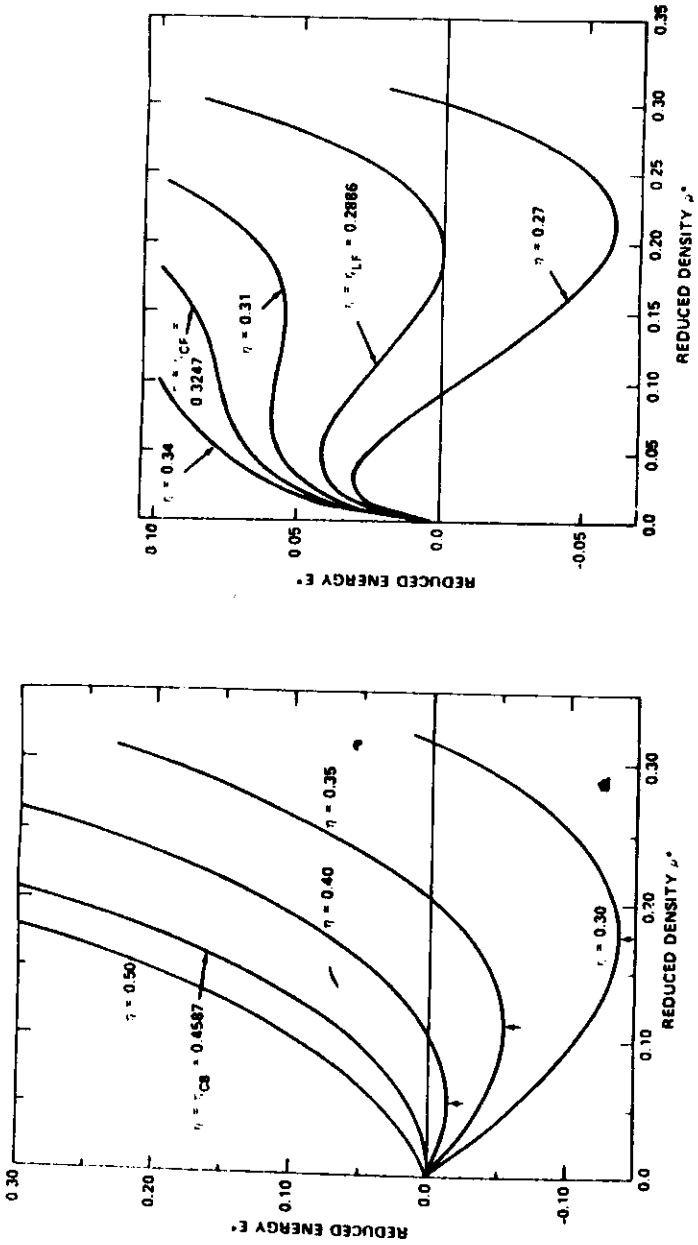

Fig. 5.2. Reduced energy vs reduced density for different values of the quantum parameter η: Bose–Einstein statistics (left), Fermi–Dirac statistics (right) (from Miller et al. [9]).

Stwalley and Nosanow concluded that H↓ is gas at $T = 0$ while T↓ is liquid. D↓ is borderline. The Letter points out the significance of research on H↓, and discusses a possible experimental approach.

D↓ has an additional interesting feature if $0.27 \leqslant \eta \leqslant 0.31$: two phase coexistence at $T = 0$. At zero pressure the system is a gas, but application of a pressure up to some critical value would cause the gas and liquid phases to coexist, separated by a meniscus. Above the critical pressure the system is a homogeneous liquid. Even if the ground state is a liquid, $\eta < 0.27$, the boiling point could be low enough to allow the study of a Fermi gas of reasonable density at very low temperature.

5.4.4. *Other calculations*

Lantto and Nieminen [35] used the exact Kolos–Wolniewicz potential to carry out variational calculations on H↓ at $T = 0$, obtaining the velocity of sound and the condensate fraction. Friend and Etters [25] found these quantities using the theory of the imperfect Bose gas. At densities below $10^{20}\,\mathrm{cm}^{-3}$, the condensate fraction is greater than 99%. (Contrast this to ^{4}He, where the condensate fraction is about 10%.) Panoff et al. [73] carried out accurate variational calculations for D↓ which indicate that it is a liquid, though very weakly bound. The binding energy is less than 50 mK. Their calculation was done for electron polarized deuterium which has a three-fold degeneracy due to nuclear spin. Nuclear polarized deuterium (prepared in a single hyperfine state) is expected to be even less weakly bound, possibly not bound at all.

5.5. *Summary of our current understanding*

H↓ remains a gas to $T = 0$. Its thermodynamic properties should be accurately described by the theory of the weakly interacting Bose gas. In particular, the transition temperature is very close to the value given by the ideal Bose gas formula. Deuterium and tritium, however, are expected to liquify.

The fact that H↓ remains a gas whereas D↓ may liquify is counterintuitive from the basis of statistics alone, for bosons tend to "fraternize" whereas fermions are "antisocial". However, the zero-point energy plays the overriding role, and this is much larger in H than in D due to the factor of two difference in mass.

6. Molecular recombination of atomic hydrogen

Any chemical which can explode merely from a change in a magnetic field must be counted among the world's most unstable species. The quest to create H ↓ is essentially a fight against hydrogen's compulsion to form molecules – a fight against recombination. In this section we describe the various routes by which hydrogen attempts to recombine. As an introduction to the problem of recombination in H ↓, we start by considering recombination in "ordinary" atomic hydrogen.

6.1. Recombination of unpolarized hydrogen

Hydrogen atoms recombine to the $^1\Sigma_g$ molecular state by the reaction

$$H + H \rightarrow H_2 + \Delta E, \tag{6.1}$$

where ΔE is the recombination energy, 4.476 eV. The reaction will not occur simply as written because a two-body collision cannot conserve momentum while simultaneously releasing kinetic energy – a third body is needed. The third body can be a photon but the rate for this process, radiative recombination, is negligible because: (a) radiative recombination is a relatively slow process at best; (b) electric dipole radiation is strictly forbidden for vibrational–rotational transitions in a homonuclear molecule. Consequently, recombination must occur by the process

$$H + H + X \rightarrow H_2 + X + \Delta E, \tag{6.2}$$

where X is another H atom, a foreign atom or molecule, or a surface.

The time evolution of density in a gas undergoing three-body recombination is described by the rate equation

$$\dot{n}_H = -K_x n_x n_H^2, \tag{6.3}$$

where K_x depends on the third body (X) and the temperature. We can roughly estimate K_H: hydrogen is most likely to recombine into a high vibrational state of the $^1\Sigma_g$ potential rather than a low-lying state because this involves a much smaller energy transfer and can take place at a larger internuclear distance. Let the radius at which recombination occurs be R_r. The density of pairs of H atoms within this distance is $\frac{1}{2}(\frac{4}{3}\pi R_r^3)n_H^2$. Recombination can take place whenever a third atom comes within distance R_r of one of these pairs. The rate of recombination is thus

$$\dot{n}_H \simeq -(\pi R_r^2) v_r n_x (\tfrac{2}{3}\pi R_r^3) n_H^2 (1 - \tfrac{1}{4}). \tag{6.4}$$

(The last factor, which is unimportant in this order of magnitude calculation, is the probability that at least one pair of the atoms is in the singlet state.) We have

$$K_H \simeq \frac{7\pi^2}{12} v_r R_r^5. \tag{6.5}$$

A room temperature the average relative speed is $v_r \cong 2 \times 10^5\ \mathrm{cm\ s^{-1}}$. Based on the potential in fig. 1.4, a reasonable choice for R_r is 2.3 Å. The result is

$$K_H \simeq 7 \times 10^{-33}\ \mathrm{cm^6\ s^{-1}}. \tag{6.6}$$

This is typical of the values measured with various third bodies, as the data in table 6.1 shows. The similarity of K for H_2, He and N_2 suggests that the nature of the third body is not terribly important.

Decay by a three-body process (with H as the third body) leads to a time dependence of the density which is markedly different from exponential decay:

$$n(t) = n(0)(1 + t/\tau)^{-1/2}, \tag{6.7}$$

Table 6.1
Three-body recombination rate constants for atomic hydrogen on various partners. From Walkhausbus and Kaufman [74]. (K is in units of $10^{-33}\ \mathrm{cm^6\ s^{-1}}$)

X	T (K)	K	X	T	K
H_2	298	8.1(4)	CO_2	295	16.4(8)
	77	18.5(22)		175	53.2(4)
He	298	7.0(4)	SF_6	295	19.5(9)
	77	12.0(15)			
N_2	295	9.1(5)			
	77	55.0(5)			

where $\tau = (2Kn^2(0))^{-1}$. For a density of $10^{17}\,cm^{-3}$ at room temperature, $\tau \sim 10^{-2}\,s$.

In most laboratory situations hydrogen recombines on surfaces rather than in the gas, which severely shortens the lifetime. If the walls are metal, the hydrogen is usually lost through chemical adsorption by processes which proceed essentially as quickly as the atoms hit the surface. For certain wall coatings, however, a hydrogen atom can make many collisions before being "lost". In the case of Teflon, for instance, up to 10^4 wall collisions can occur before an atom reacts with the surface [18]. (The reaction is $CF_2 + H \rightarrow CF + HF$.) Teflon is useful for confining atomic hydrogen at room temperature and temperatures down to 80 K, but at very low temperatures the atoms adsorb so strongly that recombination on the surface is very rapid.

6.2. *Magnetic resonance studies of unpolarized hydrogen*

Magnetic resonance studies of atomic hydrogen have provided invaluable information on how hydrogen behaves at low temperatures and on the recombination dynamics which should be important to spin-polarized hydrogen. By studying line intensities, relaxation times and frequency shifts, one can determine atomic densities and lifetimes, surface adsorption energies, sticking probabilities and collision cross-sections. Hardy et al. [3] and Morrow and Hardy [75] have reviewed much of this work.

Because an important experimental step in working with hydrogen at low temperature is cooling it first to liquid helium temperature, 4.2 K, a non-reactive surface coating is essential. As discussed in section 4.2, frozen H_2 is a natural candidate. Its effectiveness is difficult to measure with conventional surface recombination detectors at low temperature. Crampton et al. [11] solved the problem by a resonance experiment using the apparatus in fig. 6.1.

Hyperfine resonance in zero applied field was observed on the transition $(F = 0, m = 0) \rightarrow (F = 1, m = 0)$, at 1420 MHz. (The transition frequency is independent of the field to first order.) Atoms produced in a liquid nitrogen cooled discharge flowed to a glass cell inside a resonator immersed in liquid helium. A pulse of radiation at the resonance frequency induced a "$\pi/2$" transition, leaving the system in a radiating state. The frequency and various relaxation times were measured.

From the signal strength the atomic density was determined to be

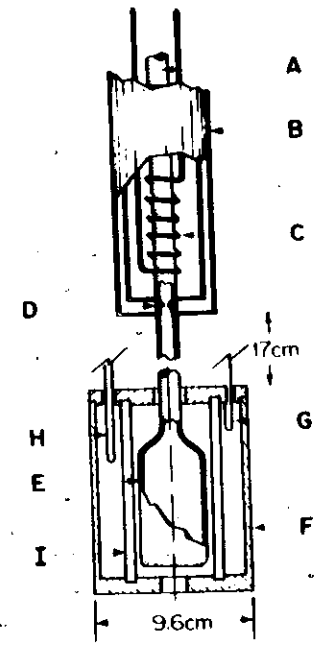

Fig. 6.1. Apparatus for observing hyperfine resonance of H at temperatures down to 4.2 K (Crampton et al. ref. [11]). The apparatus is immersed in liquid helium. A, H_2 inlet; B, Dewar, containing liquid N_2; C, rf discharge; D, orifice; E, quartz cell; F, resonant cavity, 1420 MHz; G, coupling loop; H, tuning rod.

over $10^{14}\,cm^{-3}$, and the flux of atoms was estimated to be at least $4 \times 10^{16}\,s^{-1}$. This flux is comparable to that in a robust atomic beam, but the apparatus is far simpler than a conventional hydrogen beam source.

The adsorption energy of H on H_2 was determined by measuring the hyperfine frequency. The observed frequency is shifted because the hyperfine frequency is perturbed while the atoms are adsorbed on the surface. If the frequency shift on the surface is $\delta\omega_s$, then the observed shift is

$$\Delta\omega_0 = \delta\omega_s \frac{t_a}{t_c + t_a} \simeq \delta\omega_s \frac{t_a}{t_c}, \tag{6.8}$$

where t_a is the mean adsorption time, and t_c is the mean time between

collisions. If the adsorption energy is E_b and the H atoms are free to move on the surface, then by combining the relations for the equilibrium surface density, eq. (4.1), with the gas collision rate $\gamma_c = n\bar{v}/4$, the mean adsorption time is found to be

$$t_a = \frac{\Lambda(T)}{\bar{v}} \exp(E_b/kT) . \tag{6.9}$$

The collision time is $t_c = d/\bar{v}$, where d is the mean free path, and $\bar{v}$ is the mean speed. Thus

$$\Delta\omega_0 = \delta\omega_s \frac{\Lambda(T)}{d} \exp(E_b/kT) . \tag{6.10}$$

By plotting $\Delta\omega_0$ vs $1/T$, E_b is obtained. The initial experiment [11] obtained an erroneous value due to lack of thermal equilibrium, but more careful work [44] yielded $E_b = 35.8(3)$ K. If the H atoms are frozen to specific sites on the surface, the adsorption isotherm differs from eq. 4.1 and the measurements would correspond to $E_b = 31.7(3)$ K.

The question of how rapidly H recombines on an H_2 surface is important to the technology of producing H↓, but no quantitative study has been carried out. The adsorption factor $\exp(E_b/kT)$ varies rapidly with temperature in the liquid helium range. The adsorption time at 4.2 K is 40 ns. At 1 K it is over ten years!

Hardy and Berlinsky, and their co-workers, have carried out an elegant series of hyperfine resonance experiments on unpolarized hydrogen in a helium-lined vessel at low temperatures [15, 49, 75]. The apparatus is shown in fig. 6.2. This work has yielded data on a large assortment of parameters governing the H–He system. Here we summarize the results on recombination and adsorption energy.

At "high" temperature ($T \sim 1.3$ K), the ambient pressure of He is so large that the hydrogen is lost dominantly by three-body recombination in the gas. The density of unpolarized hydrogen decays according to

$$\dot{n}_H = -K n_{He} n_H^2 , \tag{6.11}$$

which has the solution

$$n_H(t) = n_H(0) \frac{1}{1 + 2t/\tau} , \tag{6.12}$$

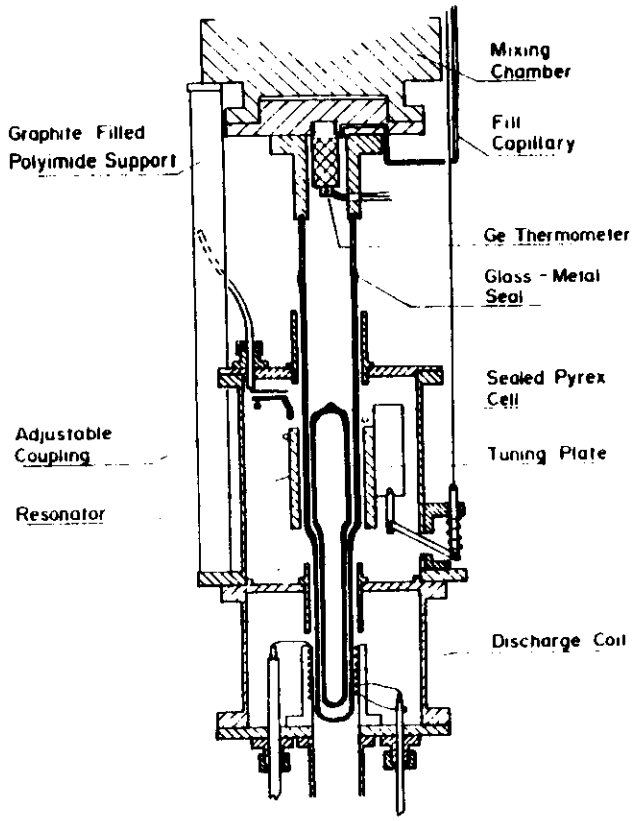

Fig. 6.2. Apparatus used by Hardy et al. to study hyperfine resonance of H on liquid helium surfaces [3]. H_2 and He are sealed in a glass cell; H is formed by an rf discharge. Courtesy of W.N. Hardy.

where $1/\tau = K n_{He} n_H(0)$. The three-body rate coefficient was found to be

$$K(\mathrm{He}, 1\ \mathrm{K}) = 2.8(3) \times 10^{-33}\ \mathrm{cm^6\ s^{-1}} . \tag{6.13}$$

This rate is slightly less than half the room temperature value. One might expect roughly the same value for K(H, 1 K).

Greben et al. [76] have carried out a theoretical study of the three-body recombination for hydrogen in helium at 1 K, evaluating the transition rates into all the available molecular states. The mole-

cules were found to form predominantly in the ortho ($I = 1$) state. They obtained $K(\mathrm{He}, 1\,\mathrm{K}) = 1.8 \times 10^{-33}\,\mathrm{cm}^6\,\mathrm{s}^{-1}$. Considering the complexity of the process, this represents impressive agreement with experiment.

At "low temperatures" (0.25–0.5 K), recombination in the gas phase is suppressed by the low vapor pressure of helium, while recombination on the surface is enhanced because the density of H on the surface is increased. The hydrogen forms a two-dimensional gas on the surface, and recombines in binary collisions. We can define the equivalent of a scattering cross section for a two-dimensional gas, a scattering "cross length" $\langle l \rangle$. The collision rate for the surface gas is

$$\gamma_s = \sigma \langle l \rangle v_r , \tag{6.14}$$

where σ is the surface density, and v_r is the relative surface speed

$$v_r = (32kT/3\pi M)^{1/2} . \tag{6.15}$$

The surface density decays according to

$$\dot{\sigma} = -\gamma_s \sigma = -\langle l \rangle v_r \sigma^2 = -K_s \sigma^2 , \tag{6.16}$$

where K_s is a two-body surface decay constant:

$$K_s = \langle l \rangle v_r . \tag{6.17}$$

The total number of atoms decays according to

$$\dot{N} = -A\dot{\sigma} , \tag{6.18}$$

where A is the area. Assuming that the surface remains in equilibrium with the volume density so that $\sigma = n\Lambda \exp(E_b/kT)$, the surface decay rate can be written in terms of an equivalent volume decay using $\dot{N} = V\dot{n} = A\dot{\sigma}$:

$$\dot{n} = \frac{A}{V}\dot{\sigma} = \frac{A}{V}\langle l \rangle v_r n^2 \Lambda^2 \exp(2E_b/kT) , \tag{6.19}$$

or

$$\dot{n} = -K_{en} n^2 . \tag{6.20}$$

K_{en} is an effective two-body volume recombination coefficient.

$$K_{en} = \frac{A}{V}\langle l \rangle v_r \Lambda^2 \exp(2E_b/kT) = K_s \frac{A}{V} \Lambda^2 \exp(2E_b/kT) . \tag{6.21}$$

By measuring K_{en} at several temperatures, Hardy et al. determined the adsorption energy of H on He^4 and He^3, and also the scattering distance $\langle l \rangle$. The results are: He^4, $E_b = 1.15(5)$ K, $\langle l \rangle = 0.20(3)$ Å; He^3, $E_b = 0.39$ K, $\langle l \rangle = 0.18$ Å.

The results of these zero-field resonance studies of hydrogen played a key role in predicting and interpreting the behavior of spin-polarized hydrogen in high field.

6.3. *Recombination in H↓ : a survey of possible mechanisms*

The stability of spin-polarized hydrogen is jeopardized by every process which can depolarize the electrons or otherwise cause triplet–singlet transitions. Prominent among these are electron exchange, as well as dipolar and spin–orbit interactions during collisions. In addition, the hyperfine interaction itself can slightly depolarize the electron in an isolated atom, providing a path to recombination. Stwalley [77] analyzed a number of these processes and showed that they do not necessarily create an experimental impediment. More recently, Kagan, Shlyapnikov and Vartanyantz [78] (KSV) have executed an exhaustive theoretical study of possible recombination processes. Their work stands as the primary theoretical reference on the subject. In this section we summarize their findings. Following the convention of fig. 1.5, note that spin-polarized hydrogen is normally comprised of states a ($m = 0$) and b ($m = -1$). (Here m is the z component of the total spin angular momentum, electron plus proton.) The remaining high-energy states are c ($m = 0$) and d ($m = +1$).

Molecular recombination requires that the two atoms form a $^1\Sigma$ state. To an excellent approximation, the only configuration available to atoms in states a and b is $^3\Sigma$. Two routes to recombination are conspicuous. The first involves the crossing of the singlet and triplet potentials. The hyperfine interaction couples the singlet and triplet states, allowing a *direct transition of* atom pairs a–a or a–b into a $^1\Sigma$ configuration. This reaction requires that the initial energy coincides with the energy of a bound state of the molecule. Because only a narrow range of energy is effective, the process is called *resonance*

recombination. The second route involves what KSV refer to as "depolarization", that is promotion of an atom to a high-energy hyperfine state, **c** or **d**. The $^1\Sigma$ configuration is then available to every pair of atoms for which one is **a** or **b** and the other is **c** or **d**. Although depolarization can occur in binary collisions, recombination requires the presence of a third body (an atom or a surface) to conserve energy and momentum. The details of these processes are summarized below.

(*A*) *Resonance recombination into a molecular state*

From fig. 4.1 it is evident that at low temperature ($kT \ll \mu B$), atoms colliding in the triplet state, $M_S = -1$, may have the same energy as a bound molecular state of the singlet potential. The hyperfine interaction couples the triplet and singlet state by admixing a small component of $m_s = 1/2$ into state **a**. As a result, singlet–triplet transitions can occur in a two-body collision, forming a quasi-molecule. The transition appears as a resonance in the scattering cross section. The quasi-molecule will in general dissociate via the same interaction which formed it (the process is called predissociation), but if it lives long enough to lose energy by an inelastic rotational or vibrational collision, the molecule becomes stabilized.

Stwalley [77] first analyzed this process, and identified resonances in H–D and D–D. The (17, 0) (i.e. $v = 17$, $J = 0$) level of HD has a binding energy of 6.8 K; this is degenerate with the $M_S = -1$ triplet level for a field of 5 T. The (21, 0) level of D_2 has energy 2.6 K, corresponding to a field of 1.9 T. The rate constant for resonance recombination depends critically on the width of the scattering resonance. In addition, it includes a threshold factor depending on the temperature and the kinetic energy required to achieve the resonance energy in the applied field. In principle, the stability of D_2 is jeopardized by the resonance at 2.6 K, but it may be possible to suppress the recombination rate by operating at a field much larger than 1.9 T. Should the HD resonance be important, its primary effect would be merely to eliminate any deuterium which is present as an impurity in the hydrogen.

KSV found that the (12, 10) state of H_2 has a binding energy of 10 K, creating a possible recombination path in H↓. The centrifugel barrier in the $J = 10$ rotational state is so high, however, that resonance recombination is unimportant.

(*B*) *Depolarization processes in pair collisions*

If an atom is depolarized (raised to a high-energy hyperfine state) during an isolated two-body collision, the depolarized atom can be expected to recombine promptly in a subsequent three-body collision or in a two-body collision on a surface. Mechanisms leading to depolarization include:

(*B1*) *Exchange interaction*. This arises from the exchange terms entering the interactions matrix elements for identical particles. It is responsible for the splitting between the singlet and triplet potential, and gives rise to the process of spin-exchange during a collision. Spin exchange occurs readily in unpolarized paramagnetic gases, but in H↓ it can occur only because **a** is not a pure eigenstate of electron spin. (The hyperfine interaction introduces a small admixture of $m_s = +1/2$.) Three types depolarizing collisions occur. An **a**–**b** collision can give rise to a $^1\Sigma$ configuration involving **b** and **c**. An **a**–**a** collision can give rise to a $^1\Sigma$ configuration involving **a**, **b**, **c**, and **d**. If the kinematic constraints could be satisfied, recombination would occur immediately. Finally, a **a**–**a** collision can give to a $^3\Sigma$ "doubly depolarized" state leaving both atoms in state **c**. In this case the atoms must seek other partners if a subsequent recombination is to occur. Note that exchange depolarization is strictly forbidden in a gas containing only **b** state atoms.

(*B2*) *Dipole interaction*. This arises from the dipolar coupling between the magnetic moments of the two electrons. It does not require hyperfine mixing, so **a**–**a**, **a**–**b**, and **b**–**b** collisions all contribute. The total electron spin S (but not its projection M_S) remains unchanged. This implies that the $^1\Sigma$ state is not formed in the collision; recombination must take place in a subsequent encounter. Normally the cross section for this process is negligible compared to spin exchange, but KSV find that at low temperature the dipolar cross section is actually larger than the exchange cross section.

(*B3*) *Spin–orbit interaction*. Coupling between the electron spin and the motional magnetic field generated during a collision by the electrostatic interaction can cause ΔM_s transitions. However, triplet-state collisions occur at such a large distance that spin–orbit effects are expected to be negligible compared to (B1) and (B2).

The exchange and dipolar interactions have small but by no means negligible cross sections. In two-body depolarization collisions, however, the magnetic energy required to flip at least one spin must be

provided at the expense of the collisional kinetic energy. This introduces a "threshold factor" $\exp(-2\mu B/kT)$ into the rate constant, and for spin-polarized hydrogen this factor is typically 10^{-20}. As a result, collisional depolarization is unimportant. KSV estimate that at a density of $10^{20}\,\mathrm{cm}^{-3}$ the lifetime due to spin depolarization in a field of 10 T is greater than one hour if the temperature is less than 0.6 K.

(*C*) *Simultaneous depolarization and recombination in three-body and surface collisions*

The "threshold factor" introduced in B can be avoided if the energy needed to flip a spin comes simultaneously from the recombination process. Even in this case, however, recombination requires a third atom or a surface to satisfy the kinematic constraints of energy and momentum conservation. Several possibilities exist.

(*C1*) *Two-body exchange interaction on a surface.* The exchange interaction during a binary collisions sets up a $^1\Sigma$ configuration, as described in (B1), and the surface allows the kinematic constraints to be satisfied. Recombination via this process has been observed experimentally; it is the principle loss mechanism at densities so far achieved. It would not take place, however, if the gas were nuclear polarized, that is, restricted to **b** state atoms only. This process is discussed below in some detail.

(*C2*) *Two-body dipole interaction on a surface.* This process is forbidden since the dipole interaction in a binary collision creates only $^3\Sigma$ configurations.

(*C3*) *Three-body exchange interaction.* Recombination in the bulk due to this process is expected to be the dominant loss mechanism for gases at high densities containing both **a** and **b** state atoms. It is forbidden in a gas containing only the **b** state.

(*C4*) *Three-body dipole interaction.* As mentioned in (B2), the dipole cross section is unexpectedly large compared to the exchange cross section at low temperature. Consequently, dipolar three-body recombination can be important, even for a gas of pure **b** state atoms. The reaction cannot occur by two-body collision on a surface; three H atoms are required. Consequently, it can only be observed at high density. KSV estimate a lifetime of one hour in a 10 T field at a density of $1 \sim 2\times 10^{17}\,\mathrm{cm}^{-3}$. Since the lifetime varies inversely with the square of the density, the process should be observable at densities somewhat above those so far studied*. If their estimate is correct, it will preclude observing

* See Postscript.

the Bose–Einstein transition in the 100–300 mK region, forcing the search to a much lower temperature, lower density region. A possible strategy for this has been pointed out by KSV, as mentioned in section 4.6.

(*D*) *Recombination via many-body processes*

As discussed in section 4.1, at very high densities many-body effects can cause spin instabilities leading to spontaneous recombination. This process was first studied by Berlinsky et al. [41], but Kagan and Shlyapnikov [43] found that these authors had overestimated the effect. KSV conclude that H↓ should be stable against many-body recombination for densities at least as high as $10^{21}\,\mathrm{cm}^{-3}$.

6.4. Recombination in a high field

For moderate densities ($n \lesssim 10^{17}\,\mathrm{cm}^{-3}$) the recombination rate for H↓ in a high magnetic field can be predicted from the results of the low field resonance experiments by a simplistic argument which turns out to be substantially correct: the recombination rate is proportional to the probability $P(B)$ that two atoms collide in a singlet electron state while adsorbed on the surface. The high-field two-body recombination collision length is then related to the low-field value by

$$\langle l(B)\rangle = \langle l(0)\rangle P(B)/P(0)\,. \tag{6.22}$$

$P(B)$ can be found from the spin eigenstates of the hyperfine Hamiltonian. In terms of the electron and proton spin state $|m_s, m_I\rangle$, the hyperfine states (fig. 1.5) are

$$\begin{aligned}
|\mathrm{a}\rangle &= \cos\theta|-+\rangle - \sin\theta|+-\rangle\,,\\
|\mathrm{b}\rangle &= |--\rangle\,,\\
|\mathrm{c}\rangle &= \sin\theta|-+\rangle + \cos\theta|+-\rangle\,,\\
|\mathrm{d}\rangle &= |++\rangle\,,
\end{aligned} \tag{6.23}$$

where $|+,-\rangle \to m_s = +1/2$, $m_I = -1/2$, etc., and $\tan 2\theta = a/[h(\gamma_e+\gamma_p)B]$. Here a is the hyperfine constant, and γ_e, γ_p are the electron and proton gyromagnetic ratios, respectively. (a/h = 1420 MHz, γ_e = 2.8 MHz/gauss, γ_p = 4.2 kHz/gauss). As $B \to 0$, $\theta \to \pi/2$, and the average probability for a collision to occur in the singlet state is $P(0) = 1/2$.

In a gas of H↓ the only states which are significantly occupied are **a** and **b**. The probability that two atoms meet in the singlet state is:

$$\begin{aligned} &|a\rangle + |a\rangle, \quad P_{aa} = \tfrac{1}{2}\sin^2\theta\cos^2\theta, \\ &|a\rangle + |b\rangle, \quad P_{ab} = \tfrac{1}{4}\sin^2\theta\cos^2\theta, \\ &|b\rangle + |a\rangle, \quad P_{ba} = \tfrac{1}{4}\sin^2\theta\cos^2\theta, \\ &|b\rangle + |b\rangle, \quad P_{bb} = 0. \end{aligned} \tag{6.24}$$

The total probability that a collision occurs in the singlet state is $\sin^2\theta\cos^2\theta$. Thus the effective collision length for the $|a\rangle$, $|b\rangle$ system is related to the zero-field length of an unpolarized system by

$$\langle l(B)\rangle = \langle l(0)\rangle \frac{\sin^2\theta\cos^2\theta}{1/2}. \tag{6.25}$$

If we denote $\sin\theta$ by $\varepsilon(B)$, then in high fields

$$\varepsilon(B) \to a/[2h(\gamma_e + \gamma_p)B] \simeq 2.53\times 10^{-2}/B, \tag{6.26}$$

$$\langle l(B)\rangle = 2\varepsilon^2 l(0) = \langle l(0)\rangle \times 1.3\times 10^{-3}/B^2, \tag{6.27}$$

where B is in tesla. The surface recombination constant K_s and the effective volume constant K_{eff} are proportional to $\langle l(B)\rangle$, or to $\varepsilon(B)^2$. At a field of 10 T the recombination rate should be inhibited by a factor of 10^5 compared to the rate at zero field.

To summarize, the dominant decay mechanism is two-body recombination on the surface, a process which can be described by an effective two-body volume decay constant for the gas. Initial experiments on spin-polarized hydrogen (see section 7.3) gave results which seemed to be consistent with this description, but an important problem has been overlooked: eq. (6.23) reveals that recombination requires that at least one atom be in state **a**: $P_{bb} = 0$. Once all the **a** state atoms have recombined, a residual gas of **b** state atoms will remain. This gas should be stable. If nuclear relaxation caused rapid equalization of the populations of the **b** and **a** states, one might expect the two states to stay in equilibrium and decay together. Statt and Berlinsky [79] recognized the critical role of nuclear relaxation in the dynamics of H↓. They pointed out that the electron–proton dipole interaction during a collision will lead to nuclear relaxation with a rate

T_1^{-1} which is proportional to the total density, and calculated the relaxation rate.

6.5. Population dynamics of H↓

The dynamical processes governing the densities n_a and n_b of atoms in the hyperfine states **a** and **b** can be described by rate equations. The following terms contribute:

Flow: Atoms are supplied by a hydrogen source to the cell at rates F_a and F_b. If the volume of the cell is V, the flux per unit volume into each of the hyperfine states is $f_a = F_a/V$, $f_b = F_b/V$.

One-body decay: The decay rate for escape from the magnetic potential well, or by any other simple loss process, is taken to be γ_0.

Recombination: Recombination requires at least one **a** atom. The rate depends on the state of the other particle. Thus, for state **b** the decay rate constant is $K_{ab}n_a$, while for state **a** it is $K_{ab}n_b + 2K_{aa}n_a$. (The factor of 2 is because in an **a**–**a** collision both atoms possess a spin "up" component.) The K's are effective two-body constants, as described in section 6.2.

Relaxation: Because the relaxation rate for the **a**–**b** transition depends on the collision rate, it is proportional to the total density. Taking G to be the constant of proportionality, the governing rate equations assume the form:

$$\begin{aligned} \dot{n}_a &= f_a - \gamma_0 n_a - K_{ab}n_a n_b - 2K_{aa}n_a^2 - G(n_a - n_b)(n_a + n_b), \\ \dot{n}_b &= f_b - \gamma_0 n_b - K_{ab}n_a n_b + G(n_a - n_b)(n_a + n_b). \end{aligned} \tag{6.28}$$

If T_1^{-1} denotes the decay rate for the population difference $n_a - n_b$, then $T_1^{-1} = 2G(n_a + n_b)$. Equations (6.28) are most meaningfully interpreted in the context of experimental studies, to which we now turn.

7. Experimental studies of H↓

7.1. First observations – the experiment of Silvera and Walraven

Two experimental challenges must be solved in order to create spin-polarized hydrogen: producing a flux of atomic hydrogen at low temperature, and constructing a storage cell lined with liquid helium.

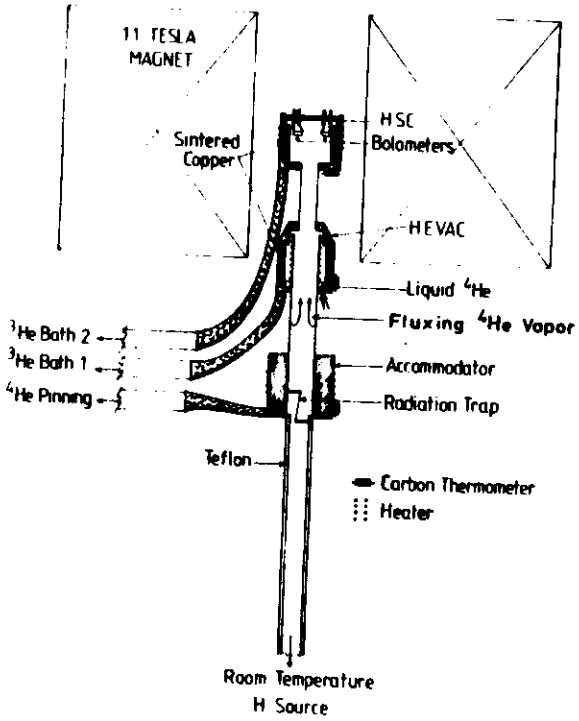

Fig. 7.1. Apparatus used by Silvera and Walraven in which H↓ was first created [13]. Courtesy of I.F. Silvera.

H↓ was first created by Silvera and Walraven [13], who invented an ingenious device, the "HEVAC", to provide the helium film and to help confine the gas. A schematic diagram of the apparatus is shown in fig. 7.1. Atomic hydrogen is supplied by a room temperature discharge and transported to a 4 K accommodator through a Teflon tube [80]. At some point the tube becomes covered by frozen H_2 which provides a non-interactive surface. The hydrogen flows through a short metal tube to a helium vapor compressor, the "HEVAC". This is a miniature diffusion pump working in reverse. Liquid helium is stored in a reservoir which is thermally pinned at 480 mK by a ^{3}He adsorption pump. A superfluid film runs up from the reservoir and then passes down the tube toward the warm (4 K) accommodator. At some point the film evaporates. The gas recondenses above the HEVAC, and flows down to the reservoir. The cell in which the H↓ accumulates is thermally pinned at 270 mK by a separate ^{3}He adsorption pump. It is located in a 6 T magnetic field and is covered by a superfluid film from the HEVAC reservoir. Thus the HEVAC simultaneously prevents the film from flowing out of the storage cell and provides a pumping action to help to compress the hydrogen.

Another innovation in the Silvera–Walraven experiment is the use of a bolometer to "burn off" the hydrogen. The bolometer is a carbon resistor suspended by fine wires. Normally it is covered by the superfluid film. If a current is supplied to the resistor, however, the film is driven off, leaving a bare surface. The hydrogen recombines on this surface, liberating a large amount of heat to the cell. Recombination appears to occur in the time it takes the atoms to hit the surface, typically a few milliseconds, and the process causes a "spike" in the temperature which is easily observed. By duplicating the thermal load from an external source, the total number of molecules is determined, and from this the density can be inferred. Silvera and Walraven obtained $n > 1.8 \times 10^{14}\,\mathrm{cm}^{-3}$.

By showing that H↓ could be created and studied in the laboratory, Silvera and Walraven's experiment played a key role in advancing the field.

7.2. *Pure magnetic confinement: the MIT experiment*

Figure 7.2 shows the apparatus used by Cline et al. [81] which differs from the technique used by Silvera and Walraven in that it relies on magnetic confinement alone to trap the hydrogen atoms. Hydrogen is provided from a liquid nitrogen temperature discharge, similar in operation to the one shown in fig. 6.1. The hydrogen is thermalized to 4.2 K in a short section covered with frozen H_2, and then flows across a narrow gap to a low temperature (300 mK) helium-lined sample tube. The helium film evaporates and recondenses in a concentric external chamber so that there is no ^{4}He vapor near the H↓. Initial experiments gave a density of $8 \times 10^{16}\,\mathrm{cm}^{-3}$ in 4 cm^3 cell.

If the atoms are confined solely by the magnetic field the mean lifetime (after the source is turned off) is

$$\tau = t_0 \exp(\mu B_0/kT)\,, \tag{7.1}$$

where B_0 is the ambient field and t_0 is the time for atoms to escape in the absence of a field. A plot of the measured lifetime vs the applied

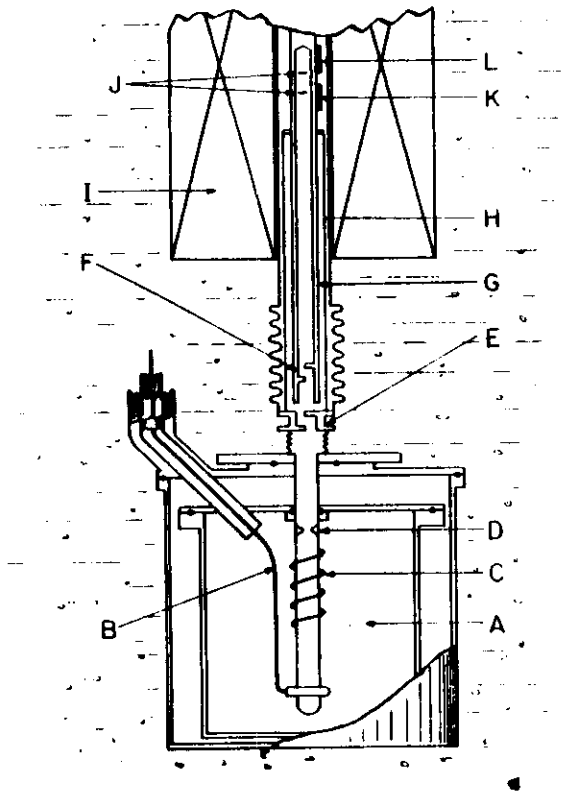

Fig. 7.2. Apparatus used by Cline et al. [81]. (A) liquid N_2; (B) H_2 inlet; (C) rf discharge, (D) orifice; (E) thermalizer, 4.2 K; (F) baffle; (G) transport tube and confinement cell; (H) helium reflexing region; (I) solenoid; (J) bolometers; (K, L) thermometers.

field B_0 is shown in fig. 7.3. For $\tau < 10^3$ s, eq. (7.1) is accurately obeyed, but at very high fields it is evident that in addition to "evaporation" out of the magnetic trap, some other decay mechanism is playing a role. These measurements were made by detecting the heat of recombination. This method is inherently destructive, which makes it difficult to map out complete decay curves. In particular, it is difficult to determine whether the decay is exponential ("one body"), or due to two- or three-body processes. To answer questions such as this, it is essential to monitor the pressure of H↓.

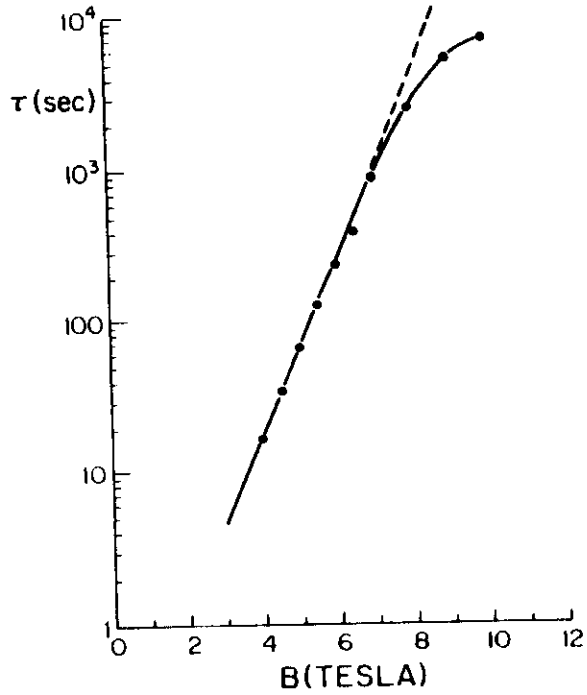

Fig. 7.3. Lifetimes of H↓ vs magnetic field [81].

7.3. *Measurement of the pressure of H↓*

Matthey et al. [48] used a capacitive transducer to monitor the pressure in a H↓ cell. The density, which was found from the pressure by the ideal gas law, was observed to decay in a curve which could be a fit by a combination of one- and two-body processes. The effective two-body rate constant, K_s was analyzed along the lines described in section 6.4. From eq. (6.25), the high-field value is related to the zero-field value by

$$K_s(B) = 2\varepsilon^2 K_s(0)\,, \tag{7.2}$$

where $\varepsilon = a/(2(\gamma_e + \gamma_p)B)$. This equation was found to hold within a factor of two, which represents reasonable agreement considering that $K_s(B)$ and $K_s(0)$ were obtained by completely different techniques, and

that they differ by a factor of 10^5. By studying the temperature dependence of $K_s(B)$ the binding energy can be found. From the slope of a logarithmic plot of the data, fig. 7.4(A), the adsorption energy was determined to be 0.89(7) K. Further confirmation of the general interpretation was obtained from study at different magnetic fields. From eqs. (6.26) and (7.2) one expects that $K_s \sim 1/B^2$; this behavior is shown in fig. 7.4(B). There was, however, no evidence for a residual stable

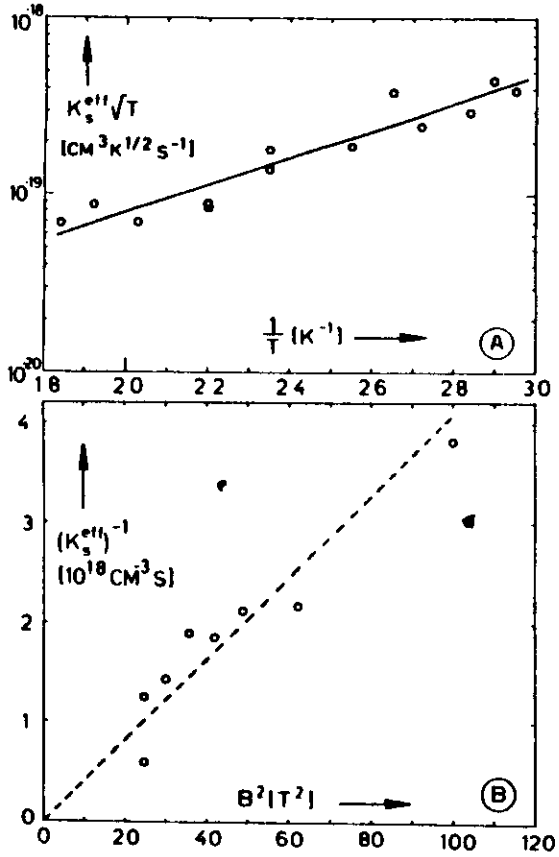

Fig. 7.4. Measurements of recombination by Mathey et al. [48]. Two-body recombination occurs on the surface; K_s^{eff} is the effective two-body rate for the gas, assuming that the gas remains in equilibrium. (A) The temperature dependence of K_s^{eff} gives the adsorption energy. (B) The magnetic field dependence of K_s^{eff} verifies that recombination occurs via hyperfine coupling in the *a* state.

component of the gas, state **b**. A subsequent experiment [50] in which exponential decay processes were eliminated also failed to display a stable component. The results could be explained by assuming that nuclear relaxation between states **a** and **b** was so rapid that as **a** decayed, **b** was also lost. However, this implied relaxation times of seconds, whereas the theory of Statt and Berlinsky [79] predicted many hours.

7.4. *Observation of nuclear polarization*

Cline et al. [16] succeeded in observing the effect of nuclear polarization on the recombination rate using a storage cell which was designed to assure that the surface film was saturated. The cell is illustrated in fig. 7.5. The source is above the cell, allowing the bottom of the cell to contain a pool of liquid helium. An experimental "fill and decay" curve is shown in fig. 7.6. The density decays rapidly until state **a** is depleted, after which it decays slowly as state **b** is lost by nuclear relaxation.

The results of this experiment are consonant with the discussion of

A) Copper rod
B) Reference capacitor
C) Capacitive pressure transducer
D) Liquid ^{4}He pool
E) Sintered copper
F) Level sensor
G) Bolometer
H) Thermometer

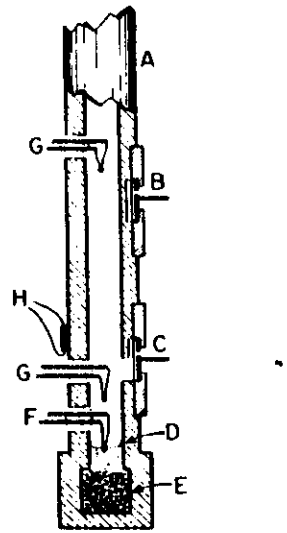

Fig. 7.5. H↓ confinement cell used by Cline et al., to obtain doubly polarized hydrogen [16]. The pool of liquid helium (D) assures that the confinement cell is covered with a saturated film.

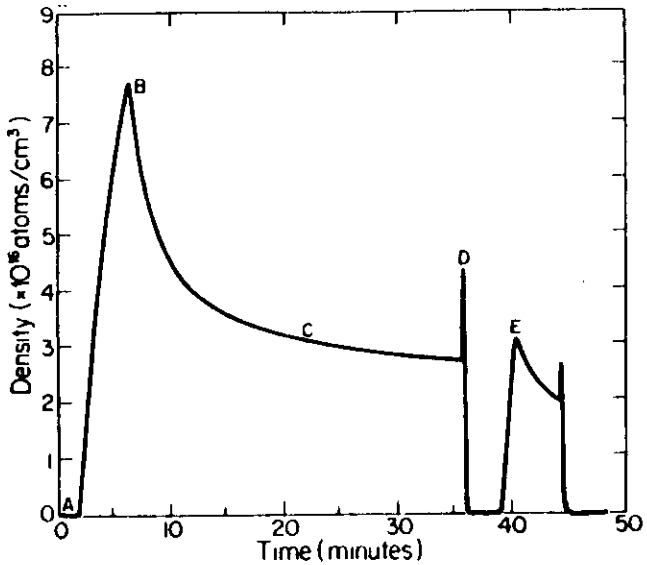

Fig. 7.6. Trace of experimental decay curve taken at 300 mK and 11 T. The noise is less than the width of the line. (A) The hydrogen source is turned on. (B) The source is turned off and the density decays rapidly as the state *a* recombines. (C) The system is now left in state *b*. It decays slowly due to nuclear relaxation to the mixed state. (D) The sample is destroyed by recombining the hydrogen on a bolometer. (E) The system is reloaded to the same density as (C). Note that the decay rate is much greater than at (C) due to the presence of the state *a*.

section 6.5. The time evolution of the densities is described by eq. (6.28) with the following simplification: $f_a = f_b \equiv f$; $K_{ab} = K_{bb} \equiv K$.

$$\dot{n}_a = f - \gamma_0 n_a - K n_a(n_b + 2n_a) - G(n_a - n_b)(n_a + n_b),$$
$$\dot{n}_b = f - \gamma_0 n_b - K n_b n_a + G(n_a - n_b)(n_a + n_b). \qquad (7.3)$$

For the decay portion of the curve $f = 0$. One-body decay was observed to be negligible, so that the only adjustable parameters were K and G. These were chosen to fit the data, often producing traces which could not be distinguished from experimental curves. Results for G and K are shown in fig. 7.7.

The temperature dependence of K yielded the adsorption energy of H on ^{4}He. The result, $E_b = 1.01(6)$ K, is in reasonable agreement with other values. Of more interest is the behavior of the nuclear relaxation rate constant, G.

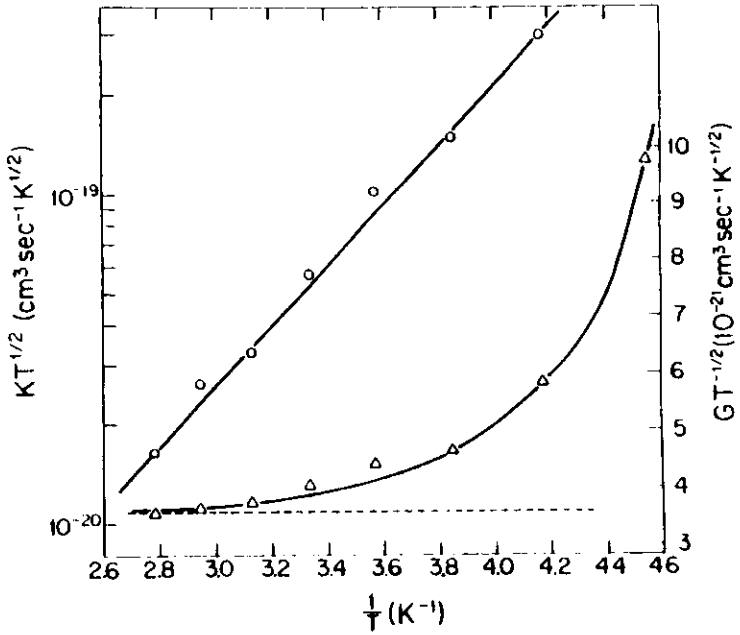

Fig. 7.7. Measurements of the recombination coefficient K and the nuclear relaxation coefficient G. Logarithmic plot of $KT^{1/2}$ (circles, left axis) vs $1/T$. Measurements were made with a field of 11 T. The solid lines are least-squares fits to the data. The dashed line indicates the gas-phase contribution to the nuclear relaxation.

Nuclear relaxation occurs by successive collisions, either in the gas or on the surface. The surface relaxation rate depends on the surface density, and so it should display a leading temperature dependence of $\exp(2E_b/kT)$. The curve for G in fig. 7.7 is plotted on the basis of this model: at high temperature the relaxation occurs primarily in the bulk giving essentially a constant relaxation rate, while at low temperature surface relaxation is important, adding a contribution which varies exponentially with $1/T$.

The decay curve, fig. 7.6, can be understood on the basis of the competition between recombination and relaxation. If the cell initially contains equal densities of **a** and **b** atoms, the gas recombines rapidly at rate $\sim 2Kn_a$. Eventually the **a** atoms are effectively eliminated, leaving a residual gas of **b** atoms. These undergo relaxation to state **a** at rate Gn_b: as soon as an atom relaxes from **b** to **a**, it recombines with a **b** atom at rate Kn_b. Under these conditions the recombination is

"bottlenecked" by the nuclear relaxation. The approximate rate equation for n_a is

$$\dot{n}_a \simeq -Kn_b n_a + Gn_b^2 . \tag{7.4}$$

In equilibrium, $Kn_a = Gn_b$. Under this condition the system has a high nuclear polarization. For state **a**, $m_I = +1/2$, while for **b**, $m_I = -1/2$. Thus the nuclear polarization is

$$P_n = \frac{n_a - n_b}{n_a + n_b} \simeq -\left(1 - \frac{G}{K}\right). \tag{7.5}$$

In the region where relaxation is dominantly in the gas, $G \ll K$, and the polarization can exceed 99%.

7.5. *Nuclear relaxation*

It is evident that nuclear relaxation plays a major role in the dynamics of H↓.

At a field of 11 T, Cline et al. [16] obtained a value for the relaxation constant for the gas phase of $G_g T^{-1/2} = 3.5(3) \times 10^{-21}\ \mathrm{cm^3\,s^{-1}\,K^{-1/2}}$. The most recent theoretical calculations by Ahn et al. [82] are in good agreement with this value. (Earlier calculations by Statt and Berlinsky [79] and by Siggia and Ruckenstein [83] differed from this result by a factor of two.) Subsequent experiments of Sprik et al. [84] using a different geometry and ^{3}He–^{4}He solutions on the wall found a value of G_g which agreed with the MIT result. It appears that volume relaxation in H↓ is understood.

Our understanding of surface relaxation is not nearly so satisfactory. The surface nuclear relaxation G_s rate is predicted to be highly anisotropic [85–88], which adds some uncertainty to the interpretation of the experimental results. Sprick et al. [84] constructed a pancake-shaped cell with a very high surface to volume ratio in order to study G_s. Their results for G_s were in good agreement with the MIT group [16]. In addition, they verified that the relaxation rate scales with the magnetic field as the theory requires. (The effective nuclear moment depends on the field due to the hyperfine coupling.) Yurke et al. [89], using a magnetic resonance method to drive the **b**–**a** transition, found similar results. Thus three experimental groups have obtained values for surface relaxation which are in reasonable agreement; however, these values are approximately *fifty times larger* than the theoretical values. It is evident that there is more to understand about surface relaxation (see Postscript). Since the recombination rate is mediated by relaxation, the solution to the problem may have important implications in choosing the best strategy to seek the Bose–Einstein transition.

7.6. *Other studies*

Spin-polarized deuterium is an attractive species for study in its role as an elementary Fermi gas. Creating D↓ presents a number of technological challenges because the dynamical rates can vary tremendously between H and D, notwithstanding that they are chemically similar. A key parameter in creating D↓ is the adsorption energy of D on ^{4}He. Silvera and Walraven [51], in an early experiment, obtained $E_b = 2.5(4)$ K from measurements of the temperature dependence of the decay rate. So far no group has produced very high densities of D↓. The binding energy of D on D_2 can be expected to be appreciably higher than for H on H_2, which would require suitable thermal redesign of the source.

^{3}He is an attractive candidate for a wall coating because the adsorption energy of H↓ can be expected to be significantly lower than for H↓ on ^{4}He. Pure ^{3}He does not provide a satisfactory surface coating; lacking superfluidity, it does not cover the entire surface and the H↓ generally recombines as fast as it enters the confinement cell. However, ^{3}He–^{4}He mixtures have been successfully used. If the ^{3}He concentration exceeds 6% phase separation occurs and a film of ^{3}He floats on the ^{3}He–^{4}He mixture. By measuring the temperature dependence of the recombination rate, Van Yperen et al. [50] obtained $E_b = 0.34(3)$ K. The binding energy was also measured using the zero-field magnetic resonance method by Jochemsen et al. [49]. The result is somewhat higher, 0.42(5) K. Heating effects on the surface due to the recombination energy are a possible explanation for the small discrepancy. Sprick et al. [84] used a combination of favorable geometry and ^{3}He rich surfaces to achieve a substantial reduction in the effective surface relaxation rate. It seems likely that ^{3}He surfaces will play a central role in the attainment of high densities of H↓.

8. Opportunities and applications for spin-polarized hydrogen

The creation of spin-polarized hydrogen and the new cold hydrogen technology opens avenues for study not only for quantum fluids but in

such diverse fields at atomic, molecular, plasma, nuclear and particle physics. This section describes some of these scientific opportunities and technical applications.

8.1. $H\downarrow$ as a quantum fluid

Observation of the Bose–Einstein transition is the most prominent goal for research on spin-polarized hydrogen, but many other aspects of this unusual quantum fluid are worth serious study. One area has already been described – two-dimensional gas of $H\downarrow$ adsorbed on a helium surface, including the search for the Kosterlitz–Thouless transition (section 4.5). Another area of interest is the study of the transport properties of $H\downarrow$ and its isotopes.

At very low temperature, where only one or two partial waves contribute to the scattering cross section, the transport properties of a gas can be radically affected by nuclear spin symmetry requirements. In some cases the cross sections drop dramatically. For example, hydrogen's exchange cross section σ_{ex} drops radidly at low temperatures. Morrow and Berlinsky [90] find that σ_{ex} approaches a limit of $5\times10^{-17}\,\mathrm{cm}^2$ at low temperature, which is only 2% of its room temperature value. The exchange collision rate decreases by a factor of about one thousand between room temperature and 0.3 K.

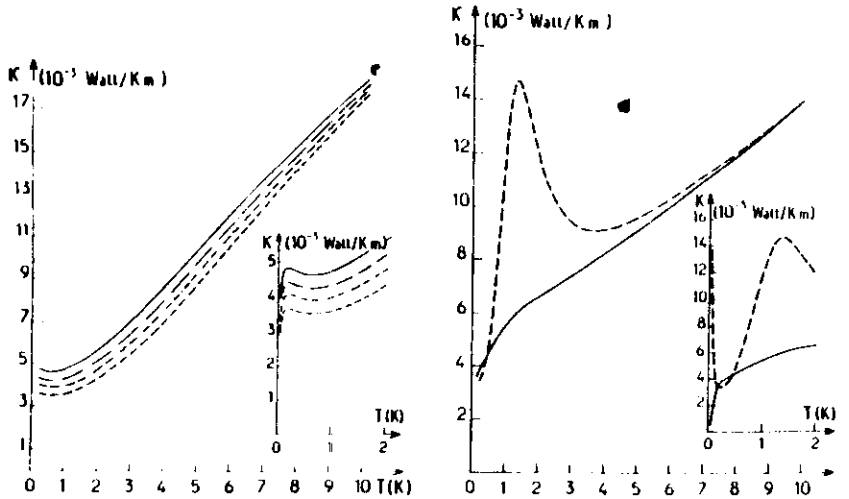

Fig. 8.1. Thermal conductivity of hydrogen isotopes as a function of temperature and polarization [22]. H (left). D (right). Courtesy of C. Lhuillier.

The thermal conductivity of $H\downarrow$ and $D\downarrow$ are also expected to exhibit dramatic behavior at low temperatures. Lhuillier and Laloë [21] have carried out a general study of the transport properties of spin-polarized gases and Lhuillier [22] has calculated spin diffusion and thermal conductivity coefficients for $H\downarrow$ and $D\downarrow$ at low temperatures. Results for the thermal conductivity κ are shown in fig. 8.1. Below 1 K, hydrogen displays a 35% variation in κ depending on the nuclear polarization. The behavior of deuterium is far more dramatic. For the completely polarized gas κ diverges at very low temperature. The reason is that S-wave scattering for fermions is forbidden for parallel nuclear spin, and P-wave scattering vanishes because of the centrifugal barrier. At 1.5 K, κ displays an anomalous peak due to cancellation of the S and D phase shifts, causing a pronounced decrease in the scattering cross section.

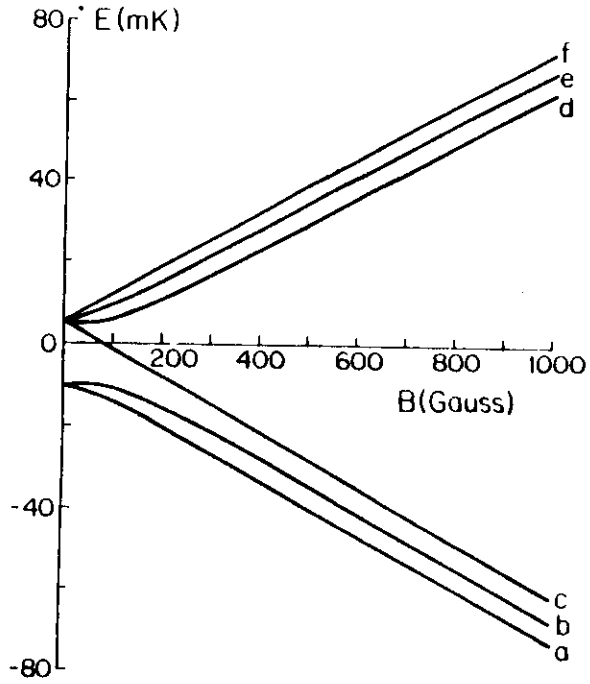

Fig. 8.2. Energy level diagram for the ground electronic state of deuterium in a magnetic field.

8.2. Spin-polarized deuterium

As described in section 5, D↓ constitutes a weakly interacting Fermi gas. Verifying the calculations of the equations of state, and finding whether or not a liquid phase exists, is an attractive experimental challenge.

The dynamics of D↓ production differ markedly from those of H↓ because of the higher adsorption energy. As table 4.1 indicates, the adsorption energy D on ^{4}He is approximately 2.4 K, in contrast to 0.9 K for H↓. Consequently, one must operate at higher temperature for a given recombination rate.

The hyperfine energy diagram of D↓ is shown in fig. 8.2. This hyperfine separation is 327 MHz, in contrast to 1420 MHz for H. The deuteron nuclear moment is $0.86\mu_N$, in contrast to $2.8\mu_N$ for the proton. As a result, the dynamics of recombination and relaxation differ considerably from those of hydrogen.

Silvera and Walraven [51] have reported the production of D↓ at low density, but the production at high density has yet to be achieved. A technical problem is that the condition for optimal transport of D from the dissociation to the low temperature region will differ considerably from those for hydrogen, due to the relatively higher adsorption energy of D on D_2 compared to H on H_2.

8.3. Application to atomic and molecular physics

Hydrogen continues to play its prominent role in atomic physics, and spin-polarized hydrogen has numerous potential applications. For example, laser spectroscopy of hydrogen can be advanced by cold hydrogen techniques. The resonance linewidth in very high resolution optical spectroscopy is generally limited by the interaction time of atoms with the light. Usually this is determined by the motion of the atoms. In such a case, reducing the temperature of the gas produces a corresponding narrowing of the resonance line. In addition, the troublesome second-order Doppler shift, proportional to the temperature of the atoms, is also reduced. The cold hydrogen techniques can be used to exploit these advantages dramatically.

The 1S–2S two-photon transition in hydrogen (243 nm) is of particular interest. The long lifetime of the metastable 2S level, 0.15 s, results in a fractional natural linewidth of this transition of less than 10^{-15}. The transition makes a superb candidate for measuring the Rydberg constant and determining the Lamb shift and isotope shifts in hydrogen, and for use as an optical frequency reference. To utilize the long lifetime of the 2S state, however, the atoms must move extremely slowly, essentially remaining at rest. There are a number of ways to produce very slow atoms using H↓ methods, including the possibility of a "fountain" experiment. A "fountain" consists of an atomic beam directed vertically up. Slow atoms fall back due to gravity, providing a long observation time. The fountain technique has never been used successfully with atoms. The problem is that in conventional atomic beams only the low speed tail of the Maxwell–Boltzmann distribution moves slowly enough for the motion to reverse within a reasonable height. The slow atoms, however, are depleted by collision with the faster atoms. By cooling hydrogen to very low temperature, however, the full velocity distribution can be used and the problem is avoided. If desired, a retarding magnetic field can be employed to further slow the beam. Hydrogen has an additional useful property: at very low temperature it is the *only* species with a significant vapor pressure, so that collisions with background gas atoms do not occur. Under such conditions one can envisage experiments with atoms which are essentially at rest.

For many applications it is not necessary to cool the hydrogen below 1 K: a helium temperature atomic beam is adequate. For example, a 4 K hydrogen atomic beam provides an excellent target for studying multiphoton processes. Hydrogen is a unique species for such studies because the multiphoton cross sections can be calculated with great accuracy, and the experimental results should be capable of straightforward analysis. Holt et al. have recently calculated the four-photon rate by a nonperturbative theory [91] making this process a particularly attractive experimental goal.

Spin-polarized hydrogen methods can be adapted to study many atomic and molecular collision processes. Charge transfer represents one potentially important area, for charge transfer collisions involving ions and atomic hydrogen are thought to play central roles in many astrophysical processes and in laboratory plasmas. For example, the reaction $H + H^- \rightarrow H_2 + e^-$ is believed to be a principle source of molecular hydrogen in astrophysical plasmas. Cross sections for capture into the accessible excited levels of H_2 have been calculated by Bieniek and Dalgarno [92], and the infrared emission spectrum has been calculated by Black et al. [93]. The high density of hydrogen available in a H↓ target should permit direct observation of the

infrared emission, a quantity never yet observed. In such an experiment the target would be a gas of H↓ confined in an "open cell" as described below.

The resonance recombination reaction described in section 6.3 represents an elementary dynamical process in molecular physics. Stwalley [77] has pointed out the interest in studying the reaction in HD and D_2 by examining the reaction rate as a function of the magnetic field. An additional "handle" on the reaction is available. By applying resonance radiation at an electron transition frequency the effective triplet–singlet interaction can be increased, broadening the resonance. Finally, it should be noted that the state-selective recombination process described in section 6.4 is a unique chemical reaction: a reaction controlled by the nuclear spin. The final spin state of the molecule can be monitored by nuclear magnetic resonance, providing a complete description of the nuclear spin dynamics during molecular recombination.

8.4. *Low temperature hydrogen maser*

The hydrogen maser is a microwave oscillator which operates on the hyperfine transition of hydrogen (1420 MHz) in a low magnetic field. Spin-selected atoms are provided by an atomic beam. In order to achieve a long interaction time with the microwave field, the atoms are "stored" in a cell coated with a non-interacting surface, generally teflon.

Maser action can be achieved at very low temperature by using ^{4}He, or possibly ^{3}He, for the wall coating. A major goal is to control the "wall shift" (the frequency shift which accompanies surface collisions described in section 6.2) by using liquid helium to coat the walls, rather than a chemical compound which is vulnerable to impurities.

Berlinsky and Hardy [94], who analyzed the systematics of such a device, have noted many potential advantages. In particular, in their study of hyperfine resonance of hydrogen in a helium-lined cell at low magnetic field (section 6.2) they found that the hyperfine frequency shift has an extremum with temperature. This occurs as the wall shift due to surface adsorption, which decreases with temperature, is offset by the pressure shift due to vapor phase collisions, which increases with temperature (see fig. 8.3). By operating at the extremum temperature the first-order variation in frequency due to temperature is eliminated. The size of the frequency shift, however, is comparable to that in a conventional maser.

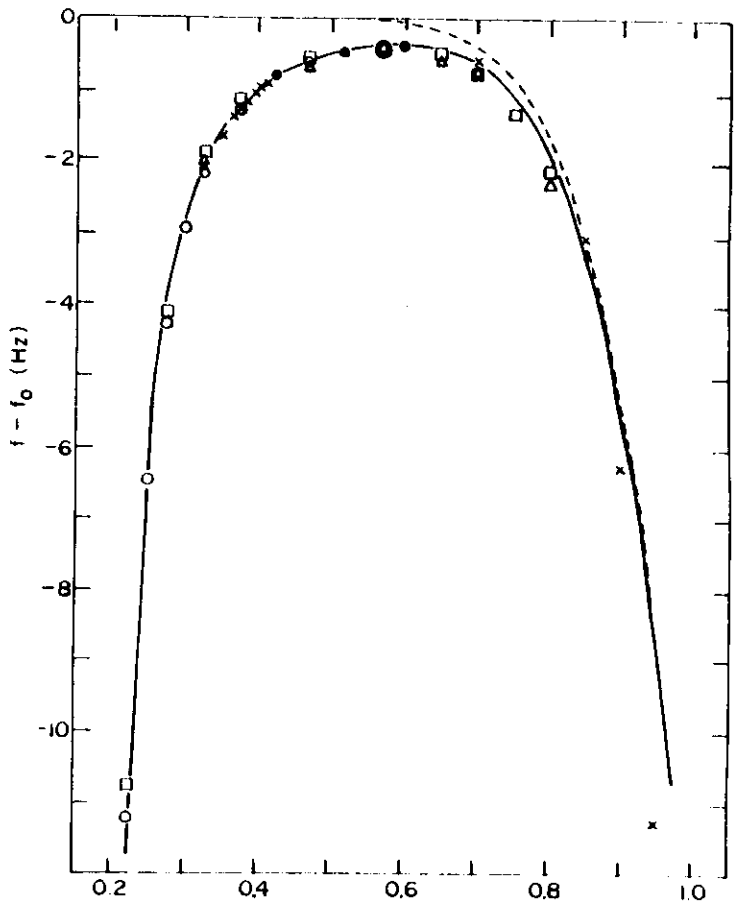

Fig. 8.3. Shift of the hyperfine frequency of hydrogen due to collisions with helium on a surface and in the gas phase, vs temperature (K) (ref. [15]). Courtesy of W.N. Hardy.

Aside from achieving a reproducible wall shift, there appear to be many other advantages to the low-temperature maser: the spin-exchange rate decreases dramatically at low temperature [90], allowing a higher atomic beam flux and higher power; intrinsic thermal noise and the second-order Doppler effect are both reduced; it becomes easier to provide an intense atomic beam due to more efficient magnetic state selection, and to control the ambient magnetic field and the mechanical stability of the microwave cavity.

8.5. Applications of magnetic resonance to H↓

Electron and nuclear spin resonance can serve as diagnostic tools for spin-polarized hydrogen, or can be employed to manipulate the population or eject atoms from a confinement cell. Because a resonance adsorption signal depends on the density of atoms and the local magnetic field, one can in principle map the density distribution in an inhomogeneous magnetic field. Walraven and Silvera [28] have proposed using this approach to detect the onset of Bose condensation.

The description of state-selective molecular recombination given in section 7.4 is based on an analysis of density decay curves for H↓ rather than on direct measurement of the nuclear polarization. By observing electron spin resonance adsorption signals, however, the density of H↓ in states **a** and **b** can be determined directly. The **a**→**d** and **b**→**c** transitions can both be observed; they are separated by the hyperfine splitting so that there is no difficulty in distinguishing them. Van Yperen et al. [95] have carried out a preliminary experiment which demonstrates feasibility of the method.

Nuclear magnetic resonance on the **b**→**a** transition can be used to measure the population difference $n_b n_a$. Yurke et al. [89] have detected the resonance by observing the recombination energy which is released as the **a** state becomes populated.

8.6. Open cell geometry

Some applications of H↓ require extracting the atoms from the cell, others involve bombarding the H↓ gas with particles from an external source. In either case it is essential to employ an "open cell" geometry, in contrast to the "closed cell" which has been used up to the present. It is easy to envisage a cylindrical storage cell in a solenoid, open at both ends, with the H↓ magnetically confined near the center. If the cell is coated with ^{4}He, however, one must face the problem of preventing the superfluid film from running out of the cell, and flowing to a high temperature region where it evaporates and wrecks the vacuum.

Figure 8.4 illustrates the principle of an open cell configuration. The helium film is trapped by a condenser surrounding the dilution refrigerator. The condenser is designed to dissipate the heat load at a high temperature stage. A series of simple baffles prevents the escape of gaseous helium, assuring that the background pressure of helium in the system is the vapor pressure at the low temperature stage.

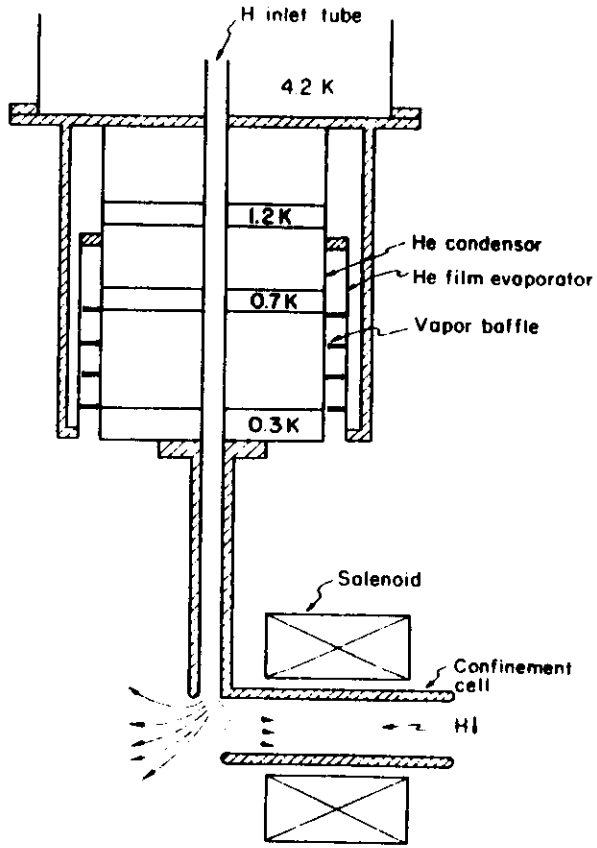

Fig. 8.4. "Open cell" design. H↓ is confined in the cell by magnetic force. The ^{4}He superfluid film flows out of the cell and is captured by a film burner at a high temperature stage of the refrigerator. The ^{4}He surface exposed to the vacuum system has a low vapor pressure.

Note that hydrogen can be introduced into the cell without a mechanical connection to the source. If the atoms are discharged near the inlet, the magnetic forces are enough to "suck in" the atoms in the correct spin state. This eliminates the troublesome transition region where the hydrogen is cooled from 4 K to below 0.3 K.

Electron spin resonance can be employed to eject spin-polarized hydrogen from its confinement cell. The transition rate must be matched to the desired escape rate; too high a rate can in principle destabilize the gas. The power required depends on the field gradients,

for the linewidth will generally be determined by the inhomogeneities. Using a power of approximately 10^{-8} W, Van Yperen et al. [95] observed the density to decay with a time constant of approximately 20 s.

8.7. *Polarized proton sources and targets for nuclear and particle physics*

Impressive technologies have been developed for providing sources of polarized particles for injection into accelerators, and for creating polarized proton targets. There are opportunities for the technology of spin-polarized hydrogen to contribute to both of these applications [96, 97].

Polarized proton ion sources provide either polarized protons ($H^+ \downarrow$) or polarized negative ions ($H^- \downarrow$). (Negative ions are more diffieult to create but they can be injected into an accelerator much more efficiently than protons.) Haeberli [98] has created an $H^- \downarrow$ source which employs a hydrogen atomic beam and charge exchange. By passing through two stages of magnetic deflection with an intermediate rf magnetic resonance region, the beam acquires high nuclear polarization. The atoms then convert to negative ions by charge exchange with fact Cs atoms: ($H + C_s^* \rightarrow H^- + C_s^+$). The intensity of such a source would be enhanced if the density of polarized atoms in the ionization region were increased. The present state of the art is a density of about $10^{12}\,cm^{-3}$. In contrast, densities of doubly-polarized hydrogen ($H \downarrow \downarrow$) greater than $10^{17}\,cm^{-3}$ have been achieved within a spin-polarized hydrogen apparatus.

One possible H^- source using spin-polarized hydrogen is shown in fig. 8.5. The open cell geometry of fig. 8.4 is combined with the Cs charge exchange method developed by Haeberli [98]. Ironically, the density provided in a conventional spin-polarized hydrogen cell is much too high for the charge exchange to work effectively. (If the density-length product is greater than about 2×10^{-15} atoms cm^{-2}, the H^- is lost by secondary charge exchange as it leaves the cell.) Consequently, the necessary $H \downarrow$ density is too low for nuclear polarization to be achieved by molecular recombination. An alternative method involves irradiating the gas with microwaves at one of the electron spin-flip transition frequencies. Atoms which undergo a transition are ejected from the cell, leaving a population of atoms in a single hyperfine state. Either the $\mathbf{a} \rightarrow \mathbf{d}$, or the $\mathbf{b} \rightarrow \mathbf{c}$ transition can be stimulated, leaving the system with $m_I = +1/2$ or $-1/2$, respectively.

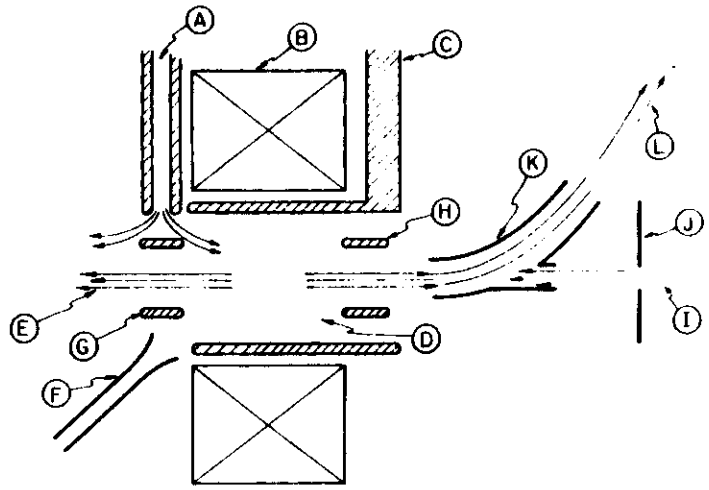

Fig. 8.5. Polarized H^- source, based on the Cs charge transfer design of Haeberli [98]. (A) H inlet; (B) solenoid; (C) cylindrical open confinement cell and connection to the dilution refrigerator; (D) stored $H \downarrow$; (E) $H \uparrow$ expelled from source; (F) ESR microwave horn; (G, H) "pusher" and "puller" electrodes for removing H^-; (I) fast Cs beam; (J) radiation shield; (K) H^- deflector; (L) polarized H^- beam.

Another approach to creating a source is shown in fig. 8.6. It uses the electron polarization of spin-polarized hydrogen to create a fast beam of $H \downarrow$ by charge exchange of fast protons with cold $H \downarrow$. The polarization is then transferred to the nucleus by passing the beam

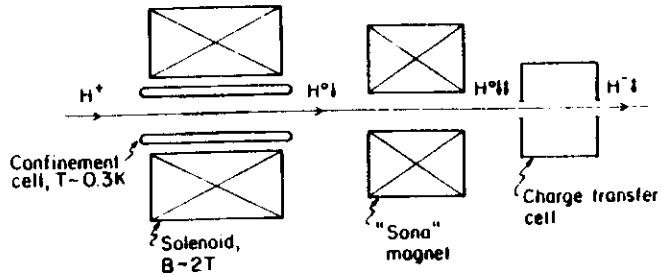

Fig. 8.6. A "fast-beam" polarized H^- source. A fast proton picks up a polarized electron by charge exchange with $H \downarrow$. The polarization is then transferred to the nucleus by passage through a "sona" magnet in which the Zeeman states, but not the hyperfine states, are inverted. Finally, the atom is converted to a negative ion by a second charge exchange collision.

through a "sona" magnet in which the magnetic field rapidly reverses, causing an inversion of the Zeeman states but not the hyperfine states.

Polarized targets can be divided into two classes: internal and external. Internal targets, which must be gaseous, are located within the accelerator so that the high energy particles pass through repeatedly. Traditionally, an intense atomic or molecular beam, a "jet", is employed. A polarized hydrogen jet has not so far been constructed because the density would be too low to be usable. By employing a cold atomic hydrogen source, however, a polarized jet may be practical. By using a 4 K source and a conventional magnetic state selector, it should be possible to achieve substantially higher beam density than from a conventional source. With a spin-polarized source even better performance should be possible. In such a source, atoms would be ejected from the storage cell by electron spin resonance. An alternative internal target would simply consist of an open hydrogen confinement cell, as shown in fig. 8.3, with the accelerator beam passing through. This design is appealing in its simplicity, but the geometry imposes severe constraints on the angular aperture for the scattered particles.

8.8. *The possibility of creating solid polarized H_2 and D_2*

For applications in nuclear and particle physics, and perhaps fusion, it would be invaluable to create nuclear-polarized solid H_2 and D_2. The techniques of spin-polarized hydrogen may make this possible.

The central idea is that the recombination reaction in $H\downarrow$ depends on the nuclear spin. If the nuclear polarization is preserved during the chemical reaction, which appears likely, than one can create polarized molecules and molecular solids.

As discussed in sections 6.4 and 7.4, a gas of $H\downarrow$ initially in states **a** and **b** acquires a high nuclear polarization as state **a** recombines, leaving a population of essentially pure **b** state atoms. This is the nascent material for creating the polarized solid. Because of nuclear relaxation, the **b** atoms decay to the **a** state but at a relatively slow rate. As soon as an atom enters the **a** state, however, it recombines in an **a**–**b** reaction. For the reaction to occur it is evident from eq. (7.3) that the **b** state $|-1/2, -1/2\rangle$ ($m_s = -1/2$, $m_I = -1/2$) must combine with the electron spin "up" component of the **a** state, $-\sin\theta|1/2, -1/2\rangle$. For both atoms $m_I = -1/2$. Thus the molecule is formed in the ortho state ($I = 1$), with $M_I = -1$.

Recombination generally leaves an H_2 molecule in a high-lying vibrational and rotational state which then relaxes to the ground state by collisional de-excitation. The nuclear spin is so weakly coupled to the rotational angular momentum that the polarization can be expected to be preserved. As a result, the molecule decays to the $J = 1$, $I = 1$, $M_I = -1$ state, the lowest rotational state of orthohydrogen. The molecules rapidly condense into a solid which is presumably covered with a film of ^{4}He. The solid could pass out of the cell under gravity, or possibly it could be removed mechanically.

A critical parameter governing applications of solid polarized H_2 is the nuclear spin-lattice relaxation time, T_1. Relaxation in molecular hydrogen at low temperature has been studied by Hardy and Berlinsky [99]. The rate is sensitive to parahydrogen impurities: for 96% pure orthohydrogen at 1.1 K, $T_1 = 78$ s. T_1 increases rapidly with decreasing temperature, however, and may be considerably longer at 0.3 K.

The general approach to creating solid polarized H_2 can also be applied to D_2, though the dynamics are quite different due to the higher adsorption energy, smaller nuclear moment and lower hyperfine frequency. Atoms are trapped in the states $|-1/2; 1, 0, -1\rangle$ ($m_s = -1/2$; $m_I = 1, 0, -1$). States $|-1/2; 0, -1\rangle$ contain small components of $|+1/2; 0, 1\rangle$, respectively, due to the hyperfine coupling, and these will eventually recombine, leaving the pure eigenstate $|-1/2, -1\rangle$. Nuclear relaxation will cause the transition $|-1/2, -1\rangle \rightarrow |-1/2, 0\rangle$. The atoms recombine to form the $I = 2$, $M_I = -2$ state of ortho-deuterium. In practice it may be desirable to employ electron and nuclear spin resonance to produce the nuclear polarization rather than to rely on state-selective recombination.

A great advantage of solid D_2 compared to H_2 is its extremely long relaxation time. At a temperature of 1.1 K, 98% para-D_2 has a relaxation time of 7.5 h [99]. At lower temperatures it is expected to be longer yet.

Polarized solids of H_2 and D_2 have potential advantages as targets for nuclear and particles scattering compared to dynamically polarized targets. In particular, the absence of foreign nuclei reduces background events, enormously enhancing the sensitivity to polarization-dependent scattering. On the other hand there are many potential technical problems in employing such a target, particularly the heat removal and target damage due to ionizing radiations. In a pulsed experiment one could conceivably employ a pellet target which is used only once.

8.9. Fusion applications

Kulsrud et al. [100] have pointed out possible advantages of using spin-polarized nucleons as fuel for a fusion plasma. In particular, if polarized deuterons and tritons are used for the reaction $D + T \rightarrow He^4 + n$, not only is the cross section increased but the reaction products are ejected anisotropically so as to enhance interaction with the magnetic field of a tokamak. (The reaction occurs via a spin 3/2 resonance of He^5, which requires that D and T have parallel spin.) The reaction $D + He^3 \rightarrow He^4 + p$ is also enhanced by using polarized particles. An added advantage of using polarized deuterons is that the reaction $D + D \rightarrow He^3 + n$ is suppressed, providing the possibility of a neutron-free plasma.

It is unexpected that nucleons could maintain their polarization in a plasma, but Kulsrud et al. find that the most obvious mechanisms for depolarization are not effective. In this regard the situation is reminiscent of the early stages of spin-polarized hydrogen research when it was realized that $H\downarrow$ might be stable in spite of numerous hypothetical destabilizing mechanisms. Nonetheless, for the present the proposal must be regarded as somewhat tentative.

To supply polarized nuclei for fusion plasmas an intense source of polarized deuterons is required, and possibly also of tritons and He^3. Large quantities of the nuclei need to be injected in a very short time, typically milliseconds, which precludes the use of low temperature atomic beams. Mechanical injection of a solid pellet is one method in use; this should be applicable to polarized solid D_2. Energy costs are a major consideration in providing large quantities of the material. By using spin resonance to select the polarization state, rather than to rely on state-selective recombination, the major thermal load on the low temperature cell is eliminated and the cooling requirements are greatly eased.

It is an open question whether the techniques for producing $H\downarrow$ and $D\downarrow$ can be applied to tritium, though the theoretical estimates of the binding energies of T on ^{4}He (table 4.1), 3.2 K, leaves it within the realm of possibility.

Postscript

Between the time these lectures were delivered and the submission of the final proofs (June 1984) there have been a number of new results relating to spin-polarized hydrogen. We summarize several of them.

P.1. Compression experiments

Experiments have been carried out in which a gas of nuclear and electron polarized hydrogen is compressed to high densities by mechanical means. Hess et al. [101, 102] used a solid piston; the gas was forced into a flat disk-shaped cell. Sprik et al. [103] exerted pressure through the liquid helium; the gas ended up in a small bubble whose shape was determined by the surface tension of the liquid. Densities as high as 4.5×10^{18} atoms/cm^3 have been reported [102]. By studying the decay of samples at high density, recombination due to the three-body dipole interaction (see C4 in section 6.3) has been observed in the bulk and on the surface. The magnitude of the effect is close to that predicted by Kagan et al. [78, 104]; however, the measured rates [102] do not show the strong dependence on magnetic field expected from the theory. It appears that three-body dipole recombination places severe limits on the densities which can be attained in spin-polarized hydrogen.

The magnitude of the surface three-body dipole recombination is so large that it caused a re-examination of earlier results on the decay of doubly-polarized hydrogen. It is now believed that the interpretation of those results in terms of an anomalously high surface two-body nuclear relaxation rate (see section 7.5) was incorrect. Computations show [105] that surface three-body recombination alone can completely account for the low-temperature decay rates, at least in the case of the earlier MIT experiments [16]. This observation clears up a worrisome discrepancy between theory and experiment. The surface two-body nuclear relaxation rate has probably never been observed, a fact consistent with the best theoretical calculations of its magnitude [82].

Compression experiments at high temperature and low magnetic fields allowed the observation of a contribution to the two-body decay due to an electronic relaxation process [103]. Atoms in the **b** state relax to the **c** state in a two-body collision; the **c** atom then recombines rapidly on the wall with a **b** atom (see B in section 6.3). The three-body decay has also been shown to exhibit a term due to the electronic relaxation [106], the **c** atom recombining with two **b** atoms in the gas.

In summary, the compression experiments have given a wealth of

experimental results to compare with the detailed calculations of relaxation and recombination mechanisms in hydrogen.

P.2. Nuclear spin waves

Nuclear spin waves have been observed in a H↓ gas by Johnson et al. [107]. They studied NMR absorption between the a and b states. Superimposed on the broad absorption peak associated with a small inhomogeneity in the magnetic field, they found a series of narrow absorption spikes corresponding to standing spin waves in the cell. The usual feature of this result is that the gas, at a density of about 10^{16} atoms/cm^3 and temperatures around 250 mK, is far from the quantum regime. The thermal deBroglie wavelength $\Lambda(T) \approx 35$ Å is much smaller than the mean spacing between atoms $n^{-1/3} \approx 460$ Å. Usually one associates collective behavior in a spin system with the overlapping of the tails of the wavefunctions of the host atoms, as one might have in a solid or liquid. In the gas, however, the effect of successive independent collisions on the spin of a given atom must accumulate in a coherent fashion. Such a behavior in dilute, non-degenerate spin-polarized gases (^{3}He as well as H↓) was predicted by Lhuillier and Laloë [21, 22]. Nacher et al. [108] have found evidence for spin waves in spin-polarized ^{3}He gas, and Gully and Mullin [109] have found similar evidence in a non-degenerate dilute liquid solution of ^{3}He in ^{4}He.

Levy and Ruckenstein [110] have formulated a theory which emphasizes the essential similarity of the physics of spin waves in ferromagnets, degenerate quantum liquids and dilute gases. They are able to calculate an absorption spectrum for H↓ which agrees very well with the spectrum measured by Johnson et al. [107]. Analysis of the spectrum allows one to determine the longitudinal spin diffusion coefficient in the gas and a parameter which measures the strength of the exchange effects in the spin-transport process.

It appears that NMR experiments of this type can provide a valuable probe of the microscopic behavior of spin-polarized hydrogen at all densities.

P.3. Critical behavior

A detailed study of the critical behavior of a dilute interacting Bose fluid has been carried out by Rasolt et al. [111]. In particular, they examined the crossover from critical behavior near the transition to ideal Bose gas behavior at low temperatures. Many of their predictions are too technical to discuss here. The most interesting result for spin-polarized hydrogen is that the crossover from mean field to critical behavior (see section 3.6) occurs at a reduced temperature $\varepsilon = (T_0 - T)/T_0$ which is proportional to $a/\Lambda(T_0)$. This gives a critical region which is considerably wider than that indicated by eq. (3.28). The reason why the simple Ginzburg criterion approach of section 3.6 gives the incorrect result is not yet understood.

P.4. Other realizations of a Bose gas

As explained in section 1, ^{4}He under normal conditions does not form a weakly interacting degenerate Bose gas. In the liquid state the density is high and the interactions, which include a hard core repulsion, are sizeable. The saturated vapor, in equilibrium with the liquid, is not dense enough at any temperature to become degenerate. Crooker et al. [112] have used an ingeneous scheme to create a weakely interacting ^{4}He gas which exhibits a Bose–Einstein like transition. They studied thin films of helium absorbed on porous Vycor glass. The glass has the geometry of a sponge: interconnected pores of the order of 60 Å in diameter take up about 40% of the apparent volume of a sample. Experiments were done at sub-monolayer coverages where the distance between mobile helium atoms was considerably greater than the atomic scattering length and comparable to the pore diameters. The phase transitions observed did not show the characteristics associated with the superfluid transition on strictly two-dimensional substrates [56, 57]; rather they resembled, at least at the higher coverages, the transition seen in the bulk liquid [113]. It is believed that the multiply connected geometry of the pores enforces three-dimensional behavior. As the coverage is decreased, the transition temperature decreases in such a way that the deBroglie wavelength at the transition is in rough proportion to the mean spacing between mobile helium atoms, as is the case for an ideal Bose gas. At low densities, on the order of 10^{19}/cm^3, the width of the critical region below the transition narrows, indicating a crossover to dilute Bose behavior. Comparison with the theory of Rasolt et al. [111] for critical behavior in a dilute Bose fluid supports this interpretation.

Another system which can be modeled as a weakly interacting Bose gas comes from the field of semiconductor physics. Excitons are a

combination of an electron and a hole in a semiconductor, bound together by Coulomb attraction. Their structure is analogous to that of a hydrogen atom; however, due to the reduction of the Coulomb interaction associated with the background medium (which can be viewed as a vacuum with a high dielectric constant), the energy scale is less and the characteristic distances are larger than in hydrogen. At low temperatures and high densities of excitons, the excitons can form biexitons (weakly bound pairs of excitons, the analogue of H_2) or even condense into a liquid state [114]. In the case of copper chloride, CuCl, the interactions between the excitons are such that the liquid state does not form, rather the low temperature state of the exitons is a gas of biexitons. Because of their low effective mass, several hundred times less than hydrogen, the biexitons would exhibit a Bose–Einstein transition at proportionately higher temperatures at the same density (see eq. 1.13). There is some evidence that such a transition may occur at temperatures of 25 to 50 K in CuCl [115]. The system is a complicated one though, and other interpretations are possible [114]. Further studies are being carried out.

Acknowledgements

We wish to acknowledge the many contributions to our research effort at MIT by R.W. Cline, and to thank the current members of the group for their assistance: D.A. Bell, H.F. Hess and G.P. Kochanski. We would also like to thank J.A. Berlinsky for many stimulating discussions. The research at MIT was sponsored by the National Science Foundation, grant DMR-8007850.

References

[1] L.H. Nosanow, J. Physique 41 (1980) C7-1.
[2] I.F. Silvera, Proc. 16th Int. Conf. Low Temperature Phys., Physica 109 & 110B (1982) 1499.
[3] W.N. Hardy, M. Morrow, R. Jochemsen and A.J. Berlinsky, 16th Int. Conf. Low Temperature Phys., Physica 109 & 110B (1982) 1964.
[4] V.F. Sears, E.C. Svensson, P. Martel and A.D.B. Woods, Phys. Rev. Lett. 49 (1982) 279.
[5] W. Kolos and L. Wolniewicz, J. Chem. Phys. 43 (1965) 2429; Chem. Phys. Lett. 24 (1974) 457.

[6] C.E. Hecht, Physica 25 (1959) 1159.
[7] J.V. Dugan, Jr. and R.D. Etters, J. Chem. Phys. 59 (1973) 6171.
[8] R.D. Etters, J.V. Dugan, Jr. and R.W. Palmer, J. Chem. Phys. 62 (1975) 313.
[9] M.D. Miller, L.H. Nosanow and L.J. Parish, Phys. Rev. Lett. 35 (1975) 581.
[10] W.C. Stwalley and L.H. Nosanow, Phys. Rev. Lett. 36 (1976) 910.
[11] S.B. Crampton, T.J. Greytak, D. Kleppner, W.D. Phillips, D.A. Smith and A. Weinrib, Phys. Rev. Lett. 42 (1979) 1039.
[12] N.W. Hardy, A.J. Berlinsky and L.A. Whitehead, Phys. Rev. Lett. 42 (1979) 1042.
[13] I.F. Silvera and J.T.M. Walraven, Phys. Rev. Lett. 44 (1980) 164.
[14] J. Physique 41 (1980) Colloque C-7. "Spin Polarized Quantum Systems", Colloque International du CNRS, 21–26 April 1980, Aussois (France), Frank Laloë, organizer.
[15] M. Morrow, R. Jochemsen, A.J. Berlinsky and W.N. Hardy, Phys. Rev. Lett. 46 (1981) 195; 47 (1981) 455.
[16] R.W. Cline, T.J. Greytak and D. Kleppner, Phys. Rev. Lett. 47 (1981) 1195.
[17] J.T. Jones, Jr., M.H. Johnson, H.L. Mayer, S. Katz and R.S. Wright, Aeronutronic Systems, Inc., (a Subsidiary of Ford Motor Company) Publication U-216, 1958.
[18] H.C. Berg and D. Kleppner, Rev. Sci. Inst. 33 (1962) 248.
[19] A. Kastler, Acto Physica Polinicia, XXXIV (1968) 693.
[20] A. Alzetta, A. Gozzini and L. Mois, C. Rendu 274 (1972) 39.
[21] C. Lhuillier and F. Laloë, J. Physique 43 (1982) 197; 43 (1982) 225.
[22] C. Lhuillier, J. Physique, 44 (1983) 1.
[23] T.J. Greytak and D. Kleppner, Bull. Am. Phys. Soc. 23 (1978) 86.
[24] E.P. Bashkin and A.E. Megerovich, Usp. Fiz. Nauk 130 (1980) 279 [Soviet Phys. Usp. 23 (1980) 156].
[25] D.G. Friend and R.D. Etters, J. Low Temp. Phys. 39 (1980) 409.
[26] V.L. Ginzburg and L.P. Pitaevski, Soviet Phys. JETP 34 (1958) 1240.
[27] E.P. Gross, J. Math. Phys. 4 (1963) 195.
[28] J.T.M. Walraven and I.F. Silvera, Phys. Rev. Lett. 44 (1980) 168.
[29] N. Bogoliubov, J. Phys. U.S.S.R. 11 (1947) 23.
[30] L. Landau, J. Phys. U.S.S.R. 5 (1941) 71.
[31] T.D. Lee, K. Huang and C.N. Yang, Phys. Rev. 106 (1957) 1135 and earlier references cited in this paper.
[32] M.E. Fisher, Rev. Mod. Phys. 46 (1974) 597.
[33] R.A. Ferrell, N. Menyhard, H. Schmidt, F. Schwabl and P. Szepfalusy, Ann. Phys. 47 (1968) 565.
[34] V.L. Ginzburg, Sov. Phys. Solid State 2 (1960) 1824.
[35] L.J. Lantto and R.M. Nieminen, J. Low Temp. Phys. 37 (1979) 1.
[36] E.D. Siggia and A.E. Ruckenstein, Phys. Rev. Lett. 44 (1980) 1423; Phys. Rev. B23 (1981) 3580.
[37] V.V. Goldman, I.F. Silvera and A.J. Leggett, Phys. Rev. B24 (1981) 2870.
[38] C.A. Condat and R.A. Guyer, Phys. Rev. B24 (1981) 2874.
[39] D.A. Huse and E.D. Siggia, J. Low Temp. Phys. 46 (1982) 137.
[40] J.M. Kosterlitz and D.J. Thouless, Prog. Low Temp. Phys., Vol. VII-B, edited by D.F. Brewer (North-Holland, 1978).
[41] A.J. Berlinsky, R.D. Etters, V.V. Goldman and I.F. Silvera, Phys. Rev. Lett. 39 (1977) 356; A.J. Berlinsky, Phys. Rev. Lett. 39 (1977) 359.
[42] L.J. Lantto and R.M. Nieminen, J. Physique 41, C7-49 (1980).

[43] Y. Kagan and G.V. Shlyapnikov, Pis'ma Zh. Eksp. Teor. Fiz. 34 (1981) 358.
[44] S.B. Crampton, J.J. Krupczak and S.P. Souza, Phys. Rev. B25 (1982) 4383.
[45] W.C. Stwalley, Chem. Phys. Lett. 88 (1982) 404.
[46] I.B. Mantz and D.O. Edwards, Phys. Rev. B20 (1979) 4518.
[47] R.H. Guyer and M.D. Miller, Phys. Rev. Lett. 42 (1979) 1754.
[48] A.P.M. Matthey, J.T.M. Walraven and I.F. Silvera, Phys. Rev. Lett. 46 (1981) 668.
[49] R. Jochemsen, M. Morrow, A.J. Berlinsky and W.N. Hardy, Phys. Rev. Lett. 47 (1981) 852.
[50] G.H. van Yperen, A.P.M. Matthey, J.T.M. Walraven and I.F. Silvera, Phys. Rev. Lett. 47 (1981) 800.
[51] I.F. Silvera and J.T.M. Walraven, Phys. Rev. Lett. 45 (1980) 1268.
[52] M.D. Miller and L.H. Nosanow, J. Low Temp. Phys. 32 (1978) 145.
[53] D.O. Edwards and I.B. Mantz, J. Physique 41 (1980) C7-257.
[54] I.F. Silvera and V.V. Goldman, Phys. Rev. Lett. 45 (1980) 915.
[55] V.V. Goldman and I.F. Silvera, Physica 107B (1981) 515.
[56] I. Rudnick, Phys. Rev. Lett. 40 (1978) 1454.
[57] D.J. Biship and J.D. Reppy, Phys. Rev. Lett. 40 (1978) 1727.
[58] D.R. Nelson and J.M. Kosterlitz, Phys. Rev. Lett. 39 (1977) 1201.
[59] D. Edwards, Physica 109 & 110 B (1982) 1531.
[60] R.A. Guyer and M.D. Miller, Phys. Rev. B25 (1982) 5749.
[61] J.E. Rutledge, W.L. McMillan, J.M. Mochel and T.E. Washburn, Phys. Rev. B18 (1978) 2155.
[62] F.M. Ellis and R.B. Hallock, Rev. Sci. Instr. 54 (1983) 751.
[63] P. Kumar, Physica 108B (1981) 939.
[64] R.A. Guyer, M.D. Miller and J. Yaple, Physica 108B (1981) 941; Phys. Rev. B25 (1982) 4570.
[65] B.G. Wilson and P. Kumar, Phys. Rev. B27 (1983) 3076.
[66] D.S. Zimmerman, Thesis, University of British Columbia, unpublished.
[67] D.S. Zimmerman and A.J. Berlinsky, Can. J. Phys., Phys. Lett. 95A (1983) 309.
[68] Y. Kagan and G.V. Shlyapnikov, preprint.
[69] P. Ehrenfest and J.R. Oppenheimer, Phys. Rev. 37 (1931) 333.
[70] V. Lefèvre-Seguin, P.J. Nacher, C. Lhuillier and F. Laloë, J. Physique 43 (1982) 1199.
[71] L.H. Nosanow, L.J. Parish and F.J. Pinski, Phys. Rev. B11 (1975) 191.
[72] W.L. McMillan, Phys. Rev. 138 (1965) A442.
[73] R.M. Panoff, J.W. Clark, M.A. Lee, K.E. Schmidt, M.H. Kalos and G.V. Chester, Phys. Rev. Lett. 48 (1982) 1675.
[74] L.P. Walkaskaus and F. Kaufman (Proc. 15th Int. Symp. Combustion, the Combustion Institute, Philadelphia, 1974).
[75] M. Morrow and W.N. Hardy, Can. J. Phys. 61 (1983) 956.
[76] J.M. Greben, A.W. Thomas and A.J. Berlinsky, Can. J. of Physics, 59 (1981) 945.
[77] W.C. Stwalley, Phys. Rev. Lett. 37 (1976) 1628.
[78] Yu. Kagan, G.V. Shlyapnikov and I.A. Vartanyantz, Zh. Eksp. Teor. Fiz. 81 (1981) 1113 [Soviet Physics JETP, 54 (1982) 590].
[79] B.W. Statt and A.J. Berlinsky, Phys. Rev. Lett. 45 (1980) 2105.
[80] J.T.M. Walraven and I.F. Silvera, Rev. of Sci. Inst. 53 (1982) 1167.
[81] R.W. Cline, D.A. Smith, T.J. Greytak and D. Kleppner, Phys. Rev. Lett. 45 (1980) 2117; J. Physique 41 (1980) C7-151.
[82] R.M.C. Ahn, J.P.H.W. v.d. Eijnde and B.J. Verhaar, Phys. Rev. B27 (1983) 5424.

[83] E.D. Siggia and A.E. Ruckenstein, Phys. Rev. B23 (1981) 3580.
[84] R. Sprik, J.T.M. Walraven, G.H. van Yperen and I.F. Silvera, Phys. Rev. Lett. 49 (1982) 153.
[85] A. Lagendijk, Phys. Rev. B25 (1982) 2054.
[86] A.E. Ruckenstein and E.D. Siggia, Phys. Rev. B25 (1982) 6031.
[87] B. Statt, Phys. Rev. B25 (1982) 6035.
[88] R.M.C. Ahn, J.P.H.W. v.d. Eijnde, C.J. Reuver, B.J. Verhaar and I.F. Silvera, Phys. Rev. B26 (1982) 452.
[89] B. Yurke, J.S. Denker, B.R. Johnson, N. Bigelow, L.P. Levy, D.M. Lee and J.H. Freed, Phys. Rev. Lett. 50 (1983) 1137.
[90] M. Morrow and A.J. Berlinsky, Can. J. Phys. 61 (1983) 1042.
[91] G.R. Holt, M.G. Raymer and W.P. Reinhardt, Phys. Rev. A27 (1983) 2971.
[92] R.J. Bieniek and A. Dalgarno, Astro. J. 228 (1979) 635.
[93] J.H. Black, A. Porter and A. Dalgarno, Astro. J. 249 (1981) 138.
[94] A.J. Berlinsky and W.N. Hardy, Proc. 13th Annual Precision Time and Timer Interval applications and Planning Meeting, Washington, D.C. 1981, NASA Conference Publications 220, p. 547.
[95] G.H. van Yperen, I.F. Silvera, J.T.M. Walraven, J. Berkhout and J.G. Brisson, Phys. Rev. Lett. 50 (1983).
[96] T.O. Niinikoski, Proc. Intern. Symp. on High-Energy Physics with Polarized Beams and Polarized Targets, Lausanne, 1980 (EXS 38, Birkhäuser Verlag, Basle and Stuttgart, 1981) p. 191.
[97] D. Kleppner and T.J. Greytak, Proceedings of the 5th Int. Conf. High Energy Spin Physics, Brookhaven 1982, G.M. Bunce, Ed., American Institute of Physics Conference Proceedings, No. 95 (1983) p. 546.
[98] W. Haeberli, Nucl. Inst. Meth. 63 (1968) 355; D. Hennies, R.S. Raymond, L.W. Anderson, W. Haeberli and H.F. Glavish, Phys. Rev. Lett. 40 (1978) 1234.
[99] W.N. Hardy and A.J. Berlinsky, Phys. Rev. B8 (1971) 4996.
[100] R.M. Kulsrud, H.P. Furth, E.J. Valeo and M. Goldhaber, Phys. Rev. Lett. 49 (1982) 1248.
[101] H.F. Hess, D.A. Bell, G.P. Kochanski, R.W. Cline, D. Kleppner and T.J. Greytak, Phys. Rev. Lett. 51 (1983) 483.
[102] H.F. Hess, D.A. Bell, G.P. Kochanski, D. Kleppner and T.J. Greytak, Phys. Rev. Lett. 52 (1984) 1520.
[103] R. Sprik, J.T.M. Walraven and I.F. Silvera, Phys. Rev. Lett. 51 (1983) 479 and 942.
[104] Yu. Kagan, G.V. Shlyapnikov, I.A. Vartanyantz and N.A. Glukhov, Pis'ma Zh. Eksp. Teor. Fiz. 35 (1982) 386 [Sov. Phys. JETP Lett. 35 (1982) 477].
[105] D.A. Bell, G.P. Kochanski, D. Kleppner and T.J. Greytak, Proc. 17th Intern. Conf. Low Temperature Phys. (1984), in press.
[106] D.A. Bell, G.P. Kochanski, L. Pollack, H.F. Hess, D. Kleppner and T.J. Greytak, Proc. 17th Intern. Conf. Low Temperature Phys. (1984), in press.
[107] B.R. Johnson, J.S. Denker, N. Bigelow, L.P. Levy, J.H. Freed and D.M. Lee, Phys. Rev. Lett. 52 (1984) 1508.
[108] P.J. Nacher, G. Testevin, M. Leduc, S.B. Crampton and F. Laloë, J. Physique Lett. 45 (1984) L441.
[109] W.J. Gully and W.J. Mullin, Phys. Rev. Lett. 52 (1984) 1810.
[110] L.P. Levy and A.E. Ruckenstein, Phys. Rev. Lett. 52 (1984) 1512.

[111] M. Rasolt, M.J. Stephen, M.E. Fisher and P.B. Weichman, Phys. Rev. Lett. (1984), in press.
[112] B.C. Crooker, E. Hebral, E.N. Smith, Y. Takano and J.D. Reppy, Phys. Rev. Lett. 51 (1983) 666.
[113] D.J. Bishop, J.E. Berthold, J.M. Parpia and J.D. Reppy, Phys. Rev. B24 (1981) 5047.
[114] J.P. Wolfe and A. Mysyrowicz, Sci. Amer. 250 (1984) 98.
[115] L.L. Chase, N. Peyghambarian, G. Grynberg and A. Mysyrowicz, Phys. Rev. Lett. 42 (1979) 1231.